Toxic si/shRNAs that kill cancer cells by targeting survival genes

William Putzbach[1,6], Quan Q. Gao[1,6], Monal Patel[1,6], Stijn van Dongen[4], Ashley Haluck-Kangas[1], Aishe A. Sarshad[5], Elizabeth Bartom[2], Kwang-Youn A. Kim[3], Denise M. Scholtens[3], Markus Hafner[5], Jonathan C. Zhao[1], Andrea E. Murmann[1] and Marcus E. Peter[1,2,*]

[1] Department of Medicine/Division Hematology/Oncology and [2] Department of Biochemistry and Molecular Genetics, [3] Department of Preventive Medicine, Feinberg School of Medicine, Northwestern University, Chicago, IL 60611, USA; [4] European Bioinformatics Institute (EMBL-EBI), Hinxton, Cambridge CB10 1SD, UK; [5] Laboratory of Muscle Stem Cells and Gene Regulation, NIAMS, NIH, Bethesda, MD 20892, USA.

Corresponding author: Marcus Peter, E-mail: m-peter@northwestern.edu, phone: 312-503-1291; FAX: 312-503-0189.

[6] Shared first authorship

Keywords:
RNAi, Fas, cancer, CRISPR, cell death, DISE, OTE

Abstract

Over 80% of multiple tested siRNAs and shRNAs targeting CD95 or CD95 ligand (CD95L) induce a form of cell death characterized by simultaneous activation of multiple cell death pathways preferentially killing transformed and cancer stem cells. We now show these si/shRNAs kill cancer cells through canonical RNAi by targeting the 3'UTR of critical survival genes in a unique form of off-target effect we call DISE (death induced by survival gene elimination). Drosha and Dicer deficient cells, devoid of most miRNAs, are hypersensitive to DISE, suggesting cellular miRNAs protect cells from this form of cell death. By testing 4666 shRNAs derived from the CD95 and CD95L mRNA sequences and an unrelated control gene, Venus, we have identified many toxic sequences - most of them located in the open reading frame of CD95L. We propose that using specific toxic RNAi-active sequences present in the genome can kill cancer cells.

Introduction

One of the most popular methods utilized to reduce gene expression in cells is RNA interference (RNAi). RNAi has been used in several studies to identify genes critical for the survival of human cancer cell lines (Cowley et al., 2014; Hadji et al., 2014; Hart, Brown, Sircoulomb, Rottapel, & Moffat, 2014; Morgens, Deans, Li, & Bassik, 2016; Wang et al., 2015). During RNAi, gene expression is inhibited by small interfering (si)RNAs, small hairpin (sh)RNAs or micro (mi)RNAs. miRNAs are generated as primary transcripts in the nucleus where they undergo processing to pre-miRNAs by the Drosha-DGCR8 complex before being exported to the cytosol by exportin 5 (Ha & Kim, 2014; Krol, Loedige, & Filipowicz, 2010). Once in the cytosol, pre-miRNAs and shRNAs are cleaved by Dicer, a type III RNase that functions in complex with TRBP, generating 21-23 nucleotide long fragments of double-stranded RNA (dsRNA) that have two nucleotide 3' overhangs (Zamore, Tuschl, Sharp, & Bartel, 2000). DsRNA fragments or chemically synthesized double stranded siRNAs are loaded into the RNA-induced silencing complex (RISC) as single stranded RNAs (the guide RNA) (Siomi & Siomi, 2009). A near-perfect complementarity between the guide strand of the si/miRNA and the target mRNA sequence results in cleavage of the mRNA (Pratt & MacRae, 2009). Incomplete complementarity results in inhibition of protein translation and contributes to mRNA degradation (Guo, Ingolia, Weissman, & Bartel, 2010). mRNA targeting is mostly determined by the seed sequence, positions 2-7/8 of the guide strand, which is fully complementary to the seed match in the 3'UTR of targeted mRNAs. Similar to miRNAs, although not fully explored, siRNAs and shRNAs also target multiple mRNAs besides the mRNAs they were designed to silence—a phenomenon commonly referred to as off-target effect (OTE)—that is generally sought to be avoided (Birmingham et al., 2006; Jackson et al., 2006; Lin et al., 2005).

The death receptor CD95 (Fas/APO-1) mediates induction of apoptosis when bound by its cognate CD95L, most prominently in the context of the immune system (Krammer, 2000). However, more recently, it has become apparent that the CD95/CD95L system has multiple tumor-promoting activities (Peter et al., 2007). CD95 signaling promotes cell growth (Chen et al., 2010), increases motility and invasiveness of cancer cells (Barnhart et al., 2004; Kleber et al., 2008), and promotes cancer stemness (Ceppi et al., 2014; Drachsler et al., 2016; Qadir et al., 2017). In fact, we reported tumors barely grew *in vivo* when the CD95 gene was deleted (Chen et al., 2010; Hadji et al., 2014). Therefore, it appeared consistent that multiple shRNAs and siRNAs targeting either CD95 or CD95L slowed down cancer cell growth (Chen et al., 2010) and

engaged a distinct form of cell death characterized by the activation of multiple cell death pathways (Hadji et al., 2014). This unique form of cell death cannot be inhibited by conventional cell death or signaling pathway inhibitors or by knockdown of any single gene in the human genome (Hadji et al., 2014); it preferentially affects transformed cells (Hadji et al., 2014) including cancer stem cells (Ceppi et al., 2014). Here we report that loading of CD95 and CD95L derived sequences (si/shRNAs targeting CD95 or CD95L) into the RISC elicits a distinct form of cell death that results from the targeting of multiple survival genes in a unique form of OTE.

Results

si/shRNAs kill cells in the absence of the targeted site

More than 80% of multiple tested shRNAs or siRNAs designed to target either CD95 or CD95L were toxic to multiple cancer cells (Hadji et al., 2014). We have now extended this analysis to Dicer substrate 27mer DsiRNAs designed to target CD95L (***Figure 1 - figure supplement 1A,*** (D. H. Kim et al., 2005)). All five DsiRNAs displayed toxicity when introduced into HeyA8 cells at 5 nM (***Figure 1 - figure supplement 1B***) reinforcing our previous observation that the majority of CD95 and CD95L targeting si/shRNAs are toxic to cancer cells. We also analyzed a data set of a genome-wide analysis of 216 cells infected with a pooled library of the TRC shRNAs (Cowley et al., 2014). Most of the shRNAs we have tested were found to be depleted in the infected cell lines included, in this study. The following shRNAs were found to be depleted in the listed percentage of the 216 cell lines tested: shL4 (99.5%), shL1 (96.8%), shR6 (88.9%), shR7 (75%), shL2 (67.1%), shR5 (38.4%, shL5 (26.4%), and shR8 (21.3%) (***Figure 1 - figure supplement 1C***). Consistent with our data, shL1 and shR6 were found to be two of the most toxic shRNAs. Again in this independent analysis, the majority of tested shRNAs (67%) targeting either CD95 or CD95L killed more than half of all tested cancer cell lines.

Interestingly, a more recent RNAi screen did not report toxicity after expressing shRNAs against CD95 or CD95L (Morgens et al., 2016). The authors of this study used a second-generation shRNA platform based on a miR-30 backbone. To determine the source of the discrepancy in the data, we generated miR-30 based Tet-inducible versions of some of our most toxic shRNAs (shL1, shL3, shL4, shR5, shR6, and shR7, ***Figure 1- figure supplement 2A***) and found none of them to be highly toxic to HeyA8 cells (***Figure 1- figure supplement 2B)***. To determine their knockdown efficiency, we induced their expression in cells carrying sensor

106 plasmids in which the fluorophore Venus was linked to either the CD95L or CD95 open
107 reading frame (ORF). Expression of most of these miR-30-based shRNAs also did not efficiently
108 silence Venus expression (***Figure 1- figure supplement 2C***). In contrast, two of our most toxic
109 shRNAs shL3 and shR6 when expressed in the Tet inducible pTIP vector not only killed HeyA8
110 cells, but also very efficiently suppressed Venus fluorescence in cells expressing the targeted
111 Venus sensor (***Figure 1- figure supplement 2D***). These data suggest that the levels of shRNAs
112 produced from the miR-30 based vector may not be sufficient to be toxic to the cancer cells.
113 Because expression levels of shRNAs are difficult to titer, we used siRNAs to determine the
114 concentration of the toxic CD95L-derived siL3 required to kill HeyA8 cells (***Figure 1- figure***
115 ***supplement 2E)***. Growth was effectively blocked (and cells died, data not shown) when siL3 was
116 transfected at 1 nM—a concentration well below the commonly used and recommended siRNA
117 concentration of 5-50 nM)—but not at 0.1 nM. These data suggest this form of toxicity does not
118 require high amounts of si- or shRNAs; however, that the low expression we achieved from the
119 miR-30 based shRNA vectors was not enough to effectively induce the toxicity. Because these
120 miR-30 based shRNA vectors were developed to reduce off-target effects, the toxicity of CD95
121 and CD95L targeting si/shRNAs described by us and others could be due to an OTE. While this
122 was a plausible explanation, the high percentage of toxic si/shRNAs derived from CD95 and
123 CD95L seemed to exclude a standard OTE and pointed at a survival activity of CD95 and
124 CD95L.

125 We therefore tested whether exogenously added recombinant CD95L protein could protect
126 cells from the toxicity of CD95L-derived shRNAs. When NB7 cells were incubated with
127 different concentrations of a soluble form of CD95L (S2), toxicity exerted by shL1 was not
128 affected (***Figure 1A, left panel***). NB7 neuroblastoma cells were chosen for these experiments
129 because they lack expression of caspase-8 (Teitz et al., 2000) and hence are completely resistant
130 to the apoptosis inducing effects of CD95L. An ostensible moderate and dose-dependent
131 protection was detected when cells were treated with a highly active leucine-zipper tagged
132 CD95L (LzCD95L) (***Figure 1A, center panel***). However, this effect is likely due to the growth-
133 promoting activities of soluble CD95L, which also significantly affected the growth of the cells
134 expressing a scrambled control shRNA (seen for both S2 and LzCD95L). The recombinant
135 LzCD95L protein was active, as demonstrated by its apoptosis-inducing capacity in CD95
136 apoptosis sensitive MCF-7 cells (***Figure 1A, right panel)***.

To test whether CD95L or CD95 proteins could protect cancer cells from death, we introduced silent mutations into the targeted sites of three very toxic shRNAs: shL1 and shL3 (both targeting CD95L) and shR6 (targeting CD95). We first introduced eight silent mutations into the sites targeted by either shL1 or shL3 (**Figure 1B**) and expressed these proteins in NB7 cells (**Figure 1C**). Both mutant constructs were highly resistant to knockdown by their cognate shRNA but still sensitive to knockdown by the other targeting shRNA (**Figure 1C**). Overexpression of these shRNA-resistant versions of the CD95L ORF did not protect the cells from shL1 or shL3, respectively (**Figure 1D**). Interestingly, expression of full length CD95L slowed down the growth of the NB7 cells right after infection with the lentivirus despite the absence of caspase-8 (data not shown). Infection with shRNAs was therefore performed 9 days after introducing CD95L when the cells had recovered and expressed significant CD95L protein levels (**Figure 1C**). We then mutated the CD95 mRNA in the targeted site of shR6 (**Figure 1E**). Neither expression of wild-type (wt) nor mutated (MUT) CD95 in MCF-7 cells (**Figure 1F**) reduced the toxicity when cells were infected with the pLKO-shR6 or another toxic lentiviral shRNA, pLKO-shR7 (**Figure 1G**). These data suggested that neither exogenously added recombinant CD95L or exogenously expressed CD95L or CD95 protein can protect cells from toxic shRNAs derived from these genes.

To determine whether we could prevent cancer cells from dying by this form of cell death by deleting the endogenous targeted sites, we used CRISPR/Cas9 gene-editing to excise sites targeted by different shRNAs and siRNAs in both alleles of the CD95 and CD95L genes. We first deleted a 41 nt piece of the CD95L gene in 293T cells, that contained the target site for shL3 (***Figure 2A, 2C***). While internal primers could not detect CD95L mRNA in three tested clones, primers outside of the deleted area did detect CD95L mRNA (***Figure 2D***, and data not shown). Three clones with this shL3 Δ41 deletion were pooled and tested for toxicity by shL3 expressed from a Tet-inducible plasmid (pTIP-shL3). Compared to a pool of control cells transfected only with the Cas9 plasmid, the 293T shL3 Δ41 cells were equally sensitive to the toxic shRNA (***Figure 2G***). This was also observed when the clones were tested individually (data not shown).

To exclude the possibility that shL3 was inducing cell death due to a unique activity of shL3 and/or 293T cells, we deleted the same 41 nt in CD95L in the ovarian cancer cell line HeyA8; We also generated HeyA8 clones in which we either removed a 64 nt region containing the target site for the siRNA siL3 in the CD95L coding sequence or a 227 nt region containing the target site for shR6 in CD95 (***Figure 2A, 2B*** and ***Figure 2 - figure supplement 1***). In all cases,

homozygous deletions were generated (***Figure 2E***). To confirm the deletion of the shR6 target site, we infected HeyA8 cells treated with the Cas9 plasmid only and HeyA8 with a homozygous deletion of the shR6 site with shR6 and, as positive controls, with shR2 (targeting the CD95 ORF) and shR6' (targeting the CD95 3'UTR). Five days after infection, CD95 mRNA was quantified by real time PCR using a primer located outside the 227bp deletion (***Figure 2F***). The mutated CD95 mRNA was still detectable in the shR6 Δ227 cells. While shR2 and shR6' (both targeting outside the deleted region) caused knockdown of CD95 mRNA in both the Cas9 expressing control and the shR6 Δ227 cells, shR6 could only reduce mRNA expression in the Cas9 control cells. These data document that HeyA8 CD95 shR6 Δ227 cells no longer harbor the sequence targeted by shR6.

Now having HeyA8 cells lacking one of three RNAi-targeted sites in either CD95 or CD95L, we could test the role of the CD95 and CD95L gene products in protecting HeyA8 cells from the death induced by either shRNA (shL3 and shR6, two different vectors: pLKO or the Tet inducible pTIP) or the siRNA siL3. In all cases, the shRNA or siRNA that targeted the deleted region was still fully toxic to the target-site deleted cells (***Figure 2H*** and ***2I***). We saw efficient growth reduction and cell death in siL3 site deleted cells transfected with as little as 1 nM siL3 (***Figure 2I***, and data not shown). These data firmly establish that cells were not dying due to the knockdown of either CD95 or CD95L.

Involvement of canonical RNAi

shRNAs and early generation naked siRNAs showed general toxicity when introduced in large amounts, presumably by eliciting an interferon (IFN) response (Marques & Williams, 2005) or by saturating the RISC (Grimm et al., 2006). However, both chemically modified siRNAs at very low concentrations and lentiviral shRNAs at an MOI<1 were still toxic (data not shown). We therefore decided to test whether the observed toxicity involved canonical RNAi and activity of the RISC. To test shRNAs or siRNAs targeting CD95L, we introduced the Venus-CD95L sensor (inset in ***Figure 3A***, right panel) into HeyA8 CD95 protein k.o. cells we had generated in the process of deleting the shR6 site (***Figure 2 - figure supplement 1*****,** clone # 2 was used for the following studies; see figure legend for strategy and characterization of the clones). While double-stranded (ds)-siL3 effectively silenced Venus expression and induced toxicity, neither the sense nor the antisense single-stranded (ss)RNAs significantly decreased Venus expression or induced toxicity (***Figure 3A***). In addition, no activity was found when ds-siL3, synthesized as

201 deoxyribo-oligonucleotides, was transfected into the cells (***Figure 3B***). Using this type of
202 analysis, we tested a number of modified siRNAs for RNAi activity and toxicity. For siRNAs to
203 be fully active they require 3' overhangs on both strands (Bernstein, Caudy, Hammond, &
204 Hannon, 2001). Converting siL3 to a blunt-ended duplex resulted in substantial loss of RNAi
205 activity and toxicity (***Figure 3C***). Due to the topology of the RISC, siRNA activity is decreased
206 by modification of the 5' end of the antisense/guide strand (Chiu & Rana, 2003). To test whether
207 cell death induced by siL3 would be affected by a bulky modification, we placed a Cy5 moiety at
208 any of the four possible ends of the siL3 duplex. Only when the siL3 duplex carried a 5'
209 modification in the guide strand did it prevent RNAi activity and toxicity; modifications in the
210 three other positions had no effect (***Figure 3C***). This was confirmed for another siRNA, siL2. To
211 test whether the toxicity of siL3 required association with a macromolecular complex, which
212 would be consistent with RISC involvement, we performed a competition experiment. HeyA8
213 cells were transfected with 10 nM of siL3, and a mutated nontoxic oligonucleotide, siL3MUT,
214 was titered in (***Figure 3D***). siL3MUT reduced the growth inhibitory activity of siL3 in a dose-
215 dependent fashion suggesting that siL3 and siL3MUT compete for the same binding site in the
216 cells, pointing at involvement of the RISC.

217 To determine involvement of RNAi pathway components in the toxicity of CD95 and
218 CD95L-derived sequences, we tested HCT116 cells deficient for either Drosha or Dicer (Y. K.
219 Kim, Kim, & Kim, 2016). Growth of parental HCT116 cells was impaired after infection with
220 shL3 or shR6 viruses (**Figure 3E**, left panel). Consistent with the requirement of Dicer to
221 process shRNAs, Dicer$^{-/-}$ cells were completely resistant to the toxic shRNAs (***Figure 3E***, center
222 panel). This was also supported by the inability of shR6 to silence CD95 protein expression in
223 these cells (***Figure 3F***). Dicer$^{-/-}$ cells were not resistant to toxic siRNAs as these cells died when
224 transfected with siL3, which is consistent with mature siRNAs not needing further processing by
225 Dicer (***Figure 3G,*** center panel). Interestingly, Drosha$^{-/-}$ cells were hypersensitive to the two
226 toxic shRNAs (***Figure 3E***, right panel, $p<0.0001$, according to a polynomial fitting model), and
227 shR6 efficiently knocked down CD95 expression in Drosha$^{-/-}$ cells (***Figure 3F***). Both Drosha$^{-/-}$
228 and Dicer$^{-/-}$ cells were much more susceptible to the toxicity induced by siL3 than parental cells
229 (***Figure 3G,*** center and right panel, $p<0.0001$, according to a polynomial fitting model). The
230 hypersensitivity of the Drosha$^{-/-}$ cells to toxic si/shRNAs and of Dicer$^{-/-}$ cells to toxic siRNAs can
231 be explained by Drosha$^{-/-}$ and Dicer$^{-/-}$ cells allowing much more efficient uptake of mature toxic

232 RNAi-active species into the RISC because they are almost completely devoid of competing
233 endogenous miRNAs (Y. K. Kim et al., 2016).

234 To determine the contribution of the siRNA seed sequence to their toxicity, we generated a
235 set of chimeric siRNAs in which we systematically replaced nucleotides of the toxic siL3 siRNA
236 with nucleotides of a nontoxic scrambled siRNA. We did this starting either from the seed end or
237 from the opposite end (***Figure 3H***). HeyA8 cells expressing both the Venus-CD95L sensor (to
238 monitor level of knockdown) and a Nuc-Red plasmid to fluorescently label nuclei (to monitor the
239 effects on cell growth) were transfected with 5 nM of the chimeric siRNAs; total green
240 fluorescence and the number of red fluorescent nuclei were quantified over time. The siL3
241 control transfected cells showed an almost complete suppression of the green fluorescence and
242 high toxicity. In the top panel of ***Figure 3H,*** the data are summarized in which siL3 nucleotides
243 were stepwise replaced with siScr nucleotides from the seed sequence end. Both RNAi and
244 toxicity were profoundly reduced when three of the terminal siL3 nucleotides were replaced with
245 the siScr nucleotides in those positions, suggesting the seed region (6mer highlighted in blue) is
246 critical for both activities. Consistently, as shown in the bottom panel of ***Figure 3H***, when siL3
247 nucleotides were replaced with siScr nucleotides from the non-seed end, neither RNAi nor the
248 toxicity was diminished until replacements affected residues in the seed region. These data
249 suggest the 6mer seed sequence of siL3 was critical for both RNAi activity and its toxicity.
250

251 **Toxic si/shRNAs cause downregulation of survival genes**

252 A general OTE by RNAi has been reported (Birmingham et al., 2006; Jackson et al., 2006; Lin et
253 al., 2005). However, this was been found to cause toxicity in most cases, and the targeted
254 mRNAs were difficult to predict (Birmingham et al., 2006). The fact that 22 of the tested CD95
255 and CD95L-targeting sh- and si/DsiRNAs were toxic to many cancer cells evoking similar
256 morphological and biological responses (Hadji et al., 2014) generated a conundrum: Could an
257 OTE trigger a specific biology? To test this, we expressed two toxic shRNAs - one targeting
258 CD95L (shL3) and one targeting CD95 (shR6) - in cells lacking their respective target sequences
259 and subjected the RNA isolated from these cells to an RNA-Seq analysis. In order to detect
260 effects that were independent of cell type, delivery method of the shRNA, or targeted gene, we
261 expressed shL3 in 293T (ΔshL3) cells using the Tet-inducible vector pTIP and shR6 in HeyA8
262 (ΔshR6) cells using the pLKO vector. In each case, changes in RNA abundance were compared
263 to cells in which expressing a non-targeting shRNA in matching vectors. Total RNA was

harvested in all cases at either the 50-hour time point (before the onset of cell death) or at the 100-hour time point (during cell death) (***Figure 4A***). To achieve high stringency, the data were then analyzed in two ways: first, using a conventional alignment-based analysis to identify genes for which the mRNA changed more than 1.5-fold (and an adjusted p-value of less than 0.05) and second, by a read-based method, in which we first identified all reads that changed >1.5-fold and then subjected each read to a BLAST search to identify the gene it was derived from. Only RNAs that were detected by both methods were considered (***Table S1***). The combination of the analyses resulted in one mRNA that was upregulated and 11 mRNAs that were downregulated (***Figure 4B***). Using an arrayed qPCR approach, most of these detected mRNA changes were validated for both cell lines (***Figure 4 - figure supplement 1A***). Interestingly, for nine of the eleven genes, published data suggest they are either highly upregulated in cancer and/or critical for the survival of cancer cells, as their inhibition or knockdown resulted in either growth reduction or induction of various forms of cell death (see legend of ***Figure 4 - figure supplement 1*** for details). Significantly, six of these eleven downregulated genes were recently identified in two independent genome-wide RNAi lethality screens to be critical for cancer cell survival (Blomen et al., 2015; Wang et al., 2015) (***Figure 4B*** and ***Figure 4 - figure supplement 1B***) (***Table S2***). Considering these two screens only identified 6.6% of human genes to be critical for cell survival, we found a significant enrichment (54.5%, p-value = 3×10^{-6} according to binomial distribution) of these survival genes among the genes downregulated during the cell death induced by either shL3 or shR6. All six survival genes are either highly amplified or mutated in human cancers (***Figure 4 - figure supplement 2A***). In addition to these six genes, GNB1 and HIST1H1C were reported to be required fitness genes in a recent high-resolution CRISPR-based screen (Hart et al., 2015). A kinetic analysis showed most of the deregulated mRNAs were downregulated early with a significant effect already at 14 hours, more than two days before the onset of cell death (***Figure 4 - figure supplement 1C*** and data not shown). This suggested the cells were dying because of the silencing of multiple critical survival genes, providing an explanation for why multiple cell death pathways were activated. We therefore call this type of cell death DISE (for Death Induced by Survival gene Elimination).

To confirm some of the downregulated genes were also critical survival genes for HeyA8 cells, we transfected HeyA8 cells with siRNA SmartPools targeting each of the eleven genes. Individual knockdown of seven of the targeted genes resulted in reduced cell growth when compared to cells transfected with a pool of scrambled siRNAs (***Figure 4C***). To mimic the effect

296 of the CD95 and CD95L-derived shRNAs, we treated HeyA8 cells with a combination of
297 siRNA pools targeting these seven genes. Remarkably, 1 nM of this siRNA mixture (35.7 pM of
298 each individual siRNA) was sufficient to effectively reduce growth of the cells (***Figure 4 -***
299 ***figure supplement 2B***) and also cause substantial cell death (***Figure 4 - figure supplement 2C***),
300 suggesting it is possible to kill cancer cells with very small amounts of siRNAs targeting a
301 network of these survival genes.

302 To test the generality of this phenomenon, we inducibly expressed another CD95L derived
303 shRNA, shL1, in 293T cells using the pTIP vector, and transfected HeyA8 cells with 25 nM
304 siL3. We subjected the cells to RNA-Seq analysis 100 hours and 48 hours after addition of Dox
305 or after transfection, respectively. To determine whether survival genes were downregulated in
306 all cases of sh/siRNA induced cell death, we used a list of 1883 survival genes and 423 genes not
307 required for survival (nonsurvival genes) recently identified in a CRISPR lethality screen (***Table***
308 ***S2***). We subjected the four ranked RNA-Seq data sets to a gene set enrichment analysis using the
309 two gene sets (***Figure 4D***). In all cases, survival genes were significantly enriched towards the
310 top of the ranked lists (most downregulated). In contrast, nonsurvival genes were not enriched.
311 One interesting feature of DISE that emerged was the substantial loss of histones. Of the 16
312 genes that were significantly downregulated in cells treated with any of the four sh/siRNAs, 12
313 were histones (***Figure 4E***). While it might be expected that dying cells would downregulate
314 highly expressed genes such as histones, we believe that losing histones is a specific aspect of
315 DISE because a detailed analysis revealed the downregulated histones were not the most highly
316 expressed genes in these cells (***Figure 4 - figure supplement 3***). In addition, almost as many
317 genes with similarly high expression were found to be upregulated in cells after DISE induction.

318 A Metascape analysis revealed genes involved in mitotic cell cycle, DNA conformation
319 change, and macromolecular complex assembly were among the most significantly
320 downregulated across all cells in which DISE was induced by any of the four sh/siRNAs (***Figure***
321 ***4F***). These GO clusters are consistent with DISE being a form of mitotic catastrophe with cells
322 unable to survive cell division (Hadji et al., 2014) and suggest a general degradation of
323 macromolecular complexes.

324

325 **Toxic si/shRNAs target survival genes in their 3'UTR**

326 To test whether the toxic shRNAs directly targeted genes through canonical RNAi, we subjected
327 the two gene lists obtained from the RNA-Seq analysis (the cell lines treated with either shL3 or

shR6 at the 50 hour time point) to a Sylamer analysis (van Dongen, Abreu-Goodger, & Enright, 2008) designed to find an enrichment of miRNA/siRNA targeted sites in the 3'UTR of a list of genes ranked according to fold downregulation (***Figure 5A***). This analysis identified a strong enrichment of the cognate seed match for shL3 and shR6 in cells treated with either of these two shRNAs. The analyses with cells treated with shRNAs for 100 hours looked similar but less significant, suggesting early targeting by the shRNAs followed by secondary events (data not shown). Enrichment in 6mers and 8mers were both detected (only 8mers shown) in the 3'UTRs but not the ORF of the ranked genes (data not shown).

Interestingly, the seed matches detected by the Sylamer analysis were shifted by one nucleotide from the expected seed match based on the 21mer coded by the lentivirus. RNA-Seq analysis performed for the small RNA fraction confirmed in all cases (shScr and shL3 in pTIP, and shScr and shR6 in pLKO), the shRNAs in the cells were cleaved in a way resulting in the predominant formation of an siRNA shifted one nucleotide away from the shRNA loop region (black arrow heads in ***Figure 5 - figure supplement 1A***). This allowed us to design toxic mature siRNAs based on the sequences of shL3 and shR6. These shRNA-to-siRNA converts were toxic to HeyA8 cells (***Figure 5 - figure supplement 1B***) confirming that the observed toxicity was not limited to the TRC shRNA platform, but based on a sequence-specific activity of the si/shRNAs.

The generalizability of the Sylamer results for shL3 and shR6 was tested with cells treated with either shL1 or siL3. In both cases, when the ranked RNA Seq data were subjected to a Sylamer analysis, the seed matches of the si/shRNA introduced were again significantly enriched in the 3'UTR of downregulated RNAs (***Figure 5 - figure supplement 2***). In none of the Sylamer analyses of the four data sets, did we see enrichment of seed matches in the 3'UTRs of downregulated RNAs that matched the passenger strand. In all cases, the only significantly enriched sequences matched the seed sequences in the guide strand of the si/shRNAs we introduced.

Our data suggested that DISE inducing si/shRNAs caused an early loss of survival genes, and at the same time downregulated RNAs through canonical RNAi targeting their 3'UTR. However, it was not clear whether the most highly downregulated survival genes were targeted in their 3'UTR by RNAi-active sequences. We determined as little as 6 nucleotides dictated whether an siRNA killed cancer cells (see ***Figure 3H***). 10 of the 11 targeted genes identified in the RNA-Seq analysis described in ***Figure 4A*** *and* ***4B*** contained multiple 6mer seed matches for either shL3 and/or shR6 (***Figure 5B***). It is therefore likely the two shRNAs, shL3 and shR6, killed cells

360 by targeting a network of genes enriched in critical survival genes through RNAi. The only
361 gene without an shL3 or shR6 seed match was HIST1H1C. Interestingly, only four of the
362 histones downregulated in cells after treatment with any of the four tested sh/siRNAs had a
363 3'UTR (underlined in ***Figure 4E***) suggesting that most histones were not directly targeted by the
364 sh/siRNAs.

365 Using multiplex qPCR, we tested whether other toxic shRNAs targeting either CD95 or
366 CD95L also caused downregulation of some of the 11 genes silenced by shL3 and shR6. HeyA8
367 cells were transfected with the toxic siRNA siL3 (RNA harvested at 80 hours) or the toxic
368 shRNAs shL1, shL3 or shR7 (RNA harvested at 100 hrs.). While shL1 did not have much of an
369 effect on the expression of these genes, shR7 caused downregulation of 7 of 11 of the same
370 genes targeted by shL3 even though the 6mer seed matches of the two shRNAs are very different
371 (CTTTGT for shL3 and GGAGGA for shR7) (***Figure 4 - figure supplement 1D***).

372 To determine whether preferential targeting of survival genes was responsible for the death
373 of the cells, we tested whether there was an association between the presence or absence of a
374 predicted seed match in the 3'UTR for the si/shRNA introduced and whether a gene would be
375 downregulated (>1.5 fold downregulated, $p<0.05$) among survival genes using the Fisher's Exact
376 test (***Figure 5C***). In almost all cases, this analysis revealed that survival genes containing a
377 predicted seed match in their 3'UTR were statistically more likely to be downregulated than
378 survival genes without such a motif. The analysis with shL1 treated cells did not reach statistical
379 significance, likely due to the fact that this shRNA was found to be very toxic and the 100 hour
380 time point may have been too late to observe evidence of significant targeting. This
381 interpretation is supported by the observation that the significance for both shL3 and shR6 to
382 target survival genes was higher at 50 hours when compared to the 100 hour time points (***Figure***
383 ***5C***) and that the Sylamer analysis of the shL1 treated cells was less significant after 100 hours of
384 treatment than any of the other Sylamer analyses (***Figure 5 - figure supplement 2***).

385 Now that we had established that the toxicity of the studied shRNAs involved targeting of
386 survival genes rather than CD95 or CD95L we had to assume that when studying a larger set of
387 shRNAs that the level of knockdown of the targeted genes and the toxicity were not strictly
388 correlated. This was confirmed for the TRC shRNAs targeting the ORF or 3'UTR of CD95 in
389 CD95 high expressing HeyA8 cells (***Figure 5 - figure supplement 3***). While some of the toxic
390 shRNAs efficiently silenced CD95 (i.e. shR6 and shR2) others did not (i.e. shR5). In summary,

our analyses suggest that cells die by DISE due to an early and selective silencing of survival genes through targeting seed matches in their 3'UTR followed by the downregulation of histones.

Identification of toxic shRNAs in the CD95L and CD95 mRNAs

The majority of commercially available si- Dsi-, and shRNAs targeting either CD95 or CD95L were highly toxic to cancer cells. We therefore asked whether these two genes contained additional sequences with similar activity. To test all shRNAs derived from either CD95L or CD95, we synthesized all possible shRNAs, 21 nucleotides long, present in the ORF or the 3'UTR of either CD95L or CD95 starting with the first 21 nucleotides after the start codon, and then shifting the sequence by one nucleotide along the entire ORF and 3'UTR (***Figure 6A***). We also included shRNAs from a gene not expressed in mammalian cells and not expected to contain toxic sequences, Venus. All 4666 oligonucleotides (700 Venus, 825 CD95L ORF, 837 CD95L 3'UTR, 987 CD95 ORF, and 1317 CD95 3'UTR shRNAs) were cloned into the Tet-inducible pTIP vector (***Figure 6B***) as five individual pools. We first tested the activity of each individual pool to be toxic and to target the Venus sensor protein (fused to either the ORF of CD95 or CD95L). NB7 cells were again used because of their resistance to the Venus-CD95L sensor which was found to be slightly toxic to CD95 apoptosis competent cells. NB7-Venus-CD95L cells infected with the Venus-targeting shRNA pool showed some reduction in fluorescence when Dox was added, however, the shRNA pool derived from the CD95L ORF was much more active in knocking down Venus (***Figure 6 - figure supplement 1A***). No significant green fluorescence reduction was detected in cells after infection with the shRNA pool derived from the CD95L 3'UTR since the targeted sequences were not part of the sensor. Similar results were obtained when NB7-Venus-CD95 cells were infected with the Venus, CD95 ORF, and CD95 3'UTR targeting shRNA pools. To determine their ability to reduce cell growth (as a surrogate marker for toxicity), we infected NB7 parental cells with each of the five pools (parental cells were used for this experiment to avoid a possible sponge effect by expressing either CD95L or CD95 sequences that were part of the Venus sensors). Interestingly, the pool of 700 shRNAs derived from Venus did not cause any toxicity (***Figure 6 - figure supplement 1B***). In contrast, the pool of the shRNAs derived from CD95L significantly slowed down growth, while no toxicity was observed when cells were infected with the pool of shRNAs derived from the CD95L 3'UTR. In the case of CD95, both the shRNAs derived from the ORF and the 3'UTR showed some toxicity. However, the shRNAs derived from the 3'UTR caused greater toxicity

423 compared to those derived from the ORF. The data suggests that overall the shRNAs derived
424 from the CD95L ORF and the CD95 3'UTR contain the most toxic sequences.

425 To determine the toxicity of each of the shRNAs in the pools, NB7 cells were infected with
426 the libraries of shRNA viruses (MOI<1), and after puromycin selection cells were pooled 1:1:1
427 (Venus ORF/CD95L ORF/CD95L 3'UTR pools or Venus ORF/CD95 ORF/CD95 3'UTR pools)
428 to allow for competition between shRNAs when Dox was added (***Figure 6B***). Cells were
429 cultured for 9 days with and without Dox to allow for cell death to occur. To identify depleted
430 shRNAs, shRNA barcodes were detected through next generation sequencing of PCR products to
431 determine the relative abundance of each shRNA in three pools: 1) the cloned plasmid libraries,
432 2) cells after infection and culture for 9 days without Dox, and 3) cells infected and cultured with
433 Dox for 9 days. A total of 71,168,032 reads were detected containing a complete sequence of one
434 of the cloned shRNAs. Virtually all shRNAs were substantially represented in the cloned
435 plasmids (***Table S3***). The shRNAs in the CD95L pool (comprised of the Venus, CD95L ORF,
436 and CD95L 3'UTR subpools) and the CD95 pool (comprised of the Venus, CD95 ORF, and
437 CD95 3'UTR subpools) were ranked from highest (most toxic) to lowest underrepresentation.
438 During this and subsequent analyses, we noticed in many cases, Dox addition did cause a
439 reduction of shRNAs, indicating an increase in toxicity; however, in other instances, infection
440 alone and without the addition of Dox was toxic. This effect was likely due to the well-described
441 leakiness of the Tet-on system (Pham, Moretti, Goodall, & Pitson, 2008), which we confirmed
442 for shR6 in NB7 cells (***Figure 6 - figure supplement 2A***). To capture all toxic shRNAs, we
443 therefore decided to split the analysis into two halves: 1) the changes in abundance after
444 infection compared to the composition in the plasmid pool (infection -Dox) and 2) the changes in
445 abundance after Dox addition compared to the infected –Dox cells (infection +Dox). In
446 subsequent analyses shRNAs underrepresented after infection are either boxed (***Figure 6C***) or
447 shown (***Figure 6D***, ***7B*** and ***Figure 7 - figure supplement 1B***) in blue and the ones
448 underrepresented after Dox addition are either boxed or shown in orange. The results for all
449 shRNAs are shown in ***Figure 6 - figure supplement 2B***. Grey dots represent all shRNAs and red
450 dots represent only the ones that were significantly underrepresented at least 5-fold.
451 Interestingly, the highest abundance of downregulated shRNAs was found in the CD95L ORF
452 and the CD95 3'UTR pools of shRNAs, which is consistent with the increased toxicity observed
453 when NB7 cells were infected with either of these two pools individually (see ***Figure 6 - figure***
454 ***supplement 1B***). The shRNAs of these two toxic pools were highly enriched in the

455 underrepresented shRNAs in the two pooled experiments (CD95L and CD95). Their toxicity
456 was also evident when all shRNAs in each pool (2362 shRNAs in the CD95L and 3004 shRNAs
457 in the CD95 pool) were ranked according to the highest fold downregulation (***Figure 6C***). The
458 three subpools in each experiment are shown separately. Thus, again this analysis identified the
459 ORF of CD95L and the 3'UTR of CD95 as the subpool in each analysis with the highest
460 enrichment of underrepresented shRNAs (***Figure 6C***).

461 This analysis allowed us to describe the toxicity landscape of CD95L and CD95 ORFs and
462 their 3'UTRs (***Figure 6D***). All shRNAs significantly underrepresented at least five-fold (red dots
463 in ***Figure 6 - figure supplement 2B***) are shown along the CD95L pool (***Figure 6D***, left) and the
464 CD95 pool (***Figure 6D***, right) sequences. For both CD95L and CD95, toxic shRNAs localized
465 into distinct clusters. The highest density of toxic sequences was found in the stretch of RNA
466 that codes for the intracellular domain of CD95L (underlined in green in ***Figure 6D***).

467

468 **Predicting shRNA toxicity - the toxicity index (TI) and GC content**

469 Our data suggest toxic shRNAs derived from either CD95L or CD95 kill cancer cells by
470 targeting a network of genes critical for survival through canonical RNAi. Therefore, we
471 wondered how many 8mer seed sequences derived from these toxic shRNAs would have
472 corresponding seed matches in the 3'UTR of critical survival genes in the human genome. Would
473 it be possible to predict with some certainty in an *in silico* analysis what shRNAs would be toxic
474 to cells? To calculate such a hypothetical toxicity index, we used the ranked CRISPR data set
475 (Wang et al., 2015) with 1883 survival genes (SGs) and 423 nonSGs. Based on our RNA-Seq
476 analyses, we hypothesized the survival genes contained more putative seed matches for toxic
477 shRNAs in their 3'UTRs than the nonsurvival genes (***Figure 7A***, left) and that the number of
478 seed matches in the 3'UTRs of survival genes divided by the number of seed matches in the
479 3'UTR of nonsurvival genes would, to some extent, predict toxicity of an si/shRNA (***Figure 7A***,
480 right).

481 To establish a Toxicity Index (TI) for each shRNA, we first gathered 3'UTR sequences for
482 1846 of the survival genes and 416 of the nonsurvival genes. We then generated a list containing
483 a normalized ratio of occurrences of every possible 8mer seed match in the 3'UTRs of the
484 survival and non-survival gene groups. This resulted in a ratio for each of the 65,536 possible
485 8mer combinations (***Table S4***), the TI. We then assigned to each of the 4666 shRNAs in our
486 screen its TI, and ranked each pool within the two experiments of our screen according to the

487 highest TI (red stippled lines in ***Figure 7B***). We then further separated the shRNAs into two
488 groups: those that were toxic just after infection and those toxic after addition of Dox (***Figure***
489 ***7B***, ***Table S5***). In each ranked list, we could now assess whether the experimentally determined
490 toxicity of shRNAs correlated with the *in silico* predicted TI. Remarkably, the highest
491 enrichment of toxic shRNAs was found amongst those with higher TI for the subpool of shRNAs
492 targeting the CD95L ORF followed by shRNAs in the subpool targeting the CD95 3'UTR. To
493 confirm the significance of this finding, we repeated the analysis 10,000 times by randomly
494 assigning 8mers and their associated TIs to the two shRNA pools and again sorted the data from
495 highest to lowest TI. The reported p-values were calculated based on these permutated datasets
496 using Mann-Whitney U tests.

497 We noticed that survival genes tend to be more highly expressed than nonsurvival genes
498 (data not shown). To address the question whether toxic si/shRNAs only target survival genes or
499 all genes that are highly expressed, we recalculated the TI based on a set of 850 highly expressed
500 and expression matched survival and nonsurvival genes (***Figure 7 - figure supplement 1A***). This
501 alternative TI tracked slightly less well with the toxic shRNAs we identified, but the enrichment
502 of toxic shRNAs towards the top of the list ranked according to the new TI was still statistically
503 significant (***Figure 7 - figure supplement 1B***). This analysis demonstrates survival genes contain
504 more seed matches for toxic shRNAs in their 3'UTR than nonsurvival genes regardless of the
505 expression level. This suggests, to a certain extent, it is possible to predict the experimental
506 toxicity of shRNAs based on the *in silico* calculated TI.

507 Our data suggest DISE results from a sequence-specific off-target activity that depends on
508 the presence of certain seed matches in the 3'UTR of survival genes. Thus, DISE inducing RISC
509 associated small RNAs behave in manner similar to miRNAs. This raised the question whether
510 these seed matches have special properties. While we did not find a sequence motif that was
511 present in all toxic si/shRNAs, we did find that sequence composition, specifically GC content,
512 which has been reported to affect the specificity of shRNAs (Gu et al., 2014; Ui-Tei et al., 2004),
513 correlated with the toxicity of shRNAs. When the GC content of the 6mer seed sequences of all
514 underrepresented shRNAs detected in the shRNA screen across the CD95L ORF was plotted we
515 found a significant correlation between the GC content and higher toxicity (indicated by
516 underrepresentation) (***Figure 7C*** *and* ***7D***). This correlation was even more pronounced when
517 plotting GC content versus the 6mer toxicity index (***Table S4***) (***Figure 7E***). While not an
518 absolute requirement, higher GC content made shRNAs more toxic, consistent with reports

demonstrating that shRNAs with high GC content in the seed region showed decreased on-target and increased off-target activity (Gu et al., 2014; Ui-Tei et al., 2004). In summary, our data suggest that si- and/or shRNAs with certain seed sequences are toxic to cancer cells by targeting critical survival genes through an RNAi mechanism independent of both Drosha and Dicer. Furthermore, the data suggest high miRNA content, presumably through competing for occupancy in the RISC, might render cells less sensitive to DISE.

Discussion

Most current uses of RNAi are aimed toward highly specific silencing with little OTE. In fact, OTEs represent one of the largest impediments to the use of RNAi in phenotypic screening applications. We now demonstrate DISE is a unique form of OTE that results in the simultaneous activation of multiple cell death pathways in cancer cells. The discovery that DISE involves loss of multiple survival genes now provides an explanation for the unique properties we described for this form of cell death, especially the observation that cancer cells have a hard time developing resistance to this cell death mechanism (Hadji et al., 2014; Murmann et al., 2017).

DISE represents a specific form of RNAi OTE

There are a number of rules that have been elucidated for designing si/shRNAs (Bramsen et al., 2009) to avoid undesired effects such as OTE (Petri & Meister, 2013), general toxicity due to the presence of toxic sequence motifs (Fedorov et al., 2006; Petri & Meister, 2013), poisoning/saturating of the RISC (Grimm et al., 2006), or evocation of an IFN response (Marques & Williams, 2005). The following arguments and evidence support our prediction that DISE is a manifestation of a novel, functionally important, conserved mechanism of genome regulation, and not the result of one of the above-mentioned effects:

1) The sheer number of toxic shRNAs embedded in CD95L or CD95. A number of genome-wide shRNA and siRNA lethality screens have revealed that 2-5% of shRNAs targeting human genes are toxic to cells. We recently reported in 12 independent arrayed shRNA lethality screens the identification of 651 genes out of about 18,000 targeted genes that are critical for the survival of 8 different cancer cell lines (Hadji et al., 2014). Many of the genes targeted by these shRNAs were actually established survival genes (as discussed in (Hadji et al., 2014)). That means that the number of shRNAs that are toxic due to a possible OTE or general toxicity would be expected to be very small. In contrast, we found that >80% of the shRNAs and siRNAs that were designed to target either CD95 or CD95L exhibited toxicity in multiple cell lines. Consistent with our data analysis a parallel genome-scale loss of function screen confirmed that the majority of the tested shRNAs derived from either CD95L and CD95 were toxic to a majority of the tested 216 cell lines when used as a pooled library (Cowley et al., 2014). These also included a number of hematopoietic cell lines suggesting that the DISE effect is not limited to solid cancers. Interestingly, in this study the authors did not consider the data on most of the CD95L and CD95 targeting shRNAs to be significant as they received

558 a low consistency score. A high consistency score predicts the observed phenotype (cell
559 death or growth reduction in this case) is caused by knocking down the targeted gene (Shao et
560 al., 2013). However, we have demonstrated here that the toxicity of an shRNA is solely
561 dependent on its seed and the transcriptome of the treated cells. Therefore, the results of every
562 shRNA should be considered individually as far as the DISE inducing effect is concerned.

563 2) High concentrations of siRNAs can saturate the RISC, preventing the access of crucial
564 endogenous miRNAs (Khan et al., 2009). We have demonstrated that, in general, 5 nM of
565 CD95L-derived siRNAs are sufficient to kill cancer cells. We have even seen very efficient
566 cell death with as little as 1 nM of siRNA (see ***Figure 2I*** *and* ***Figure 1 - figure supplement***
567 ***2E***). It is therefore unlikely we are poisoning the RISC. It has been reported that in siRNA
568 overexpression experiments, changes in mRNA expression can be caused by blocked access
569 of endogenous miRNAs to the RISC, such as the highly expressed miRNA family, let-7
570 (Khan et al., 2009). However, we can exclude such an effect in our analysis, as there was no
571 significant enrichment (or depletion) of the let-7 seed match motif (or that of any other
572 miRNA) in our analyses (black lines in ***Figure 5A***).

573 3) No IFN response was observed. We have performed multiple RNA-Seq and gene array
574 analyses of cells in which DISE was induced by multiple si/shRNAs targeting CD95 or
575 CD95L. In none of these analyses did we detect an increase in any of the known IFN response
576 genes (Schoggins et al., 2011) (data not shown). In addition, we demonstrated the latest
577 generation of Dicer optimized 27mer DsiRNAs that do not elicit an IFN response (D. H. Kim
578 et al., 2005) and the shRNAs expressed from within the cells shown to have low IFN
579 triggering activity (Robbins et al., 2006) have the same toxic activities as the standard 21mer
580 siRNAs (see ***Figure 1 - figure supplement 1A*** *and* ***1B***).

581 4) Mutation of just one position destroys activity. A major argument against DISE toxicity being
582 caused by overloading the RISC, an IFN response or the presence of known toxic sequences,
583 lies in the analysis of the chimeras we generated between siL3 and a non-toxic scrambled
584 oligonucleotide (see ***Figure 3H***). This analysis demonstrated that the seed match positions of
585 siL3 are critical for its toxicity. In fact, just replacing one nucleotide in a critical position in
586 the center of the seed match almost completely abolished toxicity of the siRNA.

587

588 **What are the requirements for an si/shRNA to induce DISE?**

589 Our data provide strong evidence that the toxicity observed is a sequence-specific event
590 caused by seed matches present in the targets of the toxic si/shRNAs rather than by a toxic motif
591 enriched in all toxic si/shRNAs (i.e. the UGGC motif described before (Fedorov et al., 2006)).
592 We did find a correlation between the toxicity of shRNAs (both predicted by the TI and
593 experimentally determined in the shRNA screen) and the GC content in their seed region. While
594 this correlation was significant, it was not a requirement as some of the most toxic si- and
595 shRNAs had a low 8mer seed GC content (shL3, 25%; shR6, 25%; siL3, 37.5%). Our data
596 suggests that survival genes may contain different types of seed matches (based on base
597 composition or sequence) when compared to nonsurvival genes. Such a distinction has indeed
598 been described before (Stark, Brennecke, Bushati, Russell, & Cohen, 2005). In a study in
599 Drosophila, it was determined that survival genes are depleted of seed matches targeted by
600 highly expressed miRNAs. These authors concluded that evolution must have selected against
601 the presence of seed matches for highly expressed miRNAs in the 3'UTR of survival genes. It is
602 therefore not surprising that a gene ontology (GO) analysis of all miRNA targets (the "targets")
603 in this study described these genes as being involved in development and differentiation (Stark et
604 al., 2005). In contrast, genes not targeted by miRNAs (the "antitargets") grouped in GO clusters
605 that were consistent with cell survival (Stark et al., 2005). A similar phenomenon was also
606 shown in mammalian cells; genes with fewer miRNA target sites, as predicted by Targetscan,
607 contained distinct enriched GO terms from those enriched in genes with many predicted target
608 sites. The genes with fewer sites were enriched in GO terms like ribosomal subunits and
609 respiratory chain, whereas target-heavy genes were more enriched in regulatory-related GO
610 terms (Zare, Khodursky, & Sartorelli, 2014). It is possible the DISE inducing si/shRNAs carry
611 seed sequences that preferentially target seed matches present in the 3'UTRs of the "anti-
612 targets". However, as our data on the miR-30 based shRNAs suggest, DISE-inducing shRNAs
613 must be expressed at a certain level to be toxic.
614

615 **DISE is caused by loading of the guide strand of toxic si/shRNAs into the RISC**

616 Part of our data was generated using a widely used first generation stem loop shRNA platform,
617 the TRC library. The TRC shRNAs have recently been found to be prone to cause OTE. Gu *et al.*
618 showed that the loop design of this system results in imprecise Dicer cleavage and, consequently,
619 the production of different mature small-RNA species that increase passenger loading, one major
620 source of OTE (Gu et al., 2012). More recently it was reported that most guide RNAs derived

621 from the TRC hairpin were shifted by 4 nt 3' of the expected 5' start site (Watanabe, Cuellar,
622 & Haley, 2016). While we did see a shift in processing of these stem loop shRNAs, we did not
623 see such a high level of imprecision in the cleavage of our toxic shRNAs. In fact, 99.4% of the
624 shR6 guide RNAs started at the same nucleotide position (***Figure 5 - figure supplement 1A***).
625 The majority of the processing of both our pTIP and pLKO-based shRNAs was shifted by one
626 nucleotide (***Figure 5 - figure supplement 1A***). This shift was consistent with the defined seed
627 matches that were detected in the Sylamer analyses. In general, one major seed match was
628 detected with one other minor species (this was less obvious for shL1, ***Figure 5 - figure***
629 ***supplement 2***). Furthermore, all four Sylamer analyses only detected enrichments in the 3'UTR
630 of downregulated mRNAs that were consistent with only the guide strand targeting the mRNA
631 and not the passenger strand. In all cases, including in cells transfected with the siRNA siL3, the
632 primary enriched sequence motifs were either 7, or 8mers present in the 3'UTR of the targeted
633 mRNAs.
634
635 **DISE has features of the RNAi OTE previously reported**
636 Our data on DISE are consistent with a number of properties of RNAi OTE that have previously
637 been reported. Similar to DISE, OTE mediated silencing requires a 6/7nt seed sequence of
638 complementarity (Birmingham et al., 2006; Jackson et al., 2006; Lin et al., 2005) and it targets
639 mRNAs in the 3'UTR (Birmingham et al., 2006). Our data on shRNAs, siRNAs, and DsiRNAs
640 suggest that DISE is not limited to one platform and requires sequence specific targeting. This
641 conclusion is also consistent with a previous report that suggested that sequence-dependent off-
642 target transcript regulation is independent of the delivery method (Jackson et al., 2006). The
643 authors found the same enrichment of 6mers and 7mers in 3'UTRs of targeted mRNAs for
644 siRNAs and shRNAs (Jackson et al., 2006).
645
646 **The role of Dicer in DISE**
647 We previously reported that Dicer$^{Exo5-/-}$ HCT116 cells (with deleted Exon 5) were at least as
648 sensitive to induction of DISE (by either shL3 or shR6) than wt cells suggesting that Dicer
649 deficient cells could be killed by DISE (Hadji et al., 2014). It is has been reported that these
650 Dicer deficient cells are hypomorphs (Ting et al., 2008) and indeed, we detected low residual
651 Dicer expression by Western blotting (Hadji et al., 2014). We have now revisited this issue with
652 HCT116 cells rendered completely deficient for Dicer using CRISPR/Cas9 gene editing (Y. K.

653 Kim et al., 2016). The fact that these Dicer$^{-/-}$ cells were now completely resistant to the toxic
654 effects of shL3 or shR6 demonstrates the complete absence of Dicer protein and activity. Similar
655 to the Drosha$^{-/-}$ cells, in the absence of mature miRNAs, which seem to attenuate DISE, Dicer$^{-/-}$
656 cells are hypersensitive to DISE induced by siRNAs.
657
658 **Open questions regarding the relevance of DISE**
659 We are proposing an entirely new concept of killing cancer cells that is based on the toxicity of
660 CD95 and CD95L derived small RNAs. Naturally, there are many open questions such as:
661 1) Is DISE part of an anti-cancer mechanism? We are proposing that DISE kills cancer cells
662 in a way that they usually cannot escape from. We have not found a way to block cancer cells
663 from dying by DISE. We provide strong evidence to suggest this is due to the simultaneous
664 targeting of multiple survival genes that result in the activation of multiple cell death pathways.
665 It will be difficult to prove cells are dying due to the preferential targeting of survival genes. It
666 may never be possible to express multiple siRNA resistant survival genes at the same time at
667 physiological levels to render cancer cells resistant to the action of countless small RNAs. This
668 prediction alone makes DISE a promising new strategy to kill cancer cells.
669 2) Does CD95L induce DISE *in vivo*? We recently found that overexpression of the CD95L
670 ORF is toxic to cancer cells and that this kills cancer cells in a manner very similar to DISE
671 induction (unpublished data). We and others have noticed upregulation of CD95L in multiple
672 stress related conditions such as treatment with chemotherapy ((Friesen, Fulda, & Debatin, 1999)
673 and data not shown). While the amount of CD95L RNA and the level of upregulation alone may
674 not be enough to induce DISE, it could result from the combined expression of multiple RNAs
675 that when generated kill cells by DISE. We view CD95L as just one of many RNAs that have
676 this activity.
677 3) Are there other genes in the human genome containing toxic seed sequences? We recently
678 identified other genes in the genome that contain DISE inducing shRNAs (Patel & Peter, 2017).
679 It is therefore possible that when cells are subjected to genotoxic or oncogenic stress that they
680 generate numerous small RNAs that can be taken up by the RISC and in combination execute
681 DISE. Hence, our analysis of CD95/CD95L will likely be applicable to other genes.
682
683 **A model for why DISE preferentially kills cancer cells**
684 We interpret the hypersensitivity of both Drosha$^{-/-}$ and Dicer$^{-/-}$ cells to DISE in the following

way: Most of the small RNAs in the cells that are loaded into the RISC are miRNAs. Using AGO pull-down experiments we determined 98.4% of AGO associated RNAs in HCT116 cells to be miRNAs (99.3% in HeyA8 cells, data not shown). It was recently reported that Drosha$^{-/-}$ cells showed a reduction of miRNA content from roughly 70-80% to 5-6%, and Dicer$^{-/-}$ cells showed a reduction down to 14-21% (Y. K. Kim et al., 2016). Since neither Drosha$^{-/-}$ nor Dicer$^{-/-}$ cells express reduced AGO2 protein levels (see subset ***Figure 3E***), it is reasonable to assume that their RISC can take up many more of the toxic DISE inducing RNAs than the RISC in wt cells explaining the super toxicity of both DISE inducing si/shRNAs and CD95L mRNAs in these cells.

We previously showed expression of either shL3 and shR6 induced DISE in immortalized normal ovarian fibroblasts much more efficiently than in matching nonimmortalized cells (Hadji et al., 2014), suggesting that this form of cell death preferentially affects transformed cells. Our data now provide an interesting model to explain the higher sensitivity of cancer cells to DISE when compared to normal cells. It is well documented that cancer cells in general have global downregulation of miRNAs when compared to normal tissues (Lu et al., 2005). This might free up the RISC for DISE inducing RNAs and would imply that miRNAs may protect normal cells from DISE.

Overall our data allow us to predict that any small RNA with DISE inducing RNAi activity that does not require Dicer processing can kill cancer cells regardless of Dicer or Drosha status. In fact, in an accompanying manuscript we demonstrate that DISE can be triggered *in vivo* to treat ovarian cancer in mouse xenografts by delivering CD95L-derived siRNAs using nanoparticles (Murmann et al., 2017). No toxicity was observed in the treated mice. These data suggest that it might be possible to develop a novel form of cancer therapy based on the DISE OTE mechanism.

Materials and methods

Reagents and antibodies

Primary antibodies for Western blot: anti-β-actin antibody (Santa Cruz #sc-47778), anti-human CD95L (BD Biosciences #556387), and anti-human CD95 (Santa Cruz #sc-715), anti-human AGO2 (Abcam #AB186733), anti-human Drosha (Cell Signaling #3364), and anti-Dicer (Cell Signaling #3363). Secondary antibodies for Western blot: Goat anti-rabbit; IgG-HRP (Southern Biotech #SB-4030-05 and Cell Signaling #7074) and Goat anti-mouse; IgG1-HRP; (Southern

717 BioTech #1070-05). Conjugated antibody isotype control for CD95 surface staining were
718 FITC-mouse anti-human CD95 (BD Biosciences #556640) and FITC-mouse IgG1, κ isotype
719 control (BD Biosciences #551954). Recombinant soluble S2 CD95L and leucine-zipper tagged
720 (Lz)CD95L were described before (Algeciras-Schimnich et al., 2003). Reagents used: propidium
721 iodide (Sigma-Aldrich #P4864), puromycin (Sigma-Aldrich #P9620), G418 (Affymetrix
722 #11379), zVAD-fmk (Sigma-Aldrich #V116, used at 20 μM), doxycycline (Dox) (Sigma-
723 Aldrich #9891), Lipofectamine 2000 (ThermoFisher Scientific #11668027), and Lipofectamine
724 RNAiMAX (ThermoFisher Scientific #13778150).
725
726 **Cell lines**
727 The ovarian cancer cell line HeyA8, the neuroblastoma cell line NB7, and the breast cancer cell
728 line MCF-7 were grown in RPMI 1640 medium (Cellgro #10-040-CM), 10% heat-inactivated
729 FBS (Sigma-Aldrich), 1% L-glutamine (Mediatech Inc), and 1% penicillin/streptomycin
730 (Mediatech Inc). The human embryonic kidney cell line 293T and Phoenix AMPHO cells were
731 cultured in DMEM (Cellgro #10-013-CM), 10% heat-inactivated FBS, 1% L-Glutamine, and 1%
732 penicillin/streptomycin.
733 HCT116 Drosha$^{-/-}$ and Dicer$^{-/-}$ cells were generated by Narry Kim (Y. K. Kim et al., 2016).
734 HCT116 parental (cat#HC19023), a Drosha$^{-/-}$ clone (clone #40, cat#HC19020) and two Dicer$^{-/-}$
735 clones (clone #43, cat#HC19023 and clone #45, cat#HC19024) were purchased from Korean
736 Collection for Type Cultures (KCTC). All HCT116 cells were cultured in McCoy's medium
737 (ATCC, cat#30-2007), 10% heat-inactivated FBS, 1% L-Glutamine, and 1% penicillin/
738 streptomycin. All cell lines were authenticated using STR profiling and tested monthly for
739 mycoplasm using PlasmoTest (Invitrogen).
740 All lentiviruses were generated in 293T cells using pCMV-dR8.9 and pMD.G packaging
741 plasmids. Retroviruses were generated in Phoenix AMPHO cells using the VSVg packaging
742 plasmid.
743 NB7 cells overexpressing wild type and mutant CD95L cDNAs used in ***Figure 1C and D***
744 were generated by infecting cells seeded at 50,000 to 100,000 cells per well on a 6-well plate
745 with empty pLenti, pLenti-CD95L-WT, pLenti-CD95L-L1MUT, and pLenti-CD95L-L3MUT
746 (described below) with 8 μg/ml polybrene. Selection was done with 3 μg/ml puromycin for at
747 least 48 hours.

748 MCF-7 cells overexpressing CD95 cDNAs used in ***Figure 1F*** were generated by seeding
749 cells at 50,000 per well in a 6-well plate followed by infection with pLNCX2-CD95 or pLNCX2-
750 CD95R6MUT (described below) in the presence of 8 µg/ml polybrene. Selection was done with
751 200 µg/ml G418 48 hours after infection for 2 weeks.
752 The HeyA8 cells used in ***Figure 3D*** carried a lentiviral Venus-siL3 sensor vector (Murmann
753 et al., 2017) and were infected with NucLight Red lentivirus (Essen Bioscience #4476) with 8
754 µg/ml polybrene and selected with 3 µg/ml puromycin and sorted for high Venus expression 48
755 hours later. HeyA8 ΔshR6 clone #2 sensor cells used in ***Figure 3A*** to ***3C*** were infected with
756 lentiviruses generated from the Venus-CD95L sensor vector (described below) to over-express
757 the Venus-CD95L chimeric transcript. Cells were sorted for high Venus expression 48 hours
758 later. NB7 cells over-expressing either the Venus-CD95L sensor or the Venus-CD95 sensor
759 (described below) used in ***Figure 6 – figure supplement 1A*** were similarly generated.
760
761 **Plasmids and constructs**
762 The Venus-CD95L ORF and Venus-CD95 ORF (full length) sensor vectors were created by sub-
763 cloning the Venus-CD95L or the Venus-CD95 inserts (synthesized as a minigene by IDT with
764 flanking XbaI RE site on the 5' end and EcoRI RE site at the 3' end in the pIDTblue vector),
765 which are composed of the Venus ORF followed by either the CD95L ORF (accession number
766 NM_000639.2) or the CD95 ORF (accession number BC012479.1) as an artificial 3'UTR (both
767 lacking the A in the start codon), respectively, into the modified CD510B vector (Ceppi et al.,
768 2014) using XbaI and EcoRI. Ligation was done with T4 DNA ligase.
769 The pLNCX2-CD95R6MUT vector was synthesized by replacing a 403bp fragment of the
770 CD95 ORF insert from the pLNCX2-CD95-WT vector (Hadji et al., 2014) with a corresponding
771 403bp fragment that had 8 silent mutation substitutions at the shR6 site (5'-
772 *GTGTCGCTGTAAACCAAACTT* -> 5'-*ATGTCGCTGCAAGCCCAATTT*-3') using BstXI (NEB
773 #R0113) and BamHI (NEB #R3136) restriction enzymes (mutant insert was synthesized in a
774 pIDTblue vector with 5' end BstXI site and 3' end BamHI RE site).
775 Dox-inducible vectors expressing shRNAs were constructed by subcloning an annealed
776 double-stranded DNA insert containing the sequence encoding the shRNA hairpin (sense strand:
777 5'-*TGGCTTTATATATCTCCCTATCAGTGATAGAGATCGNNNNNNNNNNNNNNNNNNNNN*
778 *CTCGAGnnnnnnnnnnnnnnnnnnnnnnTTTTTGTACCGAGCTCGGATCCACTAGTCCAGTGTGGG*
779 *CATGCTGCGTTGACATTGATT*-3') into the pTIP-shR6 vector (Hadji et al., 2014). BsaBI (NEB

780 #R0537) and SphI-HF (NEB #R3182) were used to digest both the pTIP-shR6 vector (to
781 excise the shR6 insert) and the double-stranded shRNA DNA cassette insert followed by ligation
782 with T4 DNA ligase. The template oligos were purchased from IDT. The poly-N represents the
783 two 21bp sequences that transcribe for the sense (*N*) and antisense (*n*) shRNA.
784 miR-30 based shRNAs were generated by The Gene Editing & Screening Core, at Memorial
785 Sloan Kettering, NY, by converting the 21mers expressed in the pLKO and pTIP vectors into
786 22mers followed by cloning into the Dox-inducible LT3REPIR vector as described (Dow et al.,
787 2012). A vector expressing an shRNA against Renilla luciferase was used as control (Dow et al.,
788 2012).
789
790 **CRISPR deletions**
791 We identified two gRNAs that target upstream and downstream of the site to be deleted. These
792 gRNAs were expected to result in the deletion of a DNA piece just large enough to remove the
793 target site. The CRISPR gRNA scaffold gene blocks were from IDT and consisted of the DNA
794 sequence 5'-*TGTACAAAAAAGCAGGCTTTAAAGGAACCAATTCAGTCGACTGGATCCGGTA*
795 *CCAAGGTCGGGCAGGAAGAGGGCCTATTTCCCATGATTCCTTCATATTTGCATATACGA*
796 *TACAAGGCTGTTAGAGAGATAATTAGAATTAATTTGACTGTAAACACAAAGATATTAGTACA*
797 *AAATACGTGACGTAGAAAGTAATAATTTCTTGGGTAGTTTGCAGTTTTAAAATTATGTTTTAA*
798 *AATGGACTATCATATGCTTACCGTAACTTGAAAGTATTTCGATTTCTTGGCTTTATATATCTT*
799 *GTGGAAAGGACGAAACACCGNNNNNNNNNNNNNNNNNNNGTTTTAGAGCTAGAAATAGC*
800 *AAGTTAAAATAAGGCTAGTCCGTTATCAACTTGAAAAAGTGGCACCGAGTCGGTGCTTTTTT*
801 *TCTAGACCCAGCTTTCTTGTACAAAGTTGGCATTA-3'* (Mali et al., 2013)*;* The poly-
802 *NNNNNNNNNNNNNNNNNNN* represents the 19nt target sequence. The two 19nt target
803 sequences for excision of the shL3 site (Δ41 deletion) were 5'-*CCTTGTGATCAATGAAACT*-3'
804 (gRNA #1) and 5'-*GTTGTTGCAAGATTGACCC*-3' (gRNA #2). The two target sequences for
805 the Δ227 deletion of the shR6 site were 5'-*GCACTTGGTATTCTGGGTC*-3' and 5'-
806 *TGTTTGCTCATTTAAACAC*-3'. The two target sequences for Δ64 deletion of the siL3 site were
807 5'-*TAAAACCGTTTGCTGGGGC*-3' and 5'-*TATCCCCAGATCTACTGGG*-3'. Target sequences
808 were identified using the CRISPR gRNA algorithm found at http://crispr.mit.edu/; only gRNAs
809 with scores over 50 were used. These 6 gene blocks were sub-cloned into the pSC-B-amp/kan
810 plasmid using the StrataClone Blunt PCR Cloning kit (Agilent Technologies #240207).

The target sites of siL3, shL3, and shR6 were homozygously deleted from target cells by co-transfecting Cas9 plasmid with each corresponding pair of pSC-B-gRNA plasmids. Briefly, 400,000 cells were seeded per well on a 6-well plate the day prior to transfection. Each well was transfected with 940 ng of Cas9-GFP plasmid (pMJ920) (Jinek et al., 2013) and 450 ng of each pSC-B-gRNA plasmid using Lipofectamine 2000. Media was replaced next day. One to two days later, cells were sorted for the top 50% population with the highest green fluorescence. Those cells were cultured for an additional week to let them recover. The cells were then sorted by FACS (BD FACSAria SORP system) directly into 96-well plates containing a 1:1 ratio of fresh media:conditioned media for single cell cloning. Approximately two to three weeks later, single cell clones were expanded and subjected to genotyping. PCR using both a primer pair that flanked the region to be deleted and another pair containing one flanking primer and one internal primer was used to screen clones for homozygous deletion. For detection of the Δ41 deletion of the shL3 site, the flanking external primers were 5'-*TCTGGAATGGGAAGACACCT*-3' (Fr primer) and 5'- *CCTCCATCATCACCAGATCC*-3' (Rev primer), and the internal Rev primer was 5'-*ATATACAAAGTACAGCCCAGT*-3'. For detection of the Δ227 deletion of the shR6 site, the flanking external primers were 5'-*GGTGTCATGCTGTGACTGTTG*-3' (Fr primer) and 5'-*TTTAGCTTAAGTGGCCAGCAA*-3' (Rev primer), and the internal Rev primer was 5'-*AAGTTGGTTTACATCTGCAC*-3'. For detection of the Δ64 deletion of the siL3 site, the flanking external primers were 5'-*CTTGAGCAGTCAGCAACAGG*-3' (Fr primer) and 5'-*CAGAGGTTGGACAGGGAAGA*-3' (Rev primer), and the internal Rev primer was 5'-*ATATGGGTAATTGAAGGGCTG*-3'. After screening the clones, Sanger sequencing was performed to confirm that the proper deletion had occurred. Three clones were pooled for each si/shRNA target site deletion except for HeyA8 ΔshR6 for which only clone #11 showed homozygous deletion of the shR6 site; clones #1 and 2 were not complete shR6 deletion mutants, but frame-shift mutations did occur in each allele (as in clone #11) making them CD95 knockout clones as depicted in ***Figure 2 - figure supplement 1A*** *and* ***B***.

Knockdown with pLKO lentiviruses

Cells were infected with the following pLKO.2 MISSION Lentiviral Transduction Particles (Sigma): pLKO.2-puro non-targeting (scramble) shRNA particles (#SHC002V), 8 non-overlapping shRNAs against human CD95L mRNA (accession number #NM_000639), TRCN0000058998 (shL1: GCATCATCTTTGGAGAAGCAA), TRCN0000058999 (shL2:

843 CCCATTTAACAGGCAAGTCCA), TRCN0000059000 (shL3:
844 ACTGGGCTGTACTTTGTATAT), TRCN0000059001 (shL4:
845 GCAGTGTTCAATCTTACCAGT), TRCN0000059002 (shL5:
846 CTGTGTCTCCTTGTGATGTTT), TRCN0000372231 (shL6:
847 TGAGCTCTCTCTGGTCAATTT), TRCN0000372232 (shL2': TAGCTCCTCAACTC
848 ACCTAAT), and TRCN0000372175 (shL5': GACTAGAGGCTTGCATAATAA), and 9 non-
849 overlapping shRNAs against human CD95 mRNA (accession number NM_000043),
850 TRCN0000218492 (shR2: CTATCATCCTCAAGGACATTA), TRCN00000 38695 (shR5:
851 GTTGCTAGATTATCGTCCAAA), TRCN0000038696 (shR6: GTGCAGA
852 TGTAAACCAAACTT), TRCN0000038697 (shR7: CCTGAAACAGTGGCAATAAAT),
853 TRCN0000038698 (shR8: GCAAAGAGGAAGGATCCAGAT), TRCN0000265627 (shR27':
854 TTTTACTGGGTACATTTTATC), TRCN0000255406 (shR6': CCCTTGTGTTT
855 GGAATTATAA), TRCN0000255407 (shR7': TTAAATTATAATGTTTGACTA), and
856 TRCN0000255408 (shR8': ATATCTTTGAAAGTTTGTATT). Infection was carried out
857 according to the manufacturer's protocol. In brief, 50,000 to 100,000 cells seeded the day before
858 in a 6-well plate were infected with each lentivirus at an M.O.I of 3 in the presence of 8 µg/ml
859 polybrene overnight. Media change was done the next day, followed by selection with 3 µg/ml
860 puromycin 24 hours later. Selection was done for at least 48 hours until puromycin killed the
861 non-infected control cells. For infection of NB7 cells over-expressing pLenti-CD95L cDNAs
862 with pLKO lentiviral particles as in ***Figure 1C*** *and* ***D***, cells were seeded at 5,000 per well on a
863 24-well plate and infected with an M.O.I. of 20 to ensure complete infection. For infection of
864 MCF-7 cells over-expressing pLNCX2-CD95 cDNAs with pLKO lentiviruses as in ***Figure 1G***,
865 cells were seeded at 7,000 per well on a 24-well plate and infected at an M.O.I. of three. 3 µg/ml
866 puromycin was added 48 hours after infection. For infection of HCT116, Drosha$^{-/-}$, and Dicer$^{-/-}$
867 cells in ***Figure 3E***, cells were seeded at 100,000 per well in a 24-well plate and infected at an
868 M.O.I of three. 3 µg/ml puromycin was added 48 hours after infection.
869

870 **Knockdown with pTIP-shRNA viruses**

871 Cells were plated at 50,000 to 100,000 cells per well in a 6-well plate. Cells were infected with
872 lentivirus generated in 293T cells from the desired pTIP-shRNA vector in the presence of 8
873 µg/ml Polybrene. Media was replaced 24 hours later. Selection was done 48 hours after infection
874 with 3 µg/ml puromycin. Induction of shRNA expression was achieved by adding 100 ng/ml

875 Dox to the media. For infection with the LT3REPIR-shRNA viruses cells were plated and
876 infected as described above for pTIP-shRNA viruses. After selection with 3 μg/ml puromycin
877 was complete, they were plated in 96-well plates and the shRNA expression was induced by
878 adding Dox (100 ng/ml) to the media. The cell confluency over time was measured using
879 Incucyte.
880
881 **Transfection with short oligonucleotides**
882 siRNAs were either purchased from Dharmacon (***Figures 2I*** and ***4D***, ***Figure 1 - figure***
883 ***supplement 1A, Figure 5 - supplement 2)*** or synthesized by IDT (***Figure 3A***) as sense and
884 antisense RNA (or DNA for ***Figure 3B, Figure 5 - supplement 1B,***) oligos and annealed. The
885 sense RNA oligonucleotides had 3' 2 deoxy-T overhangs. The antisense RNA oligos were
886 phosphorylated at the 5' end and had 3' 2 deoxy-A overhangs. siRNAs targeting CD95L (and
887 controls) were as follows: siRNA (Scr, sense: UGGUUUACAUGUUGUGUGA), siL1 (sense:
888 UACCAGUGCUGAUCAUUUA), siL2 (sense: CAACGUAUCUGAGCUCUCU), siL3 (sense:
889 GCCCUUCAAUUACCCAUAU), siL4 (sense: GGAAAGUGGCCCAUUUAAC), and
890 siL3MUT (sense: GGACUUCAACUAGACAUCU). The siL3 DNA oligos (sense:
891 GCCCTTCAATTACCCATAT) and Scr DNA oligos (sense: TGGTTTACATGTTGTGTGA)
892 were used in ***Figure 3B***. Blunt siL3 and siScr RNA oligos without the deoxynucleotide
893 overhangs as well as siL2 and siL3 RNA oligos with Cy5-labelled 5' or 3' ends (IDT) were used
894 in ***Figure 3C***. DsiRNA used in ***Figure 1 - figure supplement 1*** were Dsi13.X (sense RNA oligo:
895 CAGGACUGAG AAGAAGUAAAACCdGdT, antisense RNA oligo:
896 ACGGUUUUACUUCUUCUCAGUCCUGUA), DsiL3 (sense RNA oligo:
897 CAGCCCUUCAAUUACCCAUAUCCdCdC, antisense RNA oligo:
898 GGGGAUAUGGGUAAUUGAAGGGCUGCU), Dsi-13.2 (sense RNA oligo: AUCUU
899 ACCAGUGCUGAUCAUUUAdTdA, antisense RNA oligo:
900 UAUAAAUGAUCAGCACUGGUAAGAUUG), Dsi-13.3 (sense RNA oligo:
901 AAAGUAUACUUCCGGGGUCAAUCdTdT, antisense RNA oligo:
902 AAGAUUGACCCCGGAAGUAUACUUUGG), Dsi-13.9 (sense RNA oligo:
903 CUUCCGGGGUCAAUCUUGCAACAdAdC, antisense RNA oligo: GUUGUUGC
904 AAGAUUGACCCCGGAAGUA), and a non-targeting DsiRNA control Dsi-NC1 (Sense:5'-
905 CGUUAAUCGCGUAUAAUACGCGUdAdT, antisense:5'-
906 AUACGCGUAUUAUACGCGAUUAACGAC, IDT #51-01-14-03). Predesigned siRNA

907 SmartPools targeting the 11 downregulated genes were obtained from Dharmacon and used in
908 ***Figure 4C*** and ***Figure 4 - figure supplement 2B*** *and* ***2C***. Each siRNA SmartPool consisted of 4
909 siRNAs with On-Target*plus* modification. The following SmartPools were used: L-014208-02
910 (NUCKS1); L-012212-00 (CAPZA1); L-018339-00 (CCT3); L-013615-00 (FSTL1); L-011548-
911 00 (FUBP1); L-017242-00 (GNB1); L-014597-01 (NAA50); L-020893-01 (PRELID3B); L-
912 019719-02 (SNRPE); L-003941-00 (TFRC); L-006630-00 (HIST1H1C). On-Target*plus* non-
913 targeting control pool (D-001810-10) was used as negative control. Transfection efficiency was
914 assessed by transfecting cells with siGLO Red (Dharmacon) followed by FACS analysis.
915 HeyA8 cells (and modified cells derived from parental HeyA8 cells) were seeded at 750 cells
916 per well on a 96-well plate one day before transfection. Cells were transfected using 0.1 µl of
917 Lipofectamine RNAiMAX reagent per well. HCT116 cells (and modified cells derived from
918 parental HCT116 cells) were seeded at 4000 cells per well on a 96-well plate one day before
919 transfection. 0.2 µl of Lipofectamine RNAiMAX was used for transfection. Media was changed
920 the day after transfection.
921
922 **Soluble CD95L protein rescue experiments**
923 NB7 cells were seeded at 500 cells per well in a 96-well plate. Next day, cells were infected with
924 the scrambled pLKO lentiviruses or pLKO-shL1 lentiviruses at an M.O.I. of 20 (to achieve
925 100% transduction efficiency under conditions omitting the puromycin selection step) in the
926 presence of 8 µg/ml polybrene and 100 ng/ml of S2 CD95L or LzCD95L for 16 hrs. Media was
927 replaced the next day with media containing varying concentrations of recombinant CD95L.
928
929 **Real-time PCR**
930 Total RNA was extracted and purified using QIAZOL Lysis reagent (QIAGEN) and the
931 miRNeasy kit (QIAGEN). 200 ng of total RNA was used to generate cDNA using the High-
932 Capacity cDNA reverse Transcription kit (Applied Biosystems #4368814). cDNA was quantified
933 using Taqman Gene expression master mix (ThermoFisher Scientific #4369016) with specific
934 primers from ThermoFisher Scientific for GAPDH (Hs00266705_g1), human CD95 for ***Figure 5***
935 ***-supplement 3*** (Hs00163653_m1), human CD95 3'UTR in ***Figure 2F*** (custom probe, Fr primer:
936 *GGCTAACCCCACTCTATGAATCAAT*, Rev primer: *GGCCTGCCTGTTCAGTAACT*, Probe:
937 *CCTTTTGCTGAAATATC*), human CD95L (Hs00181226_g1 and Hs00181225_m1), the shL3
938 target site in CD95L in ***Figure 2D*** (custom probe, Fr primer: *GGTGGCCTTGTGATCAATGAAA*,

939 Rev primer: *GCAAGATTGACCCCGGAAG TATA*, Probe: *CTGGGCTGTACTTTGTATATT*),
940 and downstream of the shL3 site in ***Figure 2D*** (custom probe, Fr primer:
941 *CCCCAGGATCTGGTGATGATG*, Rev primer: *ACTGCCCCCAGGTAGCT*, Probe:
942 *CCCACATCTGCCCAGTAGT*).

943 To perform arrayed real-time PCR (***Figure 4 - figure supplement 1***), total RNA was
944 extracted and used to make cDNA as described for standard real-time PCR. For Taqman Low
945 Density Array (TLDA) profiling, custom-designed 384-well TLDA cards (Applied Biosystems
946 #43422489) were used and processed according to the manufacturer's instructions. Briefly, 50 µl
947 cDNA from each sample (200 ng total input RNA) was combined with 50 µl TaqMan Universal
948 PCR Master Mix (Applied Biosystems) and hence a total volume of 100 µl of each sample was
949 loaded into each of the 8 sample loading ports on the TLDA cards that were preloaded with
950 assays from Thermofisher Scientific for human GAPDH control (Hs99999905_m1) and for
951 detection of ATP13A3 (Hs00225950_m1), CAPZA1 (Hs00855355_g1), CCT3
952 (Hs00195623_m1), FSTL1 (Hs00907496_m1), FUPB1 (Hs00900762_m1), GNB1
953 (Hs00929799_m1), HISTH1C (Hs00271185_s1), NAA50 (Hs00363889_m1), NUCKS1
954 (Hs01068059_g1), PRELID3B (Hs00429845_m1), SNRPE (Hs01635040_s1), and TFRC
955 (Hs00951083_m1) after the cards reached room temperature. The PCR reactions were performed
956 using Quantstudio 7 (ThermoFisher Scientific). Since each of the port loads each sample in
957 duplicates on the TLDA card and because two biological replicates of each sample were loaded
958 onto two separate ports, quadruplicate Ct values were obtained for each sample. Statistical
959 analysis was performed using Student's t test. Cells were plated at 600,000 per 15 mm dish
960 (Greiner CELLSTAR, cat#P7237, Sigma) after one day of puromycin selection. Total RNA was
961 harvested at 50 hours after plating for RNAseq analysis.
962

963 **Western blot analysis**

964 Protein extracts were collected by lysing cells with RIPA lysis buffer (1% SDS, 1% Triton X-
965 100, 1% deoxycholic acid). Protein concentration was quantified using the DC Protein Assay kit
966 (Bio-Rad). 30 µg of protein were resolved on 8-12% SDS-PAGE gels and transferred to
967 nitrocellulose membranes (Protran, Whatman) overnight at 25 mA. Membranes were incubated
968 with blocking buffer (5% non-fat milk in 0.1% TBS/Tween-20) for 1 hour at room temperature.
969 Membranes were then incubated with the primary antibody diluted in blocking buffer over night
970 at 4°C. Membranes were washed 3 times with 0.1% TBS/Tween-20. Secondary antibodies were

971 diluted in blocking buffer and applied to membranes for 1 hour at room temperature. After 3
972 more additional washes, detection was performed using the ECL reagent (Amersham Pharmacia
973 Biotech) and visualized with the chemiluminescence imager G:BOX Chemi XT4 (Synoptics).
974
975 **CD95 surface staining**
976 Cell pellets of about 300,00 cells were resuspended in about 100 μl of PBS on ice. After
977 resuspension, 5 μl of either anti-CD95 primary antibody (BD #556640) conjugated with
978 fluorescein isothiocyanate (FitC), or the matching Isotype control (BD #551954), Mouse IgG1 κ
979 conjugated with FitC, were added. Cells were incubated on ice at 4°C, in the dark, for 25
980 minutes, washed twice with PBS, and percent green cells were determined by flow cytometry
981 (Becton, Dickinson).
982
983 **Cell death quantification (DNA fragmentation)**
984 A cell pellet (500,000 cells) was resuspended in 0.1% sodium citrate, pH 7.4, 0.05% Triton X-
985 100, and 50 μg/ml propidium iodide. After resuspension, cells were incubated 2 to 4 hours in the
986 dark at 4°C. The percent of subG1 nuclei (fragmented DNA) was determined by flow cytometry.
987
988 **Cell growth and fluorescence over time**
989 After treatment/infection, cells were seeded at 500 to 4,000 per well in a 96-well plate at least in
990 triplicate. Images were captured at indicated time points using the IncuCyte ZOOM live cell
991 imaging system (Essen BioScience) with a 10x objective lens. Percent confluence, red object
992 count, and the green object integrated intensity were calculated using the IncuCyte ZOOM
993 software (version 2015A).
994
995 **RNA-Seq analysis**
996 The following describes the culture conditions used to produce samples for RNA-Seq in ***Figure***
997 ***4***. HeyA8 ΔshR6 clone #11 cells were infected with pLKO-shScr or pLKO-shR6. A pool of three
998 293T ΔshL3 clones was infected with either pTIP-shScr or pTIP-shL3. After selection with
999 puromycin for 2 days, the pTIP-infected 293T cells were plated with Dox in duplicate at 500,000
1000 cells per T175 flask. The pLKO-infected HeyA8 cells were plated at 500,000 cells per flask.
1001 Total RNA was harvested 50 hours and 100 hours after plating. In addition, 293T cells were
1002 infected with either pLKO-shScr or pLKO-shL1 and RNA was isolated (100 hrs after plating) as

1003 described above for the infection with shR6. Finally, HeyA8 cells were transfected with
1004 RNAiMAX in 6-wells with siScr (NT2) or siL3 oligonucleotides (Dharmacon) at 25 nM. The
1005 transfection mix was removed after 9 hours.

1006 Total RNA was isolated 48 hours after initial transfection using the miRNeasy Mini Kit
1007 (Qiagen, Cat.No. 74004)) following the manufacturer's instructions. An on-column digestion
1008 step using the RNAse-free DNAse Set (Qiagen, Cat.No.: 79254) was included for all RNA-Seq
1009 samples.

1010 RNA libraries were generated and sequenced (Genomics Core facility at the University of
1011 Chicago). The quality and quantity of the RNA samples was checked using an Agilent bio-
1012 analyzer. Paired end RNA-SEQ libraries were generated using Illumina TruSEQ TotalRNA kits
1013 using the Illumina provided protocol (including a RiboZero rRNA removal step). Small RNA-
1014 SEQ libraries were generated using Illumina small RNA SEQ kits using the Illumina provided
1015 protocol. Two types of small RNA-SEQ sub-libraries were generated: one containing library
1016 fragments 140-150 bp in size and one containing library fragments 150-200 bp in size (both
1017 including the sequencing adaptor of about 130bp). All three types of libraries (one RNA-SEQ
1018 and two small RNA-SEQ) were sequenced on an Illumina HiSEQ4000 using Illumina provided
1019 reagents and protocols. The raw counts for RNAs were calculated by HTSeq. The sequenced
1020 reads were mapped to hg38 human genome using Tophat and bowtie2. Differential gene
1021 expression was analyzed by R Bioconductor DESeq2 package using shrinkage estimation for
1022 dispersions and fold changes to improve stability and interpretability of estimates. P values and
1023 adjusted P values were calculated using the DESeq2 package. Counts and sequences of small
1024 RNAs were extracted from raw fastq file by UNIX shell scripts and then grouped and
1025 summarized by SQL language in database tables. To extract small RNAs (shRNA sequences)
1026 adaptor sequences were remove using Trim Galore software.

1027 To identify differentially abundant RNAs in cells expressing either shL3 or shR6, using a
1028 method unbiased by genome annotation, we also analyzed the raw 100 bp reads for differential
1029 abundance. First, the second end in each paired end read was reverse complemented, so that both
1030 reads were on the same strand. Reads were then sorted and counted using the core UNIX utilities
1031 sort and uniq. Reads with fewer than 128 counts across all 16 samples were discarded. A table
1032 with all the remaining reads was then compiled, summing counts from each sequence file
1033 corresponding to the same sample. This table contained a little over 100,000 reads. The R
1034 package edgeR (http://bioinformatics.oxfordjournals.org/content/26/1/139) was used to identify

1035 differentially abundant reads, and then these reads were mapped to the human genome using
1036 blat (http://genome.cshlp.org/content/12/4/656.abstract) to determine chromosomal location
1037 whenever possible. Homer (http://homer.salk.edu/homer/) was used to annotate chromosomal
1038 locations with overlapping genomic elements (such as genes). Raw read counts in each sequence
1039 file were normalized by the total number of unique reads in the file.

1040 To identify the most significant changes in expression of RNAs both methods of RNAs-Seq
1041 analyses (alignment and read based) were used to reach high stringency. All samples were
1042 prepared in duplicate and for each RNA the average of the two duplicates was used for further
1043 analysis. In the alignment-based analysis only RNAs were considered that had a base mean of
1044 >2000 reads and were significantly deregulated between the groups (adjusted p-value <0.05).
1045 Only RNAs were scored as deregulated when they were more than 1.5 fold changed in the shL3
1046 expressing cells at both time points and in the shR6 expressing cells at either time points (each
1047 compared to shScr expressing cells) (*Table S1*). This was done because we found that the pLKO
1048 driven expression of shR6 was a lot lower than the pTIP driven expression of shL3 (see the
1049 quantification of the two shRNAs in ***Figure 5 - figure supplement 1A***) and likely was a result of
1050 the cell responses in the shR6 expressing cells were reduced. In the read based analysis, only
1051 normalized read numbers of >10 across the samples in each treatment were considered. Only
1052 RNA reads were further considered that had a variation between duplicates of less than 2 fold.
1053 Only RNAs reads were considered that showed >1.5 change between treatment groups in both
1054 cell lines and both time points (*Table S1*). Using the chromosomal localization of each read the
1055 gene of origin was determined. Finally, All RNAs were counted that showed deregulation in the
1056 same direction with both methods. This resulted in the identification of 11 RNAs that were down
1057 and 1 that was upregulated in cells exposed to the shRNAs shL3 and shR6. To determine the
1058 number of seed matches in the 3'UTR of downregulated genes, the 3'UTRs of the 11 mRNAs
1059 were extracted from the Homo sapiens gene (GRCh38.p7) dataset of the Ensembl 86 database
1060 using the Ensembl Biomart data mining tool. For each gene only the longest deposited 3'UTR
1061 was considered. Seed matches were counted in all 3'UTRs using in-house Perl scripts.

1062 GSEA used in ***Figures 4D*** was performed using the GSEA v2.2.4 software from the Broad
1063 Institute (www.http://software.broadinstitute.org/gsea); 1000 permutations were used. The
1064 Sabatini gene lists (*Table S2*) were set as custom gene sets to determine enrichment of survival
1065 genes versus the nonsurvival control genes in downregulated genes from the RNA seq data;
1066 Adjusted p-values below 0.05 were considered significantly enriched. The GO enrichment

analysis shown in ***Figure 4F*** was performed using all genes that after alignment and normalization were found to be at least 1.5 fold downregulated with an adjusted p values of <0.05, using the software available on www.Metascape.org and default running parameters.

Conversion of shL3 and shR6 to siRNAs

From the RNA-Seq analysis with HeyA8 ΔshR6 infected with pLKO-shR6 and 293T ΔshL3 clones infected pTIP-shL3, we analyzed the mature double-stranded RNAs derived from pLKO-shR6 and pTIP-shL3 and found that the most abundant RNA forms were both shifted by one nucleotide. Based on these most abundant species observed after cellular processing, we converted shL3 and shR6 sequences to siRNAs. The genomic target sequence in shL3 (21nt) is 5'-ACUGGGCUGUACUUUGUAUAU-3'. For the shL3=>siL3 sense strand, one G was added before the A on the 5' end while the last U on the 3' end was deleted, and second and third to the last ribonucleotides on the 3' end (UA) were replaced with deoxyribonucleotides for stabilization. For shL3=>siL3 antisense strand, the last three nucleotides on the 5' end (AUA) were deleted and one U and two dTs (UdTdT) were added after the last U on the 3'end. The shL3=>siL3 sense strand is 5'- GACUGGGCUGUACUUUGUAdTdA-3' and antisense strand is 5'-/5Phos/UACAAAGUACAGCCCAGUUdTdT-3'. The shR6=>siRNA was designed in a similar fashion except that two Gs instead of one G were added to the 5' end of the sense strand while UUdTdT instead of UdTdT was added to the 3' end of the antisense strand. The genomic target sequence in shR6 (21nt) is 5'-GUGCAGAUGUAAACCAAACUU-3'. The shR6=>siR6 sense strand is 5'-GGGUGCAGAUGUAAACCAAAdCdT-3' and antisense strand is 5'-/5Phos/UUUGGUUUACAUCUGCACUUdTdT-3'. Both shL3=>siL3 and ShR6=>siR6 siRNA duplexes were purchased from Dharmacon.

Construction of pTIP-shRNA libraries

The pTIP-shRNA libraries were constructed by subcloning libraries of 143nt PCR inserts of the form 5'-*XXXXXXXXXXXXXXXXXXXXXXXXXXXATAGAGATCGNNNNNNNNNNNNNNNNNNNNCTCGAGNNNNNNNNNNNNNNNNNNNNNNTTTTTGTACCGAGCTCGGATCCACTAGTCCAGTGTGGGCATGCTGCGTTGACATTGATT*-3' into the pTIP-shR6 vector after excising the shR6 insert. The poly-N region represents the 21-mer sense and antisense shRNA hairpin. The intervening CTCGAG is the loop region of the shRNA. The 5 libraries targeting Venus, CD95L ORF, CD95L 3'UTR, CD95 ORF, or CD95 3'UTR were composed of every

1099 possible 21-mer shRNA (i.e. each nearest neighbor shRNA was shifted by 1 nucleotide).
1100 These libraries were synthesized together on a chip as 143 bp single-stranded DNA oligos
1101 (CustomArray Inc, Custom 12K oligo pool). Each shRNA pool had its own unique 5' end
1102 represented by the poly-*X* region. This allowed selective amplification of a particular pool using
1103 1 of 5 unique Fr primers (CD95L ORF: 5'-*TGGCTTTATATATCTCCCTATCAGTG*-3', CD95L
1104 3' UTR: 5'-*GGTCGTCCTATCTATTATTATTCACG*-3', CD95 ORF: 5'-
1105 *TCTTGTGTCCAGACCAATTTATTTCG*-3', CD95 3'UTR: 5'-
1106 *CTCATTGACTATCGTTTTAGCTACTG*-3', Venus: 5'-*TATCATCTTTCATGATGACTTTCCGG*-
1107 3') and the common reverse primer 5'-*AATCAATGTCAACGCAGCAT*-3'. Phusion High Fidelity
1108 Polymerase (NEB #M0530) was used to amplify each library pool; standard PCR conditions
1109 were used with an annealing temperature of 61°C and 15 cycles. PCR reactions were purified
1110 using PCR Cleanup kit (QIAGEN). The pTIP-shR6 vector and each of the amplified libraries
1111 were digested with SphI-HF and BsaBI. Digested PCR products were run on either a 2%
1112 Agarose gel or a 20% polyacrylamide (29:1) gel made with 0.5 x TBE buffer. PCR products
1113 were extracted using either Gel Extraction kit (QIAGEN) for extraction from Agarose gels or via
1114 electro-elution using D-Tube Dialyzer Mini columns (Novagen #71504). Purified PCR inserts
1115 were then ligated to the linearized pTIP vector with T4 DNA ligase for 24 hours at 16°C. The
1116 ligation mixtures were transformed via electroporation in MegaX DH10B T1 cells (Invitrogen
1117 #C6400) and plated on 24 cm ampicillin dishes. At least 10 colonies per pool were picked and
1118 sequenced to verify successful library construction. After verification, all colonies per library
1119 were pooled together and plasmid DNA extracted using the MaxiPrep kit (QIAGEN). The 5
1120 pTIP-shRNA library DNA preps were used to produce virus in 293T cells.
1121

1122 **Lethality screen with pTIP-shRNA libraries**

1123 NB7 cells were seeded at 1.5 x 10^6 per 145 cm^2 dish. Two dishes were infected with each of the
1124 5 libraries with a transduction efficiency of about 10 to 20%. Media was replaced next day.
1125 Infected cells were selected with 1.5 µg/ml puromycin. Cells infected with the Venus, CD95L
1126 ORF, and CD95L 3'UTR-targeting libraries were pooled in a 1:1:1 ratio to make the CD95L cell
1127 pool. Likewise, cells infected with the Venus, CD95 ORF, and CD95 3'UTR-targeting libraries
1128 were pooled to make the CD95 receptor cell pool. The CD95 and the CD95L cell pools were
1129 plated separately each in 2 sets of duplicates seeded at 600,000 cells per 145cm^2 dish. One set
1130 received 100 ng/ml Dox, and the other one was left untreated (total of 4 dishes per combined

pool; 2 received no treatment and 2 received Dox). Cells infected with the different libraries were also plated individually in triplicate with or without Dox on a 96-well plate to assess the overall toxicity of each pool. DNA was collected from each 145cm^2 dish 9 days after Dox addition.

The shRNA barcodes were amplified from the harvested DNA template using NEB Phusion Polymerase with 4 different pairs of primers (referred to as N, N+1, N+2, and N+3) in separate reactions per DNA sample. The N pair consisted of the primers originally used to amplify the CD95L ORF library (Fr: 5'-*TGGCTTTATATATCTCCCTATCAGTG*-3' and Rev: 5'-*AATCAATGTCAACGCAGCAT*-3'). The N+1 primers had a single nucleotide extension at each 5' end of the N primers corresponding to the pTIP vector sequence (Fr: 5'-*TTGGCTTTATATATCTCCCTATCAGTG*-3' and Rev: 5'-*TAATCAATGTCAACGCAGCAT*-3'). The N+2 primers had 2 nucleotide extensions (Fr: 5'-*CTTGGCTTTATATATCTCCCTATCAGTG*-3' and Rev: 5'-*ATAATCAATGTCAACGCAGCAT*-3'), and the N+3 primers had 3 nucleotide extensions (Fr: 5'-*TCTTGGCTTTATATATCTCCCTATCAGTG*-3' and Rev: 5'-*AATAATCAATGTCAACGCAGCAT*-3'). The barcodes from the pTIP-shRNA library plasmid preparations were also amplified using Phusion Polymerase with the N, N+1, N+2, and N+3 primer pairs. The shRNA barcode PCR products were purified from a 2% Agarose gel and submitted for 100 bp paired-end deep sequencing (Genomics Core facility at the University of Chicago). DNA was quantitated using the Qubit. The 4 separate PCR products amplified using N, N+1, N+2, and N+3 were combined in equimolar amounts for each sample. Libraries were generated using the Illumina TruSeq PCR-free kit using the Illumina provided protocol. The libraries were sequenced using the HiSEQ4000 with Illumina provided reagents and protocols. Raw sequence counts for DNAs were calculated by HTSeq. shRNA sequences in the PCR pieces of genomic DNA were identified by searching all reads for the sense sequence of the mature shRNA plus the loop sequence CTCGAG. To avoid a division by zero problem during the subsequent analyses all counts of zero in the raw data were replaced with 1. A few sequences with a total read number <10 across all plasmids reads were not further considered. In the CD95L pool this was only one shRNA (out of 2362 shRNAs) (L792') and in the CD95 20 shRNAs (out of 3004 shRNAs) were not represented (R88, R295, R493, R494, R496, R497, R498, R499, R213', R215', R216', R217', R220', R221', R222', R223', R225', R226', R258', R946', R1197', R423'). While most shRNAs in both pools had a unique sequence two sequences occurred 6 times (L605', L607', L609', L611', L613', L615', and

1163 L604', L606', L608', L610', L612', L614'). In these cases, read counts were divided by 6. Two
1164 shRNAs could not be evaluated: 1) shR6 in the CD95 pool. It had a significant background due
1165 to the fact that pTIP-shR6 was used as a starting point to clone all other shRNAs. 2) shL3 was
1166 found to be a minor but significant contaminant during the infection of some of the samples. For
1167 each condition, two technical duplicates and two biological duplicates were available. To
1168 normalize reads to determine the change in relative representation of shRNAs between
1169 conditions, the counts of each shRNA in a subpool (all replicates and all conditions) was divided
1170 by the total number of shRNAs in each subpool (%). First, the mean of the technical replicates
1171 (R1 and R2) was taken. To analyze the biological replicates and to determine the changes
1172 between conditions, two analyses were performed: 1) The change in shRNA representation
1173 between the cloned plasmid library and cells infected with the library and then cultured for 9
1174 days without Dox (infection -Dox). Fold downregulation was calculated for each subpool as
1175 [(plasmid %/-Dox1 %+plasmid %/-Dox2 %)/2]. 2) The difference in shRNA composition
1176 between the infected cells cultured with (infection +Dox) and without Dox. Fold downregulation
1177 was calculated for each subpool as [(-Dox1 %/+Dox1 %)+(-Dox1 %/+Dox2 %)+(-Dox2
1178 %/+Dox1 %)+(-Dox2 %/+Dox2 %)/4]. Only shRNAs were considered that were at least 5-fold
1179 underrepresented in either of the two analyses (data in *Table S3*).
1180

1181 **The toxicity index (TI) and GC content analysis**

1182 The TI in ***Figure 7A*** is defined by the sum of the counts of a 6mer or 8mer seed match in the
1183 3'UTRs of critical survival genes divided by the seed match counts in the 3'UTRs of nonsurvival
1184 genes. We used the 1882 survival genes recently described in a CRISPR/Cas9 lethality screen by
1185 Wang et al. (Wang et al., 2015). The survival genes were defined by having a CRISPR score of
1186 <-0.1 and an adjusted p-value of <0.05. We chose as a control group to these top essential genes
1187 the bottom essential genes using inverse criteria (CRISPR score of >0.1 and adjusted p-value of
1188 <0.05) and are referring to them as the "nonsurvival genes". Both counts were normalized for the
1189 numbers of genes in each gene set. 3'UTRs were retrieved as described above. For the survival
1190 genes 1846 and for the nonsurvival genes 416 3'UTRs were found. For each gene, only seed
1191 matches in the longest 3'UTR were counted. The TI was calculated for each of the 4096 possible
1192 6mer combinations and each of the 65536 possible 8mer combinations (*Table S4*). These
1193 numbers were then assigned to the results of the shRNA screen (*Table S5*). An alternative TI was
1194 calculated in ***Figure 7 – figure supplement 1B*** and is based on the top 850 most highly

1195 expressed survival genes (all expressed >1000 average reads) and 850 expression matched
1196 genes not described to be critical for cancer cell survival were selected as controls.
1197 For the analyses in ***Figure 7C and D***, the GC content % was calculated for every 6mer in
1198 the CD95L ORF shRNA pool. The GC content % was then plotted against the log(Fold down)
1199 for each shRNA in the CD95L ORF shRNA after infection (compared to the plasmid
1200 composition) in ***Figure 7C*** and after addition of Dox (compared to cells infected but not treated
1201 with Dox) in ***Figure 7D***. In ***Figure 7E***, the log(TI) and GC content % was extracted for every
1202 possible 6mer and plotted. Pearson correlation coefficient and associated p-value were
1203 calculated in R3.3.1.
1204
1205 **Sylamer analysis**
1206 Sylamer is a tool to test for the presence of RNAi-type regulation effects from a list of
1207 differentially expressed genes, independently from small RNA measurements (van Dongen et al.,
1208 2008) (http://www.ebi.ac.uk/research/enright/software/sylamer). For short stretches of RNA (in
1209 this case length 6, 7, and 8 in length corresponding to the lengths of the determinants of seed
1210 region binding in RNAi-type binding events), Sylamer tests for all possible motifs of this length
1211 whether the motif occurrences are shifted in sequences associated with the list under
1212 consideration, typically 3'UTRs when analyzing RNAi-type binding events. A shift or
1213 enrichment of such a motif towards the down-regulated end of the gene list is consistent with
1214 upregulation of a small RNA that has the motif as the seed region. Sylamer tests in small
1215 increments along the list of genes, using a hypergeometric test on the counts of a given word,
1216 comparing the leading part of the gene list to the universe of all genes in the list. For full details
1217 refer to (van Dongen et al., 2008). Enriched motifs stand out from the back-ground of all motifs
1218 tested, as visible in the Sylamer plot. The plot consist of many different lines, each line
1219 representing the outcomes of a series of tests for a single word, performed along regularly spaced
1220 intervals (increments of 200 genes) of the gene list. Each test yields the log-transformed P-value
1221 arising from a hypergeometric test as indicated above. If the word is enriched in the leading
1222 interval the log-transformed value has its value plotted on the positive y-axis (sign changed), if
1223 the word is depleted the log-transformed value is plotted on the negative y-axis. 3' UTRs were
1224 used from Ensembl, version 76. As required by Sylamer, they were cleaned of low-complexity
1225 sequences and repetitive fragments using respectively Dust (Morgulis, Gertz, Schaffer, &
1226 Agarwala, 2006) with default parameters and the RSAT interface (Medina-Rivera et al., 2015) to

1227 the Vmatch program, also run with default parameters. Sylamer (version 12-342) was run with
1228 the Markov correction parameter set to 4.
1229
1230 **Statistical analyses**
1231 Continuous data were summarized as means and standard deviations (except for all IncuCyte
1232 experiments where standard errors are shown) and dichotomous data as proportions. Continuous
1233 data were compared using t-tests for two independent groups and one-way ANOVA for 3 or
1234 more groups. For evaluation of continuous outcomes over time, two-way ANOVA was used with
1235 one factor for the treatment conditions of primary interest and a second factor for time treated as
1236 a categorical variable to allow for non-linearity. Comparisons of single proportions to
1237 hypothesized null values were evaluated using binomial tests. Statistical tests of two independent
1238 proportions were used to compare dichotomous observations across groups.
1239 The effects of treatment on wild-type versus either Dicer$^{-/-}$ or Drosha$^{-/-}$ cells were statistically
1240 assessed by fitting regression models that included linear and quadratic terms for value over
1241 time, main effects for treatment and cell type, and two- and three-way interactions for treatment,
1242 cell-type and time. The three-way interaction on the polynomial terms with treatment and cell
1243 type was evaluated for statistical significance since this represents the difference in treatment
1244 effects over the course of the experiment for the varying cell types.
1245 To test if higher TI is enriched in shRNAs that were highly downregulated, p-values were
1246 calculated based on permutated datasets using Mann-Whitney U tests. The ranking of TI was
1247 randomly shuffled 10,000 times and the W statistic from our dataset was compared to the
1248 distribution of the W statistic of the permuted datasets. Test of enrichment was based on the
1249 filtered data of at least 5-fold difference, which we define as a biologically meaningful. Fisher
1250 Exact Tests were performed to assess enrichment of downregulated genes (i.e. >1.5
1251 downregulated with adjusted p-value <0.05) amongst genes with at least one si/shRNA seed
1252 match. All statistical analyses were conducted in Stata 14 or R 3.3.1.
1253
1254
1255 **Data availability**
1256 The accession number for the RNA-Seq and expression data reported in this manuscript are
1257 GSE87817.
1258
1259

Acknowledgements

We are grateful to Lindsay Stolzenburg and Ann Harris for helping to set up the CRISPR/Cas9 gene editing method and to Matthew Schipma for computational support. We would like to thank the Gene Editing & Screening Core, at Memorial Sloan Kettering in New York City, NY, for RNAi reagents and services. M.H. was supported by the Intramural Research Program of NIAMS. This work was funded by training grants T32CA070085 (to M.P.) and T32CA009560 (to W.P.) R50CA211271 (to J.C.Z.), and R35CA197450 (to M.E.P.).

Author contributions

W.P. planned the study and performed experiments. M.P. established the arrayed qPCR method and performed experiments, Q.Q.G., A.H., A.S., A.H.K., A.A.S, and A.E.M. performed experiments, S.D. performed the SYMALER analysis, E.B. and J.S.Z. provided biocomputational and K.A.K. and D.M.S. biostatistics support, M.H. provided assistance and discussions on the mechanism of RNAi and the RISC, and M.E.P. directed the study and wrote the manuscript.

Competing financial interests

The authors declare no competing financial interests.

1279 **Figure legends**
1280
1281 **Figure 1**
1282 **Exogenous CD95L or CD95 proteins do not protect cells from toxicity of CD95L/CD95**
1283 **derived shRNAs.**
1284 (**A**) *Left:* Percent cell confluence over time of NB7 cells after infection with either pLKO-shScr
1285 or pLKO-shL1 and concurrent treatment with different concentrations of soluble CD95L protein
1286 (S2). Two-way ANOVA was performed for pairwise comparisons of % confluence over time
1287 between shScr expressing cells untreated or treated with 100 ng/ml S2. Each data point
1288 represents mean ± SE of three replicates. *Center:* Percent cell confluence over time of NB7 cells
1289 after infection with either pLKO-shScr or pLKO-shL1 and concurrent treatment with different
1290 concentrations of leucine zipper tagged (Lz)CD95L protein. Two-way ANOVA was performed
1291 for pairwise comparisons of % confluence over time between shScr expressing cells untreated or
1292 treated with 50 ng/ml LzCD95L. Each data point represents mean ± SE of three replicates. *Right:*
1293 Percent nuclear PI staining of MCF-7 cells 24 hours after adding different amounts of LzCD95L.
1294 (**B**) Schematic of the eight silent mutations introduced to the shL1 and the shL3 target sites of
1295 CD95L. (**C**) Western blot analysis of CD95L and β-actin in NB7 cells over-expressing CD95L-
1296 WT, CD95L-L1MUT, or CD95L-L3MUT 3 days after infection with pLKO-shScr, pLKO-shL1,
1297 or pLKO-shL3. Shown is one of two repeats of this analysis. (**D**) Percent nuclear PI staining of
1298 NB7 cells expressing empty pLenti vector, CD95L-WT, CD95L-L1MUT, or CD95L-L3MUT 6
1299 days after infection with either pLKO-shScr, pLKO-shL1, or pLKO-shL3. Each bar represents
1300 mean ± SD of three replicates. (**E**) Schematic of the 8 silent mutations introduced at the shR6 site
1301 of CD95. (**F**) Western blot analysis of CD95 and β-actin in MCF-7 cells over-expressing CD95-
1302 WT or CD95-R6MUT. (**G**) Percent nuclear PI staining of MCF-7 cells expressing empty
1303 pLNCX2 vector, CD95-WT, or CD95-R6MUT 6 days after infection with pLKO-shScr, pLKO-
1304 shR6, or pLKO-shR7. Each bar represents mean ± SD of three replicates.
1305
1306 **Figure 1 - figure supplement 1.**
1307 **The majority of siRNAs and shRNAs targeting CD95L or CD95 are toxic.**
1308 (**A**) Location of target sites, growth inhibitory activities and toxicity of all tested siRNAs,
1309 DsiRNAs, and pLKO-shRNAs targeting CD95L and CD95. Experiments were performed in
1310 HeyA8 cells at an MOI of 3 for pLKO-shRNA infection, transfected with 25 nM of siRNAs, or 5
1311 nM of DsiRNAs. Color code indicates the level of growth reduction caused by each sh/siRNA.
1312 sh/siRNAs labeled with an asterisk induced significant cell death as monitored by nuclear PI
1313 staining. Both exon/intron structure and protein domains are shown for both CD95L and CD95.
1314 EC, extracellular domain; TM, transmembrane domain; IC, intracellular domain. Data on growth
1315 reduction of DsiRNAs were performed in triplicates and in two independent experiments. Data
1316 on growth reduction of siRNAs were performed in 4 replicates and in two independent
1317 experiments. Data on growth reduction of shRNAs were performed in triplicate and in two
1318 independent experiments. Data on nuclear fragmentation by siRNAs were performed in triplicate
1319 in two independent experiments. Data on nuclear fragmentation by shRNAs were performed in
1320 triplicate. (**B**) PI staining was used to quantify percent subG1 of HeyA8 cells 4 days after
1321 transfection with 5 nM of CD95L derived DsiRNAs. Data are representative of three
1322 independent experiments. Each bar represents mean ± SD of four replicates (p-value ***
1323 $p<0.0001$, unpaired t-test). (**C**) Level of underrepresentation (toxicity) of shRNAs targeting
1324 either CD95L (left column) or CD95 (right column) across 216 human cancer cell lines as
1325 described in (Cowley et al., 2014). The fraction of cell lines for which an shRNA was found to
1326 be toxic is given in percentage For shL5 data on only 197 cell lines were available. This screen

did not include shL3, but another CD95 derived shRNA we did not test (we now call shR3) was found to be toxic to 71.8% of the 216 cell lines.

Figure 1 - figure supplement 2.
Toxicity of si/shRNAs is dose dependent.
(**A**) Sequences of the 6 toxic TRC shRNAs (pLKO vector) that were converted into miR-30 based shRNAs (Tet inducible LT3REPIR vector). (**B**) Confluence over time of NB7-Venus-CD95L (left) or NB7-Venus CD95 (right) cells infected with the LT3REPIR vector minus/plus Dox to induce expression of the indicated shRNAs. (**C**) Total green fluorescence over time of the experiment shown in B. (**D**) Confluence (top) and total green fluorescence (bottom) over time of NB7-Venus-CD95L (left) or NB7-Venus CD95 (right) cells infected with the pTIP vector minus/plus Dox to induce expression of the indicated shRNAs. (**E**) Confluence over time of HeyA8 cells transfected with the indicated concentration of either siScr or siL3. Each data point represents mean ± SE of six replicates. The experiment was repeated three times.

Figure 2.
CD95 and CD95L derived si/shRNAs kill cells in the absence of the targeted sites in CD95 or CD95L.
(**A**) Schematic of the genomic locations and sequences of the gRNAs used to excise the siL3 (Δ64bp) and shL3 (Δ41bp) target sites from CD95L. PAM site is underlined. Green indicates a gRNA targeting the sense strand. Blue indicates a gRNA targeting the antisense strand. (**B**) Schematic showing the genomic locations and sequences of the gRNAs used to excise the shR6 (Δ227bp) target site. (**C**) PCR with flanking (*top panels*) and internal (*bottom panels*) primers used to confirm the Δ41 deletion in the shL3 site in 293T clones. Cells transfected with Cas9 only (Cas9) are wild-type, clone #3 is heterozygous, and clones #1 and #5 are representative of homozygous deletion clones. (**D**) Quantitative PCR for endogenous CD95L with a primer downstream of the Δ41 shL3 deletion and another primer internal to the deleted region. nd, not detectable. Each bar represents mean ± SD of three replicates. (**E**) PCR with flanking (*top row*) and internal (*bottom row*) primers used to confirm the presence of the shL3 Δ41 (*top panel*), siL3 Δ64 (*middle panel*), and shR6 Δ227 (*bottom panel*) deletions in HeyA8 clones. Mix, HeyA8 cells after transfection with Cas9 and gRNAs but before single cell cloning. (**F**) Quantitative PCR for CD95 in HeyA8 cells transfected with Cas9 plasmid (Cas9) alone, or the HeyA8 ΔshR6 clone #11. RNA was extracted 5 days after infection with pLKO-shScr, pLKO-shR6, pLKO-shR2, or pLKO-shR6' (targeting the 3'UTR). Each bar represents mean ± SD of three replicates. (**G**) Percent cell confluence over time of 293T cells (*left*) and a pool of three 293T clones with a homozygous deletion of the shL3 target site (*right*) infected with pTIP-shScr or pTIP-shL3 and treatment with or without Dox. Data are representative of two independent experiments. Each data point represents mean ± SE of six replicates. (**H**) *Left:* Percent confluence over time of HeyA8 cells infected with pLKO-shScr, pLKO-shR6, or pLKO-shL3. *Center:* Percent confluence over time of a HeyA8 clone with a homozygous deletion of the shR6 target site infected with either pLKO-shScr or pLKO-shR6. *Right:* Percent confluence over time of a pool of three HeyA8 clones with a homozygous deletion of the shL3 site infected with either pLKO-shScr or pLKO-shL3. Data are representative of two independent experiments. Each data point represents mean ± SE of three replicates. (**I**) Percent confluence over time of a pool of three HeyA8 clones harboring a homozygous deletion of the siRNA siL3 target site after transfection with different concentrations of siScr or siL3. Data are representative of three independent experiments. Each data point represents mean ± SE of three replicates.

Figure 2 - figure supplement 1.
Knockout of CD95 in HeyA8 cells.
(**A**) PCR showing a Δ227 shR6 deletion and insertions in HeyA8 clones #1 and #2. (**B**) Schematic of the Δ227 deletion in allele #1 and partial insertion of a pSC-B plasmid fragment in allele #2 in HeyA8 clone #2 based on Sanger sequencing of isolated bands from PCR shown in A. Note, cl#1 and #2 have the expected Δ227 shR6 deletion in one allele and an insertion in the other. cl#11 has a homozygous Δ227 shR6 deletion. The deleted region is shown in green containing the shR6 target site in red. pSC-B vector sequences are shown in blue letters, and the insertion is shown in orange. (**C**) Western blot for CD95 and β-actin in Cas9-control transfected HeyA8 cells and HeyA8 shR6 k.o. clones #1, #2, and #11. Shown is one of two repeats of this analysis. (**D**) Surface staining for CD95 in parental HeyA8 cells and HeyA8 shR6 knockout clones #1, #2, and #11. Shown is one of two repeats of this analysis. (**E**) Images showing apoptosis induction with LzCD95L treatment (4.5 hrs) in parental HeyA8 cells but not in clone #2.

Figure 3.
Toxicity of CD95L derived siRNAs involves canonical RNAi activity.
(**A**) Percent cell confluence (*left*) and total green object integrated intensity (*right*) over time of a HeyA8 CD95 knockout clone (ΔR6 cl#2) expressing the Venus-CD95L sensor either untreated (Ctr) or after transfection with 25 nM of single-stranded sense, single-stranded antisense, or double-stranded (ds) siScr or siL3 siRNAs. The CD95L sensor is schematically shown and comprises the Venus ORF fused to the CD95L ORF lacking the A of the ATG start codon (X). Data are representative of two independent experiments. Each data point represents mean ± SE of three replicates. (**B**) Percent cell confluence (*left*) and total green object integrated intensity (*right*) over time of the HeyA8 CD95L sensor cell used in *Figure 3A* after transfection with 5 nM siScr or siL3 double-stranded RNA (dsRNA) or double-stranded DNA (dsDNA). Data are representative of two independent experiments. Each data point represents mean ± SE of three replicates. (**C**) Summary of experiments to test whether siL3 and siL2 siRNAs modified as indicated (*left*) were active (check mark) or not (X) in reducing green fluorescence or cell growth (both >70% reduction at end point) when transfected at 25 nM (except for blunt end oligonucleotides which were used at 5 nM and compared to 5 nM of siL3) into HeyA8 CD95L sensor cells used in *Figure 3A*. Endpoints were 164 hours for blunt end siRNA transfection, 180 hrs for modified siL3 and 144 hrs for modified siL2 siRNA transfections. Every data row is based on cell growth and green fluorescence quantification data executed as shown in A. Each analysis was done in triplicate and based on two independent repeats. (**D**) Red object count over time of HeyA8 cells (expressing NucRed) after transfection with different ratios of siL3 and mutant siL3 (siL3MUT). Data are representative of two independent experiments. Each data point represents mean ± SE of three replicates. (**E**) Percent cell confluence over time of HCT116 parental (*left*) or Dicer$^{-/-}$ (clone #43, another Dicer$^{-/-}$ clone, #45, gave a similar result, data not shown), or Drosha$^{-/-}$ (*right*) cells after infection with either shScr, shL3 or shR6 pLKO viruses. Inserts show the level of protein expression levels of Drosha/Dicer and AGO2 levels in the tested cells. Data are representative of three independent experiments. Each data point represents mean ± SE of four replicates. Drosha$^{-/-}$ cells were more sensitive to toxic shRNAs than wt cells ($p<0.0001$, according to a polynomial fitting model). (**F**) Western blot analysis of HCT116 wt, Dicer$^{-/-}$ or Drosha$^{-/-}$ cells 4 days after infection with either pLKO-shScr or pLKO-shR6. (**G**) Percent cell confluence over time of HCT116 wt, Dicer$^{-/-}$ (clone #43) and Drosha$^{-/-}$ cells after transfection with 25 nM siScr or siL3. Data are representative of four independent experiments (Dicer$^{-/-}$ clone #45, gave a similar result, data not shown). Each data point represents the mean ±

SE of four replicates. Data in insert confirm similar uptake of transfected siRNA (25 nM of siGLO Red) into wild-type, Dicer$^{-/-}$ and Drosha$^{-/-}$ cells. Dicer$^{-/-}$ and Drosha$^{-/-}$ cells were more sensitive to siL3 than wt cells ($p<0.0001$, according to a polynomial fitting model). (**H**) Percent reduction in Venus expression (green) and in cell number (red object count (red)) over time of HeyA8 cells expressing the Venus-CD95L sensor and red nuclei after transfection with 5 nM of different chimeric siRNAs generated by substituting nucleotides in the toxic siL3 with the scrambled siRNA sequence beginning at either the seed match end (top) or the opposite end (bottom) of siL3 after 188 hours. The schematic in the middle shows the sequence of siL3 and the siScr siRNA (both sense and antisense strands). The 6mer seed sequence region of siL3 (positions 2 to 7) is highlighted in light blue. Nucleotides shared by siScr and siL3 are shown in grey font. Data are representative of two independent experiments. Each data point represents mean of three replicates. In another independent experiment cells were transfected with 25 nM with a very similar result (data not shown).

Figure 4.

Toxic shRNAs derived from CD95 and CD95L cause downregulation of critical survival genes.

(**A**) Schematic of RNA-Seq work flow for total RNA sample prepared both before (50 hrs) and during (100 hrs) DISE after expressing either shR6 or shL3 from different vector systems (i.e. pLKO-shR6 and pTIP-shL3) in different cells (HeyA8 shR6 Δ227 cells and 293T shL3 Δ41 cells). (**B**) One mRNA was up and 11 mRNAs were downregulated in the cells treated with toxic shL3 and shR6 as shown in *Figure 4A*. mRNAs shown in red were found to be essential cancer survival genes in two genome-wide lethality screens. The number of essential genes was enriched from 6.6% of the tested genes (Blomen et al., 2015; Wang et al., 2015) to 54.5% in our study ($p=3 \times 10^{-6}$ according to binomial distribution). (**C**) The level of growth inhibition observed in HeyA8 cells transfected with siRNA SmartPools (25 nM) individually targeting the listed survival genes. Targeting the seven genes shown significantly reduced cell growth compared to cells transfected with a siScr pool at 140 hrs (samples done in quadruplicate in two independent experiments) with an ANOVA $p<0.05$. (**D**) Gene set enrichment analysis for a group of 1846 survival genes (*top 4 panels*) and 416 nonsurvival genes (*bottom 4 panels*) identified in a genome-wide CRISPR lethality screen (Wang et al., 2015) after introducing Dox-inducible shL3 in 293T ΔshL3 cells (*left-most panels*), shR6 in HeyA8 ΔshR6 cells (*center-left panels*), shL1 in parental 293T cells (*center-right panels*), and siL3 in HeyA8 cells (*right-most panels*). Scrambled sequences served as controls. p-values indicate the significance of enrichment. (**E**) Schematics showing all RNAs at least 1.5 fold downregulated (adj p-value <0.05) in cells treated as in *Figure 4A*. Histones that are underlined contain a 3'UTR. (**F**) Metascape analysis of the 4 RNA Seq data sets analyzed. The boxed GO term clusters were highly enriched in all data sets.

Figure 4 - figure supplement 1.

Down-regulation of critical survival genes after treatment with CD95 and CD95L-derived shRNAs and siRNAs.

(**A**) Arrayed quantitative PCR of genes found to be down-regulated (or upregulated as with ATP13A3) in *Figure 4B* both in 293T ΔshL3-pTIP-shL3 cells 50 hrs post-Dox treatment and HeyA8 ΔshR6-pLKO-shR6 100 hrs post infection and puromycin selection. Data are representative of two independent experiments. Each bar represents mean ± SD of two biological replicates and two technical replicates (p-value *<0.05, **<0.005, unpaired t-test). (**B**) Venn diagram showing overlap of genes determined to be down-regulated with both read-based and

1471 alignment-based analyses of the RNA-Seq data depicted in *Figure 4A* with the critical
1472 survival genes found in the Sabatini and Brummelkamp studies (Blomen et al., 2015; Wang et
1473 al., 2015), all listed in ***Table S2***. The Venn diagram was generated using
1474 http://bioinformatics.psb.ugent.be/webtools/Venn. (**C**) Kinetic quantitative PCR of the down-
1475 regulated genes in the 293T ΔshL3 pTIP-shL3 cells. RNA was collected at 14 hrs, 26 hrs, and 50
1476 hrs after treatment with Dox. NS, not significant. Each bar represents mean ± SD of
1477 quadruplicates (p-value *<0.05, **<0.005, unpaired t-test). (**D**) Table showing which genes were
1478 significantly (p<0.05) down-regulated >1.5 fold (indicated by an "X") in parental HeyA8 cells
1479 80 hrs after transfection with siL3 or 100 hrs after infection and puromycin selection with
1480 pLKO-shL1, pLKO-shL3, or pLKO-shR7.
1481 The following describes the 11 genes that were significantly downregulated after introducing the
1482 toxic shRNAs shL3 or shR6 into cancer cells (see ***Figure 4B***) and some of their cancer relevant
1483 activities:
1484 1) CAPZA1 (capping actin protein of muscle Z-line alpha subunit 1) is an actin capping protein.
1485 CAPZA1 knockdown has been reported to cause disassembly of autophagosomes (Mi et al.,
1486 2015). It is overexpressed in malignant melanoma (Sun et al., 2011).
1487 2) CCT3 (chaperonin containing TCP1 subunit 3) is part of a chaperone complex that folds
1488 various proteins including actin and tubulin. CCT3 is required for proper mitotic progression
1489 (Zhang et al., 2016).
1490 3) FSTL1 (follistatin-like 1) is a putative activin-binding protein. Knockdown of FSTL1 in lung
1491 cancer cells resulted in mitotic arrest followed by apoptosis promoted by the activation of
1492 caspase-3 and -9 (Bae et al., 2016). FSTL1 is downregulated during cellular senescence of
1493 human mesenchymal stem cells (Yoo, Choi, & Kim, 2013).
1494 4) FUBP1 (far upstream element binding protein 1). A lack of FUBP1 causes a cell-autonomous
1495 defect in the maintenance of fetal and adult hematopoietic stem cells (HSCs). FUBP1-
1496 deficient adult HSCs exhibit significant transcriptional changes, including upregulation of the
1497 cell-cycle inhibitor p21 and the pro-apoptotic Noxa molecule, suggesting they undergo
1498 apoptosis (Rabenhorst et al., 2015). In addition, FUBP1 binds to an upstream element of the c-
1499 myc promoter and regulates c-myc mRNA level, thus regulating proliferation (Jang et al.,
1500 2009). Finally, FUBP1 is upregulated in many tumors and acts as an oncoprotein by
1501 stimulating proliferation and inhibiting apoptosis (Baumgarten et al., 2014).
1502 5) GNB1 (G-protein beta submit 1) is tumor-promoting in breast cancer. Data suggest that GNB1
1503 plays an important role in the mTOR-related anti-apoptosis pathway (Wazir, Jiang, Sharma, &
1504 Mokbel, 2013).
1505 6) HIST1H1C. A specific role of this particular histone in cancer cell survival has not yet been
1506 described. (Knockdown causes cell cycle arrest in MCF-7 cells;
1507 (http://journals.plos.org/plosgenetics/ article?id=10.1371%2Fjournal.pgen.1000227)).
1508 7) NAA50 (N(alpha)-acetyltransferase 50, NatE catalytic subunit) is required for sister chromatid
1509 separation *in vivo* (Hou, Chu, Kong, Yokomori, & Zou, 2007).
1510 8) NUCKS1 (nuclear casein kinase and cyclin dependent kinase substrate 1) is a chromatin-
1511 associated protein with a role in the DNA damage response. Knocking down NUCKS1 causes
1512 chromosomal breaks (Parplys et al., 2015).
1513 9) PRELID3B (PRELI domain containing 3B) is an inner mitochondrial protein. Knocking down
1514 PRELID3B decreases cell viability (http://www.genecards.org/cgi-
1515 bin/carddisp.pl?gene=PRELID3B).
1516 10) SNRPE (small nuclear ribonucleoprotein polypeptide E). siRNA-mediated depletion of
1517 SNRPE stimulated autophagy and led to a marked reduction of cell viability in breast, lung,

1518 and melanoma cancer cell lines, whereas it had little effect on the survival of the
1519 nonmalignant MCF-10A breast epithelial cells (Quidville et al., 2013).
1520 11) TFRC (transferrin receptor). Blocking TFRC function with a neutralizing antibody inhibits
1521 cell proliferation and survival (Pham et al., 2014). Suppression of TFRC led to apoptosis of
1522 renal cells (Gui et al., 2013) and cell cycle arrest in esophageal squamous cell carcinoma cells
1523 (Chan et al., 2014).
1524
1525 **Figure 4 - figure supplement 2.**
1526 **Characterization of the six genes downregulated in shL3 and shR6 treated cells and found**
1527 **to be critical survival genes in lethality screens.**
1528 (**A**) The six downregulated survival genes were queried individually using default settings with
1529 all studies selected in the cBioPortal for Cancer Genomics hosted by Memorial Sloan Kettering
1530 Cancer Center (http://www.cbioportal.org/) (Cerami et al., 2012; Gao et al., 2013). Datasets with
1531 alterations in 5 out of the 6 essential genes reporting both copy number alterations and
1532 mutational data were included. To avoid reporting duplicate datasets, The Cancer Genome Atlas
1533 publications were excluded. After filtering, 33 datasets representing cancers from 23 different
1534 sites reported alterations in the downregulated survival genes. (**B**) Percent confluence over time
1535 of HeyA8 cells transfected with increasing concentrations of a pool of siRNAs (28 different
1536 siRNAs) targeting 7 different genes: CCT3, TFRC, NAA50, FUBP1, PRELID3B, GNB1 and
1537 FSTL1. Each siRNA SmartPool was comprised of 4 individual siRNAs. Data are representative
1538 of two independent experiments. Values were calculated from samples done in quadruplicates
1539 shown as mean ± SE. (**C**) PI staining used to quantify percent subG1 for cells 4 days after
1540 transfection with 1 nM and 5 nM of combined siRNA pools targeting the 7 different survival
1541 genes as in *B*. Data are representative of two independent experiments. Values were calculated
1542 from samples done in quadruplicates shown as mean ± SD. *** $p<0.0001$, unpaired t-test.
1543
1544 **Figure 4 - figure supplement 3.**
1545 **Histones are downregulated in all forms of DISE but are not the most highly expressed**
1546 **genes in cells.**
1547 MA plots comparing the expression level (counts per million, CPM) and fold change in the four
1548 RNA Seq data sets in this study. Shown are all RNAs that were >1.5 fold deregulated with an
1549 adjusted p-value of <0.01. Significantly downregulated RNAs are shown in green, upregulated
1550 RNAs in cyan. All 73 histones are shown as dark blue dots and the 12 histones downregulated in
1551 all 4 data sets are shown as red dots.
1552
1553 **Figure 5.**
1554 **DISE inducing si/shRNAs target critical survival genes through RNAi.**
1555 (**A**) Sylamer plots for the list of genes in the shL3 experiment (left) and the shR6 experiment
1556 (right) ordered from down-regulated to up-regulated. The most highly enriched sequence is
1557 shown which in each case is the 8mer seed match of the introduced shRNA. The red line
1558 corresponds to a p-value threshold of 0.05 after Bonferroni correction for the number of words
1559 tested (65536). Bonferroni-adjusted p-values are shown. The unadjusted p-values are 1.58E-24
1560 and 1.35E-26, respectively. The black line represents the sequences carrying the let-7 8mer seed
1561 match. (**B**) Location of the 6mer seed matches of either shL3 or shR6 in the 3'UTRs of the 11
1562 genes (shown at scale) identified in the RNA-Seq experiment described in *Figure 4A*. Red font
1563 indicates a critical survival gene. (**C**) A series of six 2x2 contingency tables comparing whether
1564 or not a critical survival gene is downregulated after treatment with the indicated siRNA or
1565 shRNA to whether or not its 3'UTR contains at least 1 seed match for the introduced sh/siRNA.

1566 p-values were calculated using Fisher's Exact Test to determine any significant relationship
1567 between gene downregulation and presence of seed matches in 3'UTR.
1568
1569 **Figure 5 - figure supplement 1.**
1570 **Quantification of the mature shRNA forms.**
1571 (**A**) Graphical representation of the percentage of the different Dicer cut sites to produce the
1572 mature passenger (top) and guide (bottom) strands of 3 shRNAs expressed from two vectors. All
1573 analyses were performed with cells 50 hrs after either Dox addition (in pTIP expressing cells) or
1574 infection with the pLKO virus. Letters in green: vector sequences; black: passenger and guide
1575 strands of shRNAs; Arrow heads label the most highly cleaved residues; the darker the arrow
1576 head the more highly cleaved. Numbers in yellow box represent total number of reads detected
1577 for passenger and guide strands. (**B**) Percent cell confluence in HeyA8 cells after transfection
1578 with shL3=>siL3 (shL3 converted to an siRNA) or shR6=>siR6 (shR6 converted to an siRNA).
1579 Conversion was based on the most common mature double-stranded RNA form produced as
1580 indicated by the results in *A*. Data are representative of two independent experiments. Each bar
1581 represents mean ± SE of four replicates. Insert: percent DNA fragmentation in the same samples.
1582 Data are representative of two independent experiments. Each bar represents mean ± SD of four
1583 replicates, *** $p<0.0001$, unpaired t-test.
1584
1585 **Figure 5 - figure supplement 2.**
1586 **Identification of seed matches targeted by shL1 and siL3.**
1587 Sylamer plots for the list of genes in the shL1 experiment (293T cells 100 hrs after infection with
1588 pLKO-shL1) (left) and the siL3 experiment (48 hrs after transfection of HeyA8 cells with siL3)
1589 (right) ordered from down-regulated to up-regulated. The most highly enriched sequences are
1590 shown which in each case is the 7mer seed match of the introduced shRNA. The red line
1591 corresponds to a p-value threshold of 0.05 after Bonferroni correction for the number of words
1592 tested. Bonferroni-adjusted p-values are shown.
1593
1594 **Figure 5 - figure supplement 3.**
1595 **Activity to knockdown CD95 does determine shRNA toxicity.**
1596 HeyA8 cells infected with the indicated shRNAs in the pLKO vector were analyzed for toxicity
1597 (top, % percent reduction at half maximal confluency), CD95 expression by Western blot
1598 analysis (center, 2 days after puromycin addition) and qPCR analysis (bottom, 3 days after
1599 puromycin addition). Shown data are representative of two independent experiments. +++,
1600 >75%; ++, >50%; +, >10%; -, <10% growth reduction.
1601
1602 **Figure 6.**
1603 **Identifying all toxic shRNAs derived from CD95L and CD95.**
1604 (**A**) Schematic showing the cloned shRNAs covering the ORF of Venus and the ORFs and
1605 3'UTRs of CD95L and CD95. The 3'UTR is displayed as a dashed line because it was not
1606 included in the full-length Venus-CD95L/CD95 sensors. (**B**) Work-flow of pTIP-shRNA library
1607 synthesis, shRNA screen and data analysis. (**C**) Ranked fold reduction of shRNAs spanning
1608 Venus and CD95L (ORF and 3'UTR) (*left 3 panels*) and Venus and CD95 (ORF and 3'UTR)
1609 (*right 3 panels*). The ranked lists were separated into the shRNAs derived from Venus (top), the
1610 ORFs (center) and the 3'UTRs (bottom). The p-value of enrichment for each ranked set of
1611 shRNAs is given. Only the parts of the ranked lists are shown with the downregulated shRNAs.
1612 For all 6 panels, the top section of each panel (boxed in blue) contains the data on shRNAs
1613 downregulated after infection of cells and cultured for 9 days without Dox when compared to the

1614 composition of the shRNA plasmid library and the bottom half (boxed in orange) contains the
1615 data on shRNAs downregulated after culture with Dox for 9 days when compared to the culture
1616 without Dox. P-values were calculated using Mann Whitney U tests with a one-sided alternative
1617 that the rank was lower. (**D**) The location of all shRNAs significantly downregulated at least 5
1618 fold along the sequences of Venus, CD95L ORF, CD95L 3'UTR (left panel) and Venus, CD95
1619 ORF, and CD95 3'UTR (right panel). The top half of each sub panel (blue ticks) shows the
1620 shRNAs downregulated after infection and the bottom half (orange ticks) contains the data on
1621 shRNAs downregulated after culture with Dox for 9 days. Significance of enrichment in the
1622 different subpanels is shown. p-values were calculated according to statistical tests of two
1623 proportions. Each data set was compared to the corresponding Venus distribution. Green line:
1624 sequence that corresponds to the intracellular domain of CD95L.
1625
1626 **Figure 6 - figure supplement 1.**
1627 **Toxicity and RNAi of individual shRNA pools.**
1628 (**A**) *Top panels:* Green object intensity over time of NB7 Venus-CD95L sensor cells infected
1629 with the pTIP-Venus shRNA pool (*left panel*), pTIP-CD95L ORF shRNA pool (*center panel*), or
1630 pTIP-CD95L 3'UTR shRNA pool (*right panel*) with or without Dox treatment. *Bottom panels:*
1631 Green object intensity over time of NB7 Venus-CD95 sensor cells infected with the pTIP-Venus
1632 shRNA pool (*left panel*), pTIP-CD95 ORF shRNA pool (*center panel*), or pTIP-CD95 3'UTR
1633 shRNA pool (*right panel*) with or without Dox treatment. Values were calculated from samples
1634 done in quadruplicates shown as mean ± SE. (**B**) Percent confluence over time of parental NB7
1635 cells infected with the pTIP-Venus shRNA pool (*top left panel*), pTIP-CD95L ORF shRNA pool
1636 (*top center panel*), pTIP-CD95L 3'UTR shRNA pool (*top right panel*), pTIP-CD95 ORF-shRNA
1637 pool (*bottom center panel*), and pTIP-CD95 3'UTR shRNA pool (*bottom right panel*) with or
1638 without Dox treatment. Values were calculated from samples done in triplicate shown as mean ±
1639 SE. P-values were calculated using two-way ANOVA with a factor for Dox treatment and a
1640 factor for time. Similar data were obtained when either HCT116 or 293T cells were treated with
1641 each of the five shRNA pools (data not shown).
1642
1643 **Figure 6 - figure supplement 2.**
1644 **Fold change in shRNA representation after infection of NB7 cells and after treatment with**
1645 **Dox.**
1646 (**A**) Change in green fluorescence (top panels) and percent cell confluence (bottom panels) over
1647 time of NB7 cells expressing either Venus-CD95 (left panels) or Venus-CD95L (right panels).
1648 Cells were infected with the Tet-inducible pTIP-shR6 virus, selected for two days with
1649 puromycin and then subjected to an analysis in the IncuCyte Zoom. No Dox was added. Two
1650 other inducible constructs (pTIP-shL1 and pTIP-shL3) were tested in the same way and no
1651 evidence of leakiness was observed (data not shown), supporting the finding in the shRNA
1652 screen that certain shRNA constructs display leakiness while others do not. Values were
1653 calculated from samples done in triplicate shown as mean ± SE. (**B**) Scatterplot showing the fold
1654 change of shRNAs after infection of cells and culture for 9 days without Dox when compared to
1655 the composition of the shRNA plasmid library (X axis) and the fold change of shRNAs after
1656 culture with Dox for 9 days when compared to the culture without Dox (Y axis). The red dots are
1657 the shRNAs that were significantly downregulated at least 5 fold. The number of shRNAs
1658 labeled in red in each quartile is given in blue. Two of the shRNAs tested before are labeled in
1659 green.
1660
1661 **Figure 7.**

In silico prediction of DISE activity tracks with experimental determined toxicity of shRNAs.

(**A**) *Left:* Schematic showing the preferential targeting of seed matches present in the 3'UTRs (red marks) of survival genes by toxic si/shRNAs. *Right:* The toxicity index (TI) is the normalized ratio of the number of 6mer or 8mer seed matches present in a list of survival genes versus a list of nonsurvival genes. (**B**) Fold downregulation versus ranked (8mer seed matched based) Toxicity Index for shRNAs of the Venus/CD95L pool (*left three panels*) and the Venus/CD95 pool (*right three panels*). Orange and blue tick marks indicate the same as in *Figure 6D*. To test if higher TI is enriched in shRNAs that were highly downregulated, p-values were calculated based on permutated datasets using Mann-Whitney U tests. The ranking of TI was randomly shuffled 10,000 times and the W statistic from our dataset was compared to the distribution of the W statistic of the permutated datasets. (**C, D**) Plot of fold downregulation of toxic shRNAs derived from CD95L ORF of the toxicity screens -Dox (left) or +Dox (center) versus GC content the 6mer seed in each shRNA. (**E**) Plot of the log(TI) of all 4092 possible 6mers versus GC content of the seeds. Pearson correlation coefficient and significance (p values) are given.

Figure 7 - figure supplement 1.

DISE does not just target all highly expressed genes.

(**A**) Correlation between 850 survival genes (genes identified as critical survival genes in two genome-wide lethality screens (Blomen et al., 2015; Wang et al., 2015) and expressed at least at 100 reads in all of the 16 control RNA Seq samples in this study) and 850 expression matched nonsurvival genes (genes not identified as critical survival genes in two genome-wide lethality screens (Blomen et al., 2015; Wang et al., 2015) and expressed at least at 100 reads in all of the 16 control RNA Seq samples in this study). (**B**) Reanalysis of the CD95L ORF data in *Figure 7B* using two alternative ways to calculate the toxicity index (TI). *Left:* the analysis shown in *Figure 7B* with the data ranked using the original TI (using all known 3'UTRs for each gene group). *Center*: analysis with the data ranked using the original TI but based on only the longest 3'UTR for each gene. *Right*: analysis with the data ranked using the new TI based on expression matched SGs and nonSGs identified in A and using the longest 3'UTR for each gene. To test if higher TI is enriched in shRNAs that were highly downregulated, p-values were calculated based on permutated datasets using Mann-Whitney U tests.

Supplementary Tables:

Table S1: Results of the RNA-Seq analysis used to generate *Figure 4B*.

Table S2: Gene lists used in this work.

Table S3: shRNA screen data.

Table S4: The 6mer and 8mer toxicity index.

Table S5: Correlation between experimental shRNA toxicity and TI.

References

Algeciras-Schimnich, A., Pietras, E. M., Barnhart, B. C., Legembre, P., Vijayan, S., Holbeck, S. L., & Peter, M. E. (2003). Two CD95 tumor classes with different sensitivities to antitumor drugs. *Proc Natl Acad Sci U S A, 100*(20), 11445-11450.

Bae, K., Park, K. E., Han, J., Kim, J., Kim, K., & Yoon, K. A. (2016). Mitotic cell death caused by follistatin-like 1 inhibition is associated with up-regulated Bim by inactivated Erk1/2 in human lung cancer cells. *Oncotarget, 7*(14), 18076-18084. doi: 10.18632/oncotarget.6729

Barnhart, B. C., Legembre, P., Pietras, E., Bubici, C., Franzoso, G., & Peter, M. E. (2004). CD95 ligand induces motility and invasiveness of apoptosis-resistant tumor cells. *EMBO J, 23*(15), 3175-3185.

Baumgarten, P., Harter, P. N., Tonjes, M., Capper, D., Blank, A. E., Sahm, F., . . . Mittelbronn, M. (2014). Loss of FUBP1 expression in gliomas predicts FUBP1 mutation and is associated with oligodendroglial differentiation, IDH1 mutation and 1p/19q loss of heterozygosity. *Neuropathol Appl Neurobiol, 40*(2), 205-216. doi: 10.1111/nan.12088

Bernstein, E., Caudy, A. A., Hammond, S. M., & Hannon, G. J. (2001). Role for a bidentate ribonuclease in the initiation step of RNA interference. *Nature, 409*(6818), 363-366. doi: 10.1038/35053110

Birmingham, A., Anderson, E. M., Reynolds, A., Ilsley-Tyree, D., Leake, D., Fedorov, Y., . . . Khvorova, A. (2006). 3' UTR seed matches, but not overall identity, are associated with RNAi off-targets. *Nat Methods, 3*(3), 199-204. doi: 10.1038/nmeth854

Blomen, V. A., Majek, P., Jae, L. T., Bigenzahn, J. W., Nieuwenhuis, J., Staring, J., . . . Brummelkamp, T. R. (2015). Gene essentiality and synthetic lethality in haploid human cells. *Science, 350*(6264), 1092-1096. doi: 10.1126/science.aac7557

Bramsen, J. B., Laursen, M. B., Nielsen, A. F., Hansen, T. B., Bus, C., Langkjaer, N., . . . Kjems, J. (2009). A large-scale chemical modification screen identifies design rules to generate siRNAs with high activity, high stability and low toxicity. *Nucleic Acids Res, 37*(9), 2867-2881. doi: 10.1093/nar/gkp106

Ceppi, P., Hadji, A., Kohlhapp, FJ., Pattanayak, A., Hau, A., Xia, L., . . . Peter, M. E. (2014). CD95 and CD95L promote and protect cancer stem cells. *Nature Commun, 5*, 5238.

Cerami, E., Gao, J., Dogrusoz, U., Gross, B. E., Sumer, S. O., Aksoy, B. A., . . . Schultz, N. (2012). The cBio cancer genomics portal: an open platform for exploring multidimensional cancer genomics data. *Cancer Discov, 2*(5), 401-404. doi: 10.1158/2159-8290.CD-12-0095

Chan, K. T., Choi, M. Y., Lai, K. K., Tan, W., Tung, L. N., Lam, H. Y., . . . Law, S. (2014). Overexpression of transferrin receptor CD71 and its tumorigenic properties in esophageal squamous cell carcinoma. *Oncol Rep, 31*(3), 1296-1304. doi: 10.3892/or.2014.2981

Chen, L., Park, S. M., Tumanov, A. V., Hau, A., Sawada, K., Feig, C., . . . Peter, M. E. (2010). CD95 promotes tumour growth. *Nature, 465*(7297), 492-496.

Chiu, Y. L., & Rana, T. M. (2003). siRNA function in RNAi: a chemical modification analysis. *RNA, 9*(9), 1034-1048.

Cowley, G. S., Weir, B. A., Vazquez, F., Tamayo, P., Scott, J. A., Rusin, S., . . . Hahn, W. C. (2014). Parallel genome-scale loss of function screens in 216 cancer cell lines for the identification of context-specific genetic dependencies. *Sci Data, 1*, 140035. doi: 10.1038/sdata.2014.35

Dow, L. E., Premsrirut, P. K., Zuber, J., Fellmann, C., McJunkin, K., Miething, C., . . . Lowe, S. W. (2012). A pipeline for the generation of shRNA transgenic mice. *Nat Protoc, 7*(2), 374-393. doi: 10.1038/nprot.2011.446

Drachsler, M., Kleber, S., Mateos, A., Volk, K., Mohr, N., Chen, S., . . . Martin-Villalba, A. (2016). CD95 maintains stem cell-like and non-classical EMT programs in primary human glioblastoma cells. *Cell death & disease, 7*, e2209. doi: 10.1038/cddis.2016.102

Fedorov, Y., Anderson, E. M., Birmingham, A., Reynolds, A., Karpilow, J., Robinson, K., . . . Khvorova, A. (2006). Off-target effects by siRNA can induce toxic phenotype. *RNA, 12*(7), 1188-1196. doi: 10.1261/rna.28106

Friesen, C., Fulda, S., & Debatin, K. M. (1999). Cytotoxic drugs and the CD95 pathway. *Leukemia, 13*(11), 1854-1858.

Gao, J., Aksoy, B. A., Dogrusoz, U., Dresdner, G., Gross, B., Sumer, S. O., . . . Schultz, N. (2013). Integrative analysis of complex cancer genomics and clinical profiles using the cBioPortal. *Science signaling, 6*(269), pl1. doi: 10.1126/scisignal.2004088

Grimm, D., Streetz, K. L., Jopling, C. L., Storm, T. A., Pandey, K., Davis, C. R., . . . Kay, M. A. (2006). Fatality in mice due to oversaturation of cellular microRNA/short hairpin RNA pathways. *Nature, 441*(7092), 537-541. doi: 10.1038/nature04791

Gu, S., Jin, L., Zhang, Y., Huang, Y., Zhang, F., Valdmanis, P. N., & Kay, M. A. (2012). The loop position of shRNAs and pre-miRNAs is critical for the accuracy of dicer processing in vivo. *Cell, 151*(4), 900-911. doi: 10.1016/j.cell.2012.09.042

Gu, S., Zhang, Y., Jin, L., Huang, Y., Zhang, F., Bassik, M. C., . . . Kay, M. A. (2014). Weak base pairing in both seed and 3' regions reduces RNAi off-targets and enhances si/shRNA designs. *Nucleic Acids Res, 42*(19), 12169-12176. doi: 10.1093/nar/gku854

Gui, S., Sang, X., Zheng, L., Ze, Y., Zhao, X., Sheng, L., . . . Tang, M. (2013). Intragastric exposure to titanium dioxide nanoparticles induced nephrotoxicity in mice, assessed by physiological and gene expression modifications. *Part Fibre Toxicol, 10*, 4. doi: 10.1186/1743-8977-10-4

Guo, H., Ingolia, N. T., Weissman, J. S., & Bartel, D. P. (2010). Mammalian microRNAs predominantly act to decrease target mRNA levels. *Nature, 466*(7308), 835-840.

Ha, M., & Kim, V. N. (2014). Regulation of microRNA biogenesis. *Nat Rev Mol Cell Biol, 15*(8), 509-524. doi: 10.1038/nrm3838

Hadji, A., Ceppi, P., Murmann, A. E., Brockway, S., Pattanayak, A., Bhinder, B., . . . Peter, M.E. (2014). Death induced by CD95 or CD95 ligand elimination. *Cell Reports, 10*, 208-222.

Hart, T., Brown, K. R., Sircoulomb, F., Rottapel, R., & Moffat, J. (2014). Measuring error rates in genomic perturbation screens: gold standards for human functional genomics. *Mol Syst Biol, 10*, 733. doi: 10.15252/msb.20145216

Hart, T., Chandrashekhar, M., Aregger, M., Steinhart, Z., Brown, K. R., MacLeod, G., . . . Moffat, J. (2015). High-Resolution CRISPR Screens Reveal Fitness Genes and Genotype-Specific Cancer Liabilities. *Cell, 163*(6), 1515-1526. doi: 10.1016/j.cell.2015.11.015

Hou, F., Chu, C. W., Kong, X., Yokomori, K., & Zou, H. (2007). The acetyltransferase activity of San stabilizes the mitotic cohesin at the centromeres in a shugoshin-independent manner. *J Cell Biol, 177*(4), 587-597. doi: 10.1083/jcb.200701043

Jackson, A. L., Burchard, J., Schelter, J., Chau, B. N., Cleary, M., Lim, L., & Linsley, P. S. (2006). Widespread siRNA "off-target" transcript silencing mediated by seed region sequence complementarity. *RNA, 12*(7), 1179-1187. doi: 10.1261/rna.25706

Jang, M., Park, B. C., Kang, S., Chi, S. W., Cho, S., Chung, S. J., . . . Park, S. G. (2009). Far upstream element-binding protein-1, a novel caspase substrate, acts as a cross-talker

between apoptosis and the c-myc oncogene. *Oncogene, 28*(12), 1529-1536. doi: 10.1038/onc.2009.11

Jinek, M., East, A., Cheng, A., Lin, S., Ma, E., & Doudna, J. (2013). RNA-programmed genome editing in human cells. *Elife, 2*, e00471. doi: 10.7554/eLife.00471

Khan, A. A., Betel, D., Miller, M. L., Sander, C., Leslie, C. S., & Marks, D. S. (2009). Transfection of small RNAs globally perturbs gene regulation by endogenous microRNAs. *Nat Biotechnol, 27*(6), 549-555.

Kim, D. H., Behlke, M. A., Rose, S. D., Chang, M. S., Choi, S., & Rossi, J. J. (2005). Synthetic dsRNA Dicer substrates enhance RNAi potency and efficacy. *Nat Biotechnol, 23*(2), 222-226. doi: 10.1038/nbt1051

Kim, Y. K., Kim, B., & Kim, V. N. (2016). Re-evaluation of the roles of DROSHA, Export in 5, and DICER in microRNA biogenesis. *Proc Natl Acad Sci U S A, 113*(13), E1881-1889. doi: 10.1073/pnas.1602532113

Kleber, S., Sancho-Martinez, I., Wiestler, B., Beisel, A., Gieffers, C., Hill, O., . . . Martin-Villalba, A. (2008). Yes and PI3K Bind CD95 to Signal Invasion of Glioblastoma. *Cancer Cell, 13*(3), 235-248.

Krammer, P. H. (2000). CD95's deadly mission in the immune system. *Nature, 407*(6805), 789-795.

Krol, J., Loedige, I., & Filipowicz, W. (2010). The widespread regulation of microRNA biogenesis, function and decay. *Nat Rev Genet, 11*(9), 597-610.

Lin, X., Ruan, X., Anderson, M. G., McDowell, J. A., Kroeger, P. E., Fesik, S. W., & Shen, Y. (2005). siRNA-mediated off-target gene silencing triggered by a 7 nt complementation. *Nucleic Acids Res, 33*(14), 4527-4535. doi: 10.1093/nar/gki762

Lu, J., Getz, G., Miska, E.A., varez-Saavedra, E., Lamb, J., Peck, D., . . . Golub, T.R. (2005). MicroRNA expression profiles classify human cancers. *Nature, 435*(7043), 834-838.

Mali, P., Yang, L., Esvelt, K. M., Aach, J., Guell, M., DiCarlo, J. E., . . . Church, G. M. (2013). RNA-guided human genome engineering via Cas9. *Science, 339*(6121), 823-826. doi: 10.1126/science.1232033

Marques, J. T., & Williams, B. R. (2005). Activation of the mammalian immune system by siRNAs. *Nat Biotechnol, 23*(11), 1399-1405. doi: 10.1038/nbt1161

Medina-Rivera, A., Defrance, M., Sand, O., Herrmann, C., Castro-Mondragon, J. A., Delerce, J., . . . van Helden, J. (2015). RSAT 2015: Regulatory Sequence Analysis Tools. *Nucleic Acids Res, 43*(W1), W50-56. doi: 10.1093/nar/gkv362

Mi, N., Chen, Y., Wang, S., Chen, M., Zhao, M., Yang, G., . . . Yu, L. (2015). CapZ regulates autophagosomal membrane shaping by promoting actin assembly inside the isolation membrane. *Nat Cell Biol, 17*(9), 1112-1123. doi: 10.1038/ncb3215

Morgens, D. W., Deans, R. M., Li, A., & Bassik, M. C. (2016). Systematic comparison of CRISPR/Cas9 and RNAi screens for essential genes. *Nat Biotechnol, 34*(6), 634-636. doi: 10.1038/nbt.3567

Morgulis, A., Gertz, E. M., Schaffer, A. A., & Agarwala, R. (2006). A fast and symmetric DUST implementation to mask low-complexity DNA sequences. *J Comput Biol, 13*(5), 1028-1040. doi: 10.1089/cmb.2006.13.1028

Murmann, A. E., McMahon, K. M., Halluck-Kangas, A., Ravindran, N., Patel, M., Law, C., . . . Peter, M. E. (2017). Induction of DISE in ovarian cancer cells in vivo. *BioRxive*.

Parplys, A. C., Zhao, W., Sharma, N., Groesser, T., Liang, F., Maranon, D. G., . . . Wiese, C. (2015). NUCKS1 is a novel RAD51AP1 paralog important for homologous recombination and genome stability. *Nucleic Acids Res, 43*(20), 9817-9834. doi: 10.1093/nar/gkv859

Patel, M., & Peter, M.E. (2017). Identification of DISE-inducing shRNAs by monitoring cellular responses. *BioRxive*.

Peter, M. E., Budd, R. C., Desbarats, J., Hedrick, S. M., Hueber, A. O., Newell, M. K., . . . Lynch, D. H. (2007). The CD95 receptor: apoptosis revisited. *Cell, 129*(3), 447-450.

Petri, S., & Meister, G. (2013). siRNA design principles and off-target effects. *Methods Mol Biol, 986*, 59-71. doi: 10.1007/978-1-62703-311-4_4

Pham, D. H., Moretti, P. A., Goodall, G. J., & Pitson, S. M. (2008). Attenuation of leakiness in doxycycline-inducible expression via incorporation of 3' AU-rich mRNA destabilizing elements. *Biotechniques, 45*(2), 155-156. doi: 10.2144/000112896

Pham, D. H., Powell, J. A., Gliddon, B. L., Moretti, P. A., Tsykin, A., Van der Hoek, M., . . . Pitson, S. M. (2014). Enhanced expression of transferrin receptor 1 contributes to oncogenic signalling by sphingosine kinase 1. *Oncogene, 33*(48), 5559-5568. doi: 10.1038/onc.2013.502

Pratt, A. J., & MacRae, I. J. (2009). The RNA-induced silencing complex: a versatile gene-silencing machine. *J Biol Chem, 284*(27), 17897-17901. doi: 10.1074/jbc.R900012200

Qadir, A. S., Ceppi, P., Brockway, S., Law, C., Mu, L., Khodarev, N. N., . . . Peter, M. E. (2017). CD95/Fas Increases Stemness in Cancer Cells by Inducing a STAT1-Dependent Type I Interferon Response. *Cell Rep, 18*(10), 2373-2386. doi: 10.1016/j.celrep.2017.02.037

Quidville, V., Alsafadi, S., Goubar, A., Commo, F., Scott, V., Pioche-Durieu, C., . . . Andre, F. (2013). Targeting the deregulated spliceosome core machinery in cancer cells triggers mTOR blockade and autophagy. *Cancer Res, 73*(7), 2247-2258. doi: 10.1158/0008-5472.CAN-12-2501

Rabenhorst, U., Thalheimer, F. B., Gerlach, K., Kijonka, M., Bohm, S., Krause, D. S., . . . Zornig, M. (2015). Single-Stranded DNA-Binding Transcriptional Regulator FUBP1 Is Essential for Fetal and Adult Hematopoietic Stem Cell Self-Renewal. *Cell Rep, 11*(12), 1847-1855. doi: 10.1016/j.celrep.2015.05.038

Robbins, M. A., Li, M., Leung, I., Li, H., Boyer, D. V., Song, Y., . . . Rossi, J. J. (2006). Stable expression of shRNAs in human CD34+ progenitor cells can avoid induction of interferon responses to siRNAs in vitro. *Nat Biotechnol, 24*(5), 566-571. doi: 10.1038/nbt1206

Schoggins, J. W., Wilson, S. J., Panis, M., Murphy, M. Y., Jones, C. T., Bieniasz, P., & Rice, C. M. (2011). A diverse range of gene products are effectors of the type I interferon antiviral response. *Nature, 472*(7344), 481-485. doi: 10.1038/nature09907

Shao, D. D., Tsherniak, A., Gopal, S., Weir, B. A., Tamayo, P., Stransky, N., . . . Mesirov, J. P. (2013). ATARiS: computational quantification of gene suppression phenotypes from multisample RNAi screens. *Genome Res, 23*(4), 665-678. doi: 10.1101/gr.143586.112

Siomi, H., & Siomi, M. C. (2009). On the road to reading the RNA-interference code. *Nature, 457*(7228), 396-404. doi: 10.1038/nature07754

Stark, A., Brennecke, J., Bushati, N., Russell, R. B., & Cohen, S. M. (2005). Animal MicroRNAs confer robustness to gene expression and have a significant impact on 3'UTR evolution. *Cell, 123*(6), 1133-1146. doi: 10.1016/j.cell.2005.11.023

Sun, D., Zhou, M., Kowolik, C. M., Trisal, V., Huang, Q., Kernstine, K. H., . . . Shen, B. (2011). Differential expression patterns of capping protein, protein phosphatase 1, and casein kinase 1 may serve as diagnostic markers for malignant melanoma. *Melanoma Res, 21*(4), 335-343. doi: 10.1097/CMR.0b013e328346b715

Teitz, T., Wei, T., Valentine, M. B., Vanin, E. F., Grenet, J., Valentine, V. A., . . . Kidd, V. J. (2000). Caspase 8 is deleted or silenced preferentially in childhood neuroblastomas with amplification of MYCN. *Nat Med, 6*(5), 529-535.

Ting, A. H., Suzuki, H., Cope, L., Schuebel, K. E., Lee, B. H., Toyota, M., . . . Baylin, S. B. (2008). A requirement for DICER to maintain full promoter CpG island hypermethylation in human cancer cells. *Cancer Res, 68*(8), 2570-2575. doi: 10.1158/0008-5472.CAN-07-6405

Ui-Tei, K., Naito, Y., Takahashi, F., Haraguchi, T., Ohki-Hamazaki, H., Juni, A., . . . Saigo, K. (2004). Guidelines for the selection of highly effective siRNA sequences for mammalian and chick RNA interference. *Nucleic Acids Res, 32*(3), 936-948. doi: 10.1093/nar/gkh247

van Dongen, S., Abreu-Goodger, C., & Enright, A. J. (2008). Detecting microRNA binding and siRNA off-target effects from expression data. *Nat Methods, 5*(12), 1023-1025. doi: 10.1038/nmeth.1267

Wang, T., Birsoy, K., Hughes, N. W., Krupczak, K. M., Post, Y., Wei, J. J., . . . Sabatini, D. M. (2015). Identification and characterization of essential genes in the human genome. *Science, 350*(6264), 1096-1101. doi: 10.1126/science.aac7041

Watanabe, C., Cuellar, T. L., & Haley, B. (2016). Quantitative evaluation of first, second, and third generation hairpin systems reveals the limit of mammalian vector-based RNAi. *RNA Biol, 13*(1), 25-33. doi: 10.1080/15476286.2015.1128062

Wazir, U., Jiang, W. G., Sharma, A. K., & Mokbel, K. (2013). Guanine nucleotide binding protein beta 1: a novel transduction protein with a possible role in human breast cancer. *Cancer Genomics Proteomics, 10*(2), 69-73.

Yoo, J. K., Choi, S. J., & Kim, J. K. (2013). Expression profiles of subtracted mRNAs during cellular senescence in human mesenchymal stem cells derived from bone marrow. *Exp Gerontol, 48*(5), 464-471. doi: 10.1016/j.exger.2013.02.022

Zamore, P. D., Tuschl, T., Sharp, P. A., & Bartel, D. P. (2000). RNAi: double-stranded RNA directs the ATP-dependent cleavage of mRNA at 21 to 23 nucleotide intervals. *Cell, 101*(1), 25-33. doi: 10.1016/S0092-8674(00)80620-0

Zare, H., Khodursky, A., & Sartorelli, V. (2014). An evolutionarily biased distribution of miRNA sites toward regulatory genes with high promoter-driven intrinsic transcriptional noise. *BMC Evol Biol, 14*, 74. doi: 10.1186/1471-2148-14-74

Zhang, Y., Wang, Y., Wei, Y., Wu, J., Zhang, P., Shen, S., . . . Yu, L. (2016). Molecular chaperone CCT3 supports proper mitotic progression and cell proliferation in hepatocellular carcinoma cells. *Cancer Lett, 372*(1), 101-109. doi: 10.1016/j.canlet.2015.12.029

Figure 1

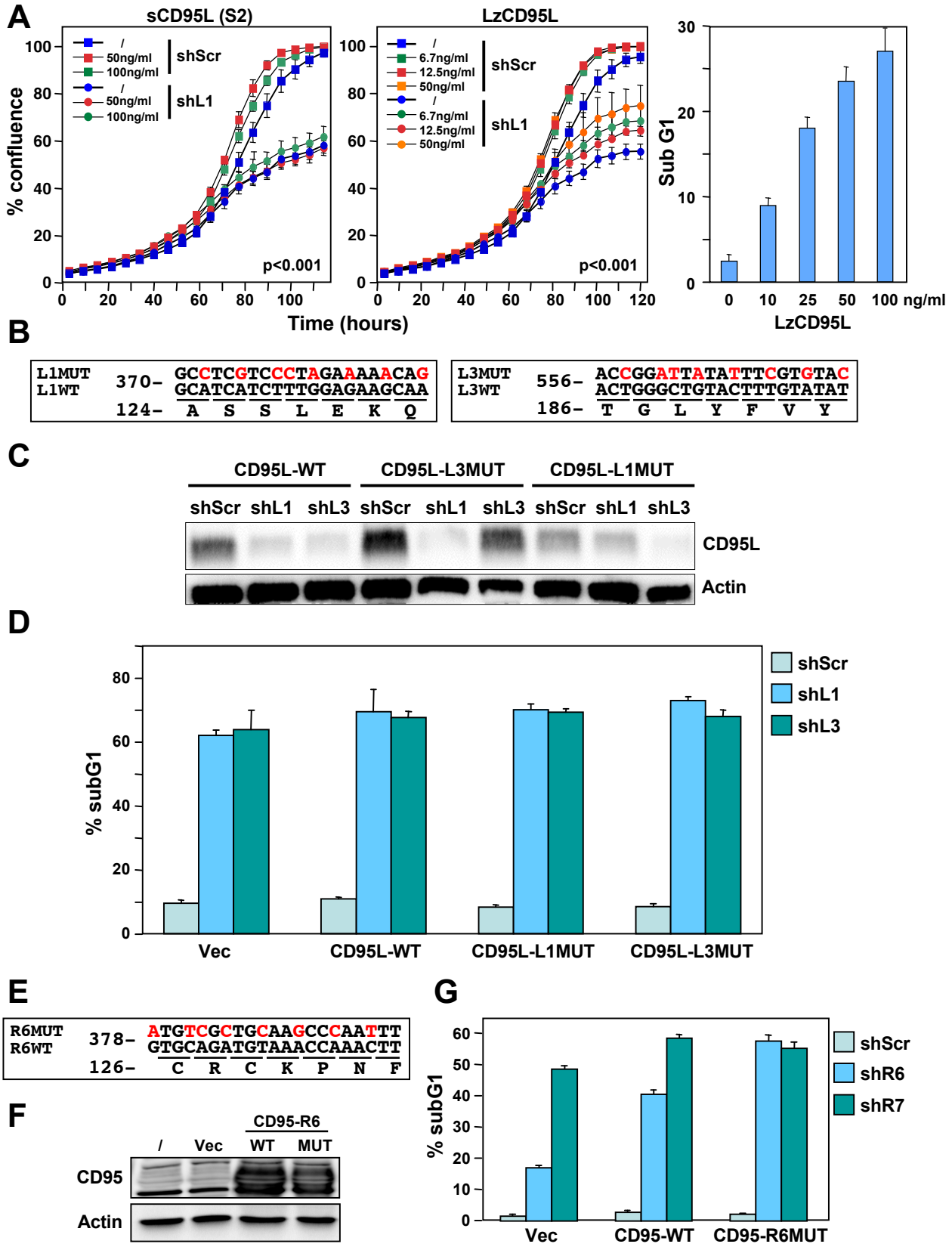
A
sCD95L (S2)
LzCD95L
% confluence
Time (hours)
shScr
shL1
/
50ng/ml
100ng/ml
6.7ng/ml
12.5ng/ml
p<0.001
Sub G1
LzCD95L
0 10 25 50 100 ng/ml
B
L1MUT 370- GCCTCGTCCCTAGAAAAACAG
L1WT GCATCATCTTTGGAGAAGCAA
124- A S S L E K Q
L3MUT 556- ACCGGATTATATTTCGTGTAC
L3WT ACTGGGCTGTACTTTGTATAT
186- T G L Y F V Y
C
CD95L-WT
CD95L-L3MUT
CD95L-L1MUT
shScr shL1 shL3 shScr shL1 shL3 shScr shL1 shL3
CD95L
Actin
D
% subG1
shScr
shL1
shL3
Vec
CD95L-WT
CD95L-L1MUT
CD95L-L3MUT
E
R6MUT 378- ATGTCGCTGCAAGCCCAATTT
R6WT GTGCAGATGTAAACCAAACTT
126- C R C K P N F
F
CD95-R6
/ Vec WT MUT
CD95
Actin
G
% subG1
shScr
shR6
shR7
Vec
CD95-WT
CD95-R6MUT

Figure 1 - figure supplement 1

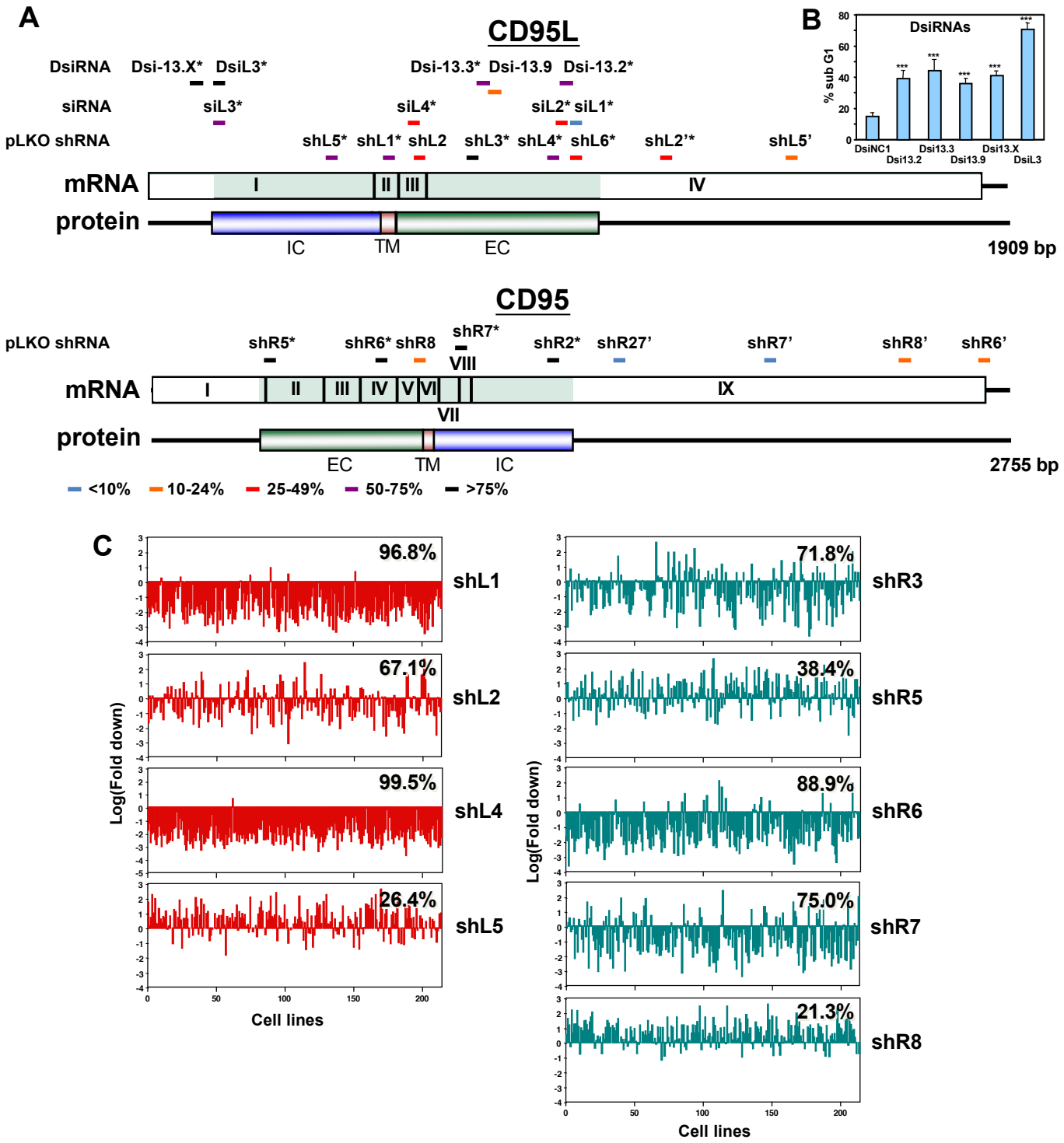

Figure 1 - figure supplement 2

A

```
shL1 - GCATCATCTTTGGAGAAGCAA        shR5 - GTTGCTAGATTATCGTCCAAA
shL3 - ACTGGGCTGTACTTTGTATAT        shR6 - GTGCAGATGTAAACCAAACTT
shL4 - GCAGTGTTCAATCTTACCAGT        shR7 - CCTGAAACAGTGGCAATAAAT
```

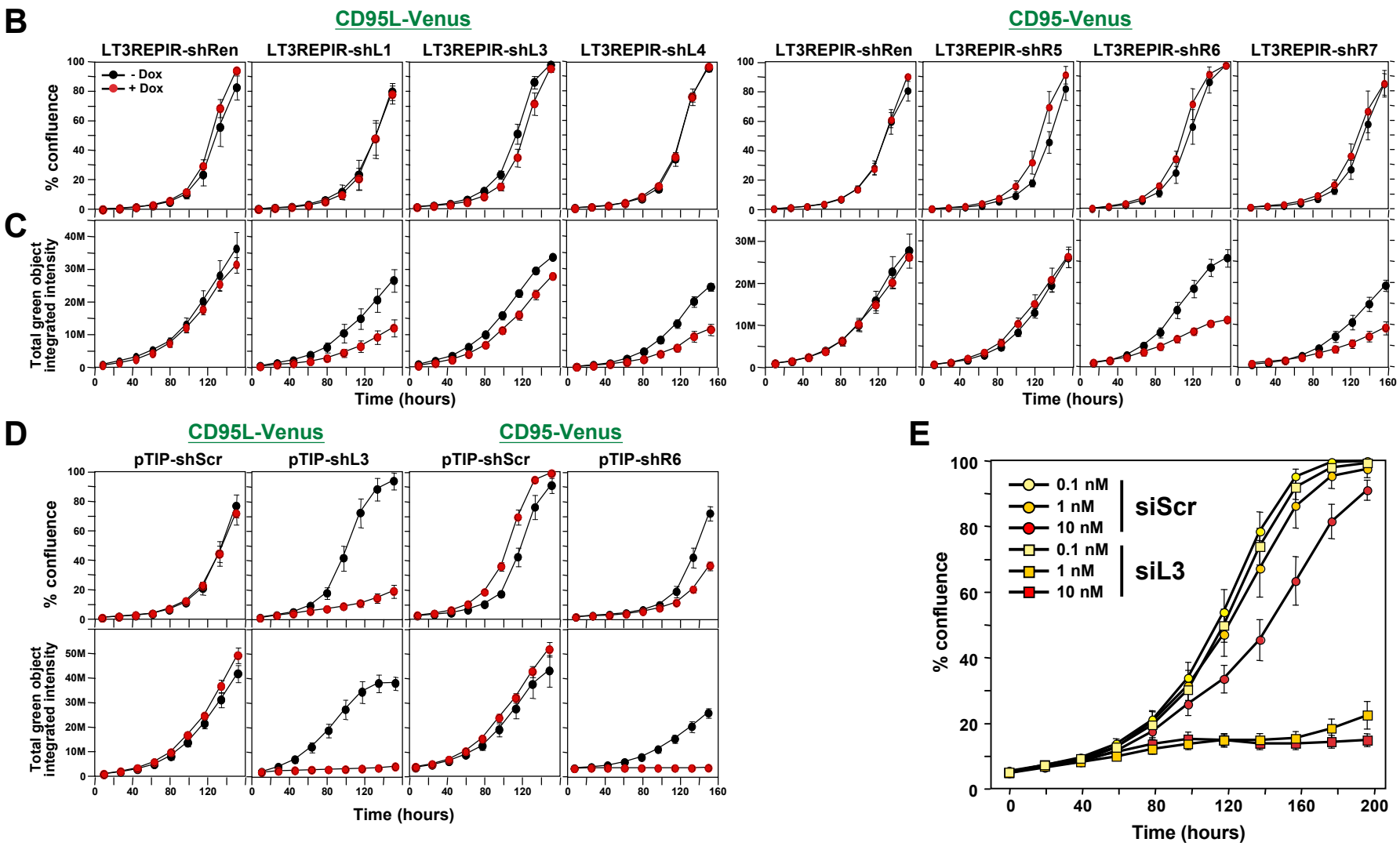

Figure 2

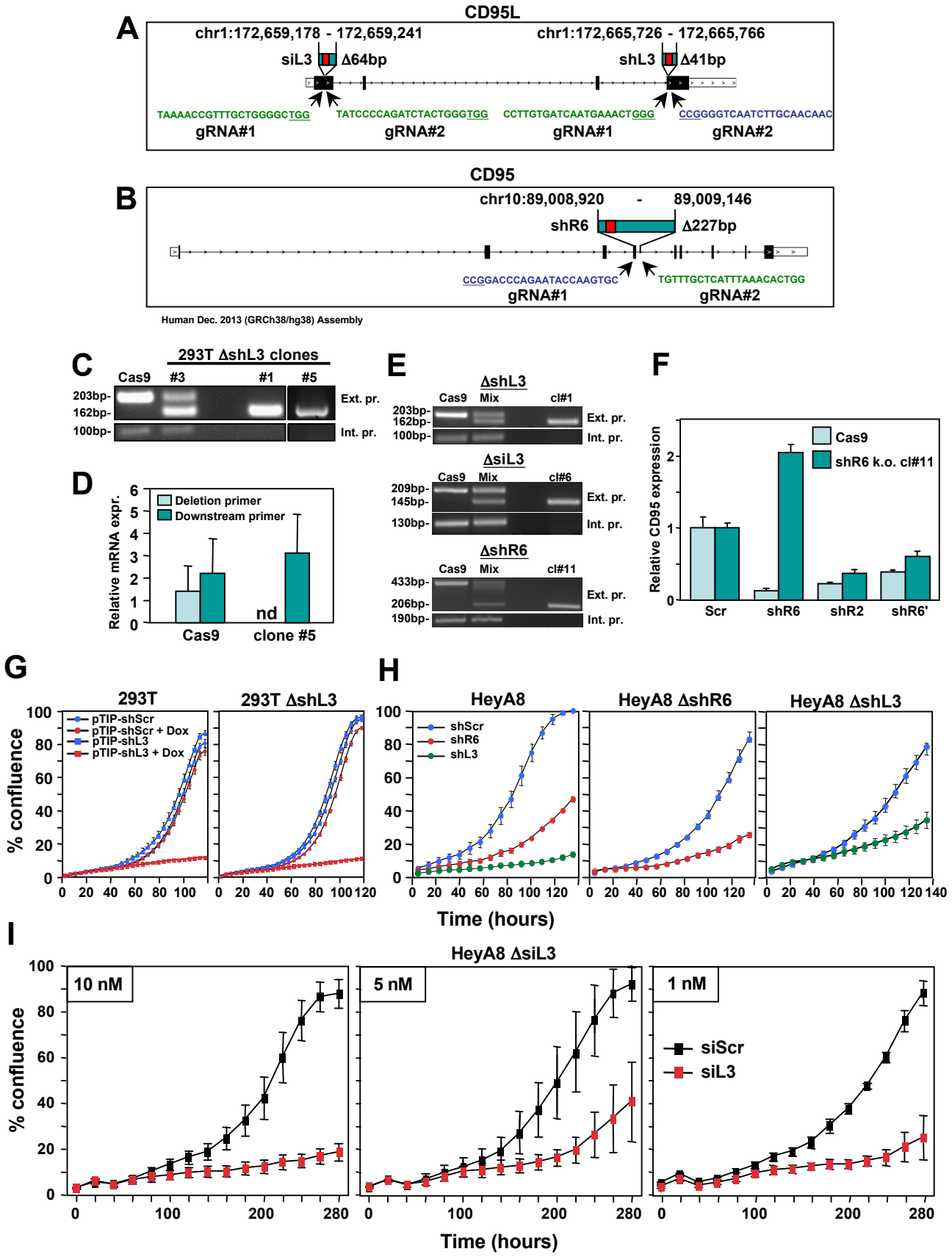
A
CD95L
chr1:172,659,178 - 172,659,241
chr1:172,665,726 - 172,665,766
siL3
Δ64bp
shL3
Δ41bp
TAAAACCGTTTGCTGGGGCTGG
TATCCCCAGATCTACTGGGTGG
CCTTGTGATCAATGAAACTGGG
CCGGGGTCAATCTTGCAACAAC
gRNA#1
gRNA#2
gRNA#1
gRNA#2
B
CD95
chr10:89,008,920 - 89,009,146
shR6
Δ227bp
CCGGACCCAGAATACCAAGTGC
TGTTTGCTCATTTAAACACTGG
gRNA#1
gRNA#2
Human Dec. 2013 (GRCh38/hg38) Assembly
C
293T ΔshL3 clones
Cas9
#3
#1
#5
203bp-
162bp-
100bp-
Ext. pr.
Int. pr.
D
Relative mRNA expr.
Deletion primer
Downstream primer
nd
Cas9
clone #5
E
ΔshL3
Cas9
Mix
cl#1
203bp-
162bp-
100bp-
Ext. pr.
Int. pr.
ΔsiL3
Cas9
Mix
cl#6
209bp-
145bp-
130bp-
Ext. pr.
Int. pr.
ΔshR6
Cas9
Mix
cl#11
433bp-
206bp-
190bp-
Ext. pr.
Int. pr.
F
Relative CD95 expression
Cas9
shR6 k.o. cl#11
Scr
shR6
shR2
shR6'
G
293T
293T ΔshL3
% confluence
pTIP-shScr
pTIP-shScr + Dox
pTIP-shL3
pTIP-shL3 + Dox
H
HeyA8
HeyA8 ΔshR6
HeyA8 ΔshL3
shScr
shR6
shL3
Time (hours)
I
HeyA8 ΔsiL3
% confluence
10 nM
5 nM
1 nM
siScr
siL3
Time (hours)

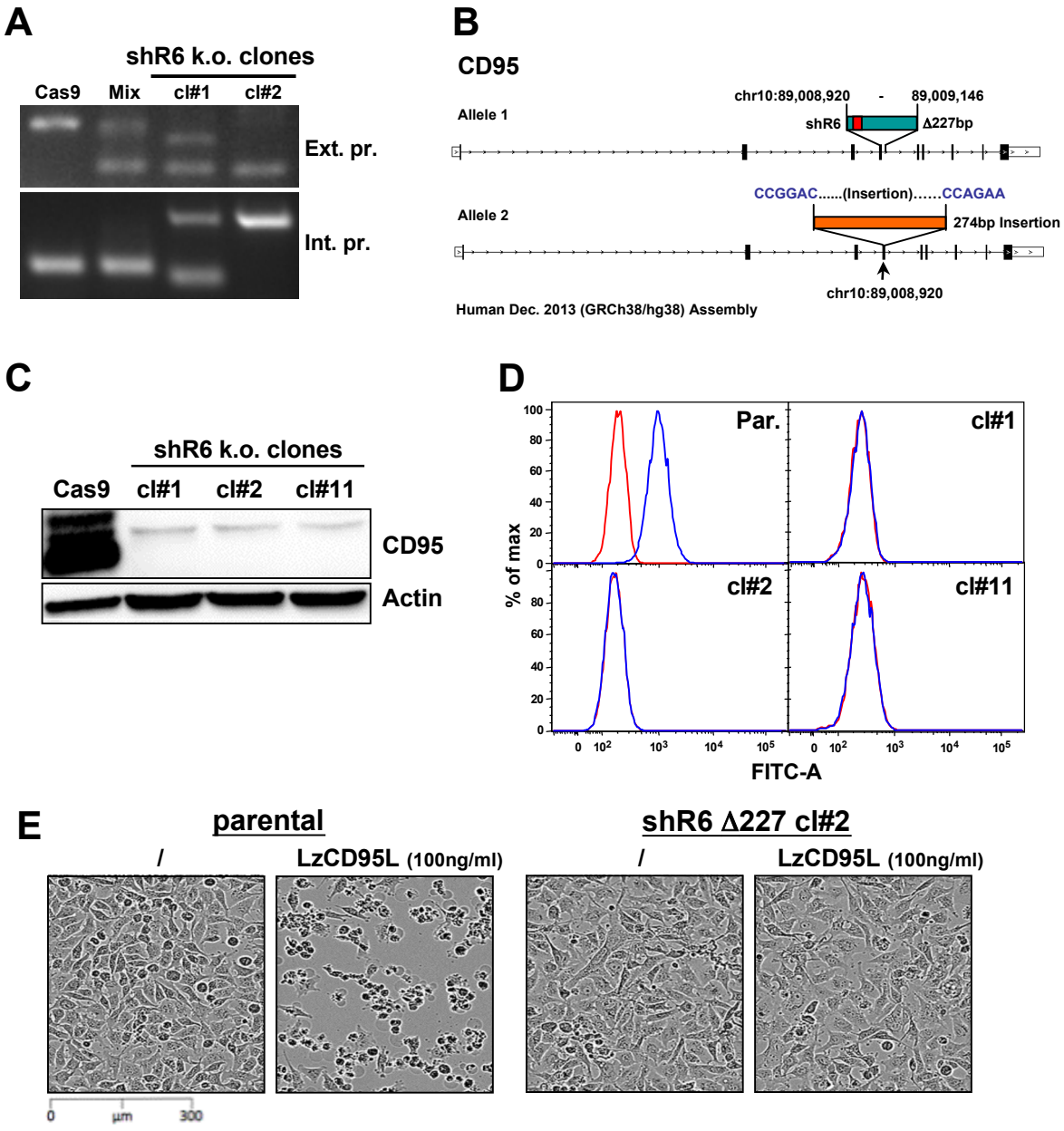
A
shR6 k.o. clones
Cas9
Mix
cl#1
cl#2
Ext. pr.
Int. pr.
B
CD95
chr10:89,008,920 - 89,009,146
Allele 1
shR6
Δ227bp
CCGGAC.....(Insertion).....CCAGAA
Allele 2
274bp Insertion
chr10:89,008,920
Human Dec. 2013 (GRCh38/hg38) Assembly
C
shR6 k.o. clones
Cas9
cl#1
cl#2
cl#11
CD95
Actin
D
Par.
cl#1
cl#2
cl#11
% of max
FITC-A
E
parental
shR6 Δ227 cl#2
/
LzCD95L (100ng/ml)
/
LzCD95L (100ng/ml)
0
µm
300

Figure 3

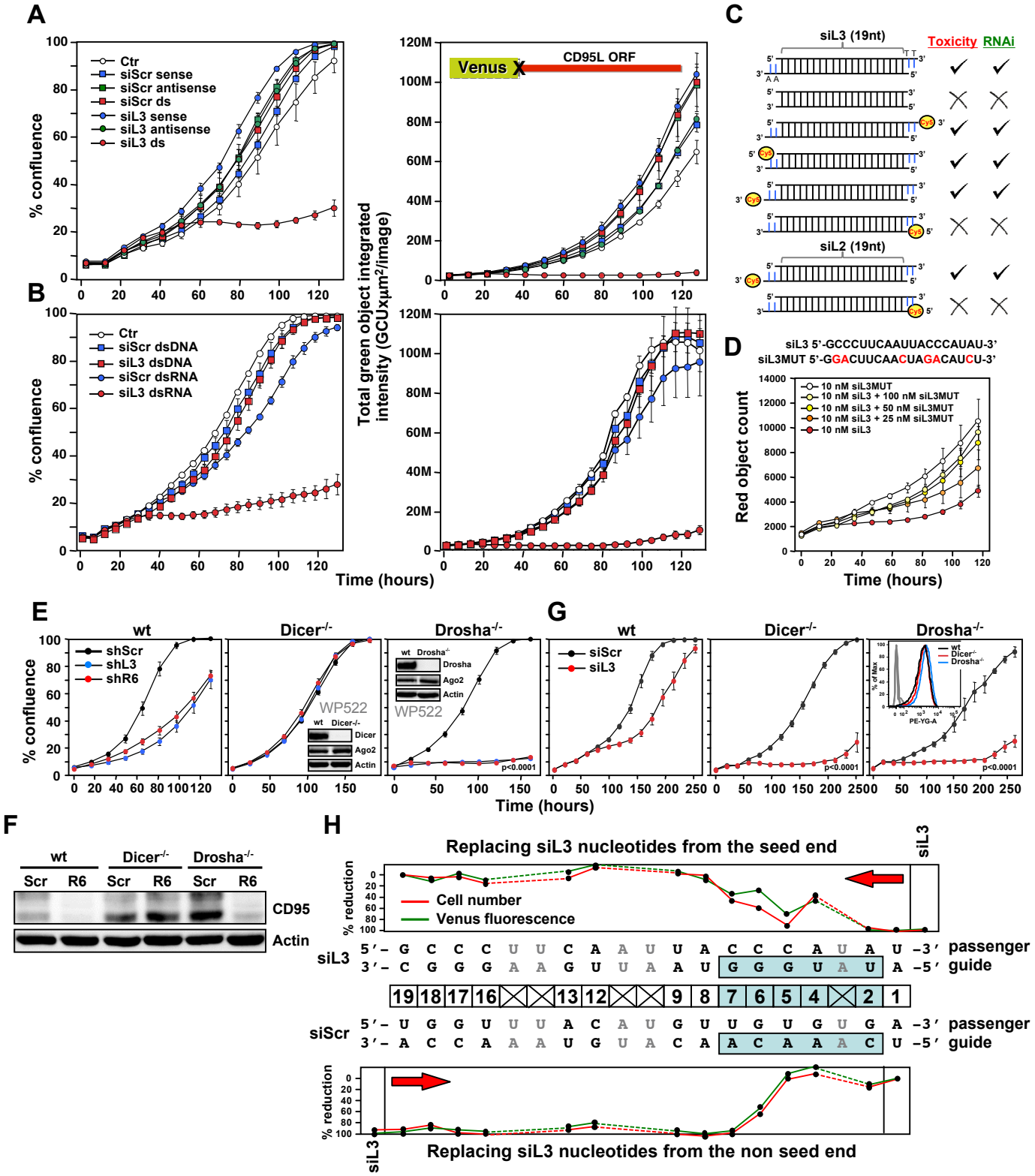
A
B
C
D
E
F
G
H
% confluence
Total green object integrated intensity (GCUxμm²/image)
Time (hours)
Ctr
siScr sense
siScr antisense
siScr ds
siL3 sense
siL3 antisense
siL3 ds
siScr dsDNA
siL3 dsDNA
siScr dsRNA
siL3 dsRNA
Venus
CD95L ORF
siL3 (19nt)
siL2 (19nt)
Toxicity
RNAi
siL3 5'-GCCCUUCAAUUACCCAUAU-3'
siL3MUT 5'-GGACUUCAACUAGACAUCU-3'
Red object count
10 nM siL3MUT
10 nM siL3 + 100 nM siL3MUT
10 nM siL3 + 50 nM siL3MUT
10 nM siL3 + 25 nM siL3MUT
10 nM siL3
wt
Dicer-/-
Drosha-/-
shScr
shL3
shR6
siScr
siL3
WP522
Drosha
Ago2
Actin
Dicer
p<0.0001
PE-YG-A
% of Max
Scr
R6
CD95
Replacing siL3 nucleotides from the seed end
Cell number
Venus fluorescence
% reduction
siL3
passenger
guide
siScr
Replacing siL3 nucleotides from the non seed end

Figure 4

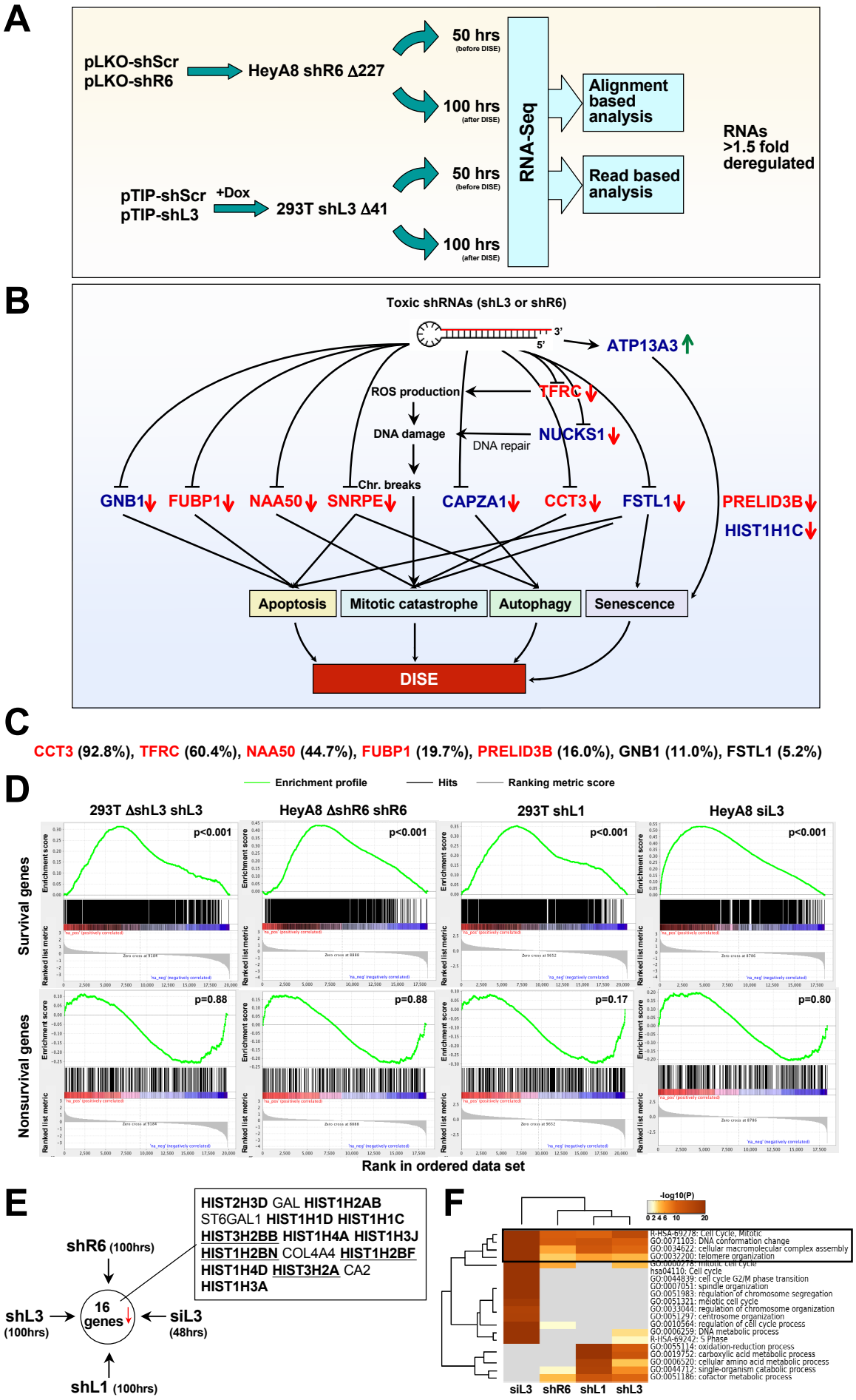
A
pLKO-shScr
pLKO-shR6
HeyA8 shR6 Δ227
pTIP-shScr
pTIP-shL3
+Dox
293T shL3 Δ41
50 hrs (before DISE)
100 hrs (after DISE)
50 hrs (before DISE)
100 hrs (after DISE)
RNA-Seq
Alignment based analysis
Read based analysis
RNAs >1.5 fold deregulated
B
Toxic shRNAs (shL3 or shR6)
3'
5'
ATP13A3
ROS production
TFRC
DNA damage
NUCKS1
DNA repair
Chr. breaks
GNB1
FUBP1
NAA50
SNRPE
CAPZA1
CCT3
FSTL1
PRELID3B
HIST1H1C
Apoptosis
Mitotic catastrophe
Autophagy
Senescence
DISE
C
CCT3 (92.8%), TFRC (60.4%), NAA50 (44.7%), FUBP1 (19.7%), PRELID3B (16.0%), GNB1 (11.0%), FSTL1 (5.2%)
D
Enrichment profile
Hits
Ranking metric score
293T ΔshL3 shL3
HeyA8 ΔshR6 shR6
293T shL1
HeyA8 siL3
Survival genes
Nonsurvival genes
p<0.001
p<0.001
p<0.001
p<0.001
p=0.88
p=0.88
p=0.17
p=0.80
Enrichment score
Ranked list metric
Rank in ordered data set
E
shR6 (100hrs)
shL3 (100hrs)
16 genes
siL3 (48hrs)
shL1 (100hrs)
HIST2H3D GAL HIST1H2AB
ST6GAL1 HIST1H1D HIST1H1C
HIST3H2BB HIST1H4A HIST1H3J
HIST1H2BN COL4A4 HIST1H2BF
HIST1H4D HIST3H2A CA2
HIST1H3A
F
-log10(P)
0 2 4 6 10 20
R-HSA-69278: Cell Cycle, Mitotic
GO:0071103: DNA conformation change
GO:0034622: cellular macromolecular complex assembly
GO:0032200: telomere organization
GO:0000278: mitotic cell cycle
hsa04110: Cell cycle
GO:0044839: cell cycle G2/M phase transition
GO:0007051: spindle organization
GO:0051983: regulation of chromosome segregation
GO:0051321: meiotic cell cycle
GO:0033044: regulation of chromosome organization
GO:0051297: centrosome organization
GO:0010564: regulation of cell cycle process
GO:0006259: DNA metabolic process
R-HSA-69242: S Phase
GO:0055114: oxidation-reduction process
GO:0019752: carboxylic acid metabolic process
GO:0006520: cellular amino acid metabolic process
GO:0044712: single-organism catabolic process
GO:0051186: cofactor metabolic process
siL3
shR6
shL1
shL3

Figure 4 - figure supplement 1

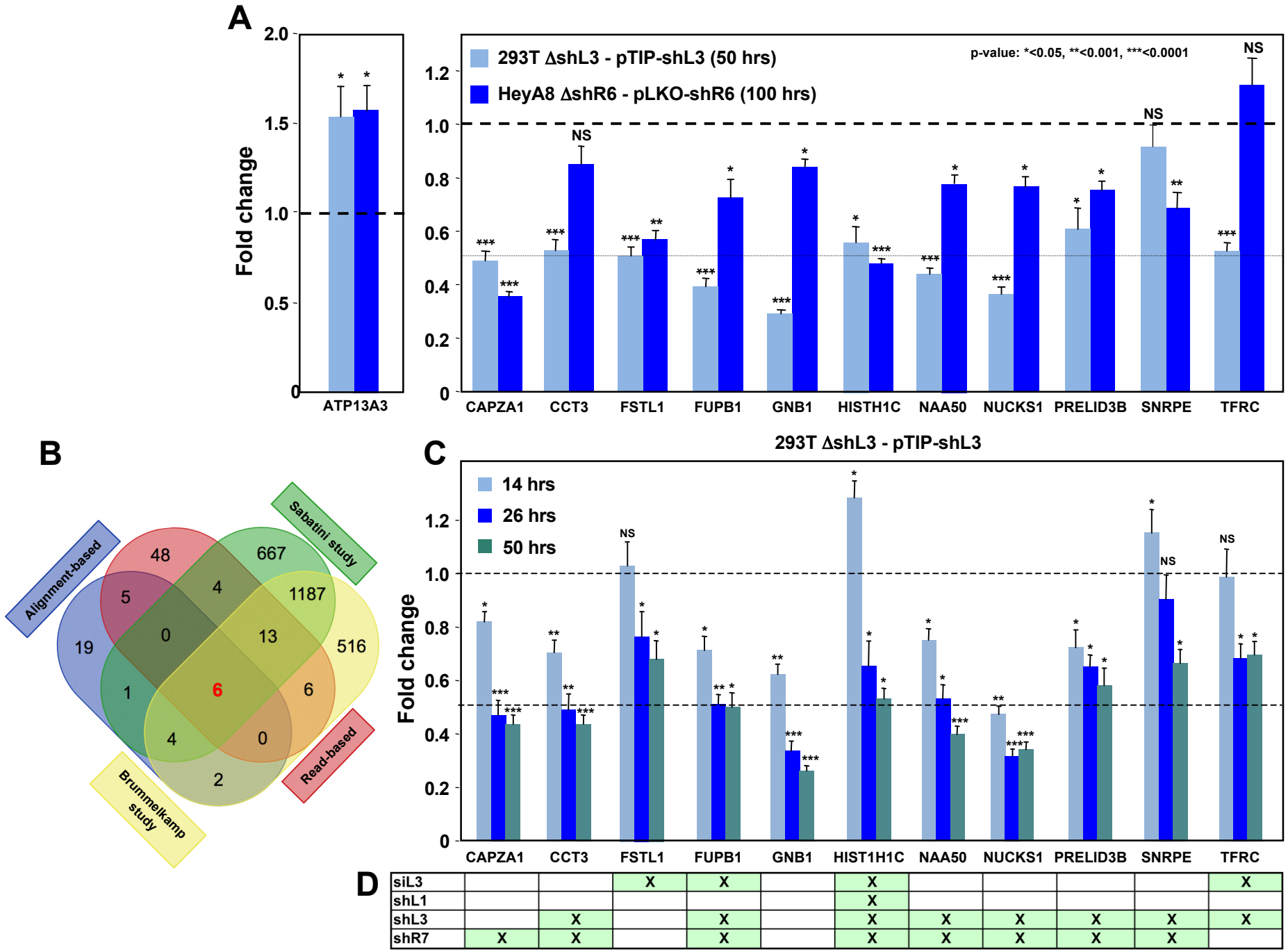

Figure 4 - figure supplement 2

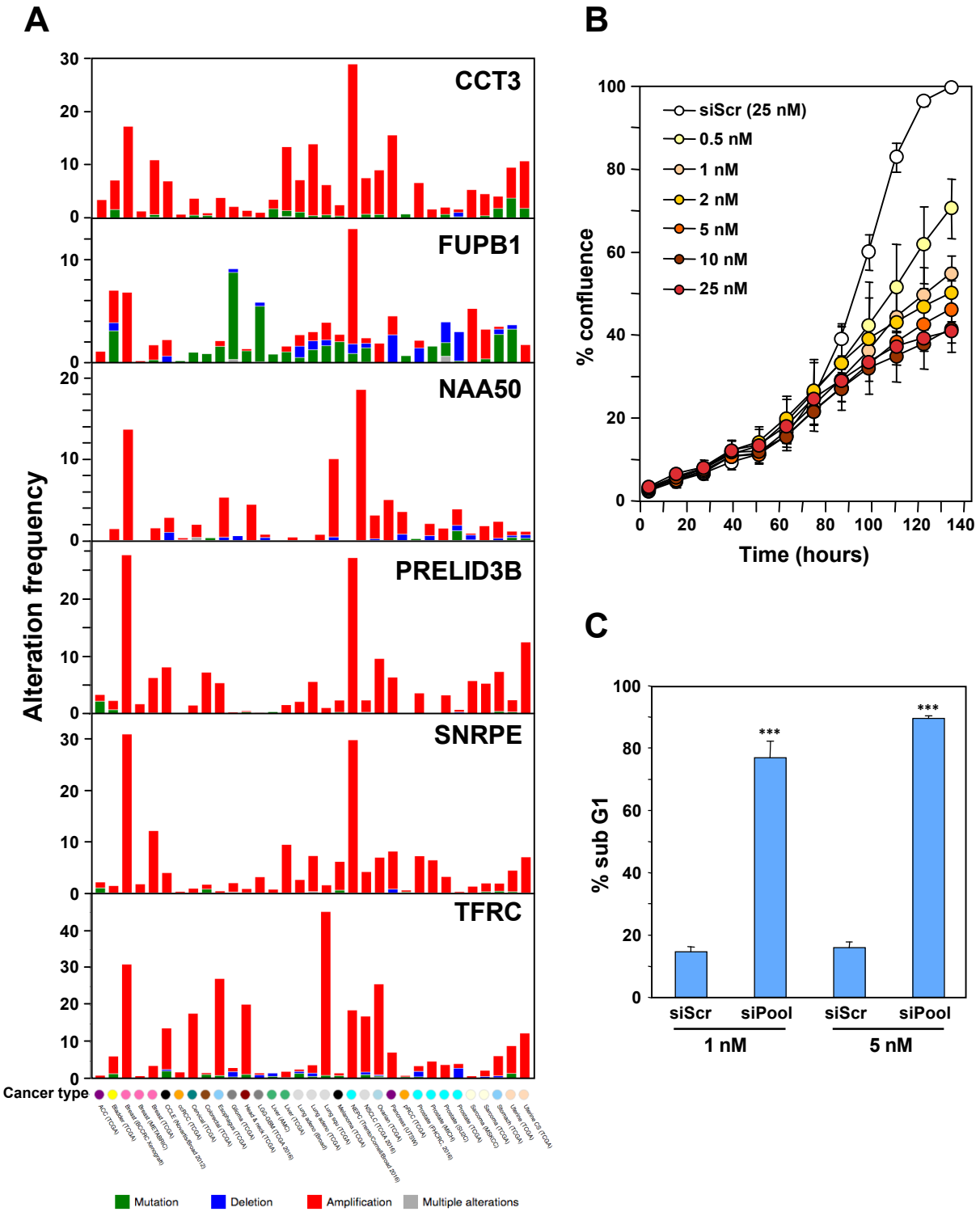

Figure 4 - figure supplement 3

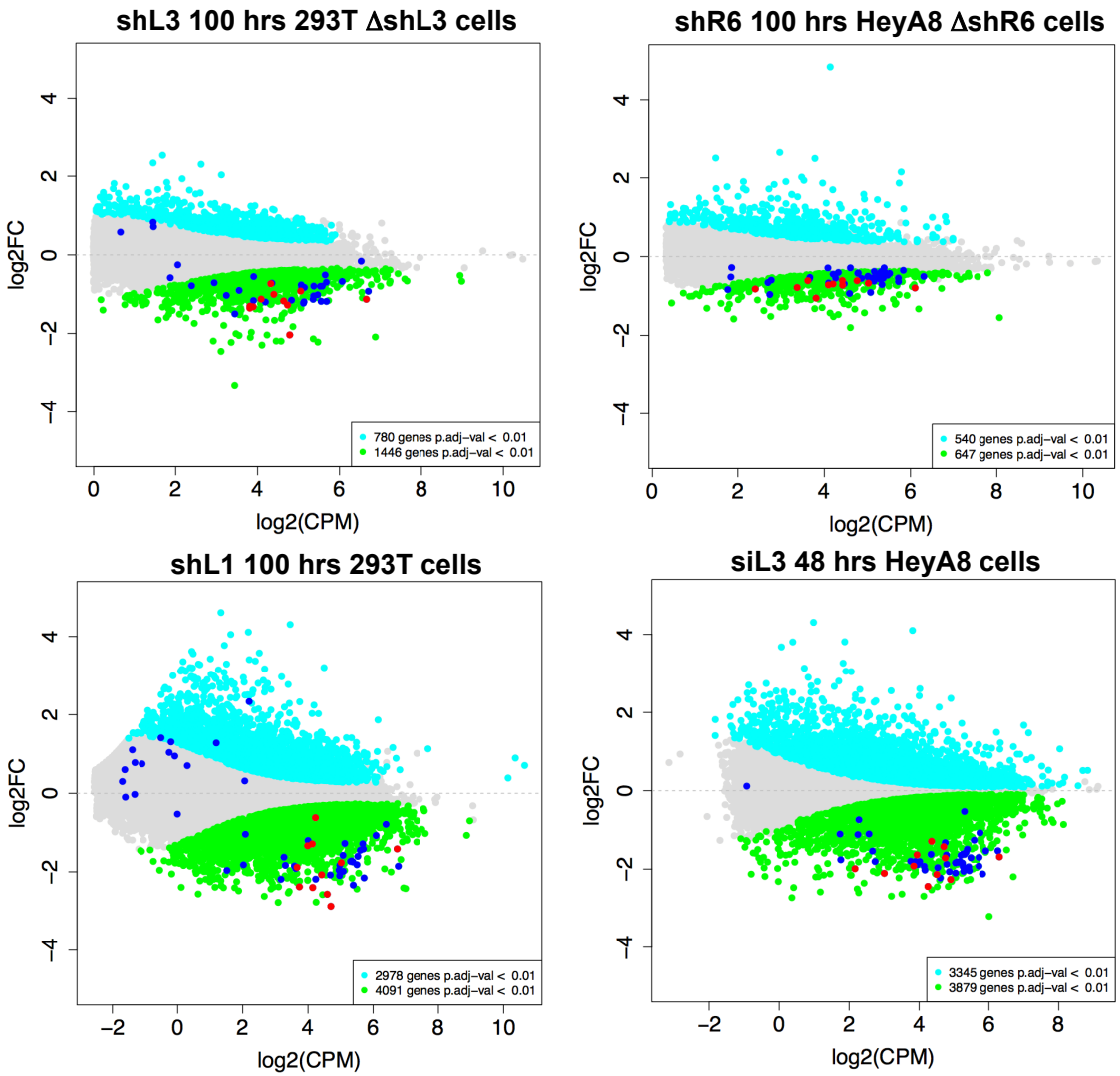

Figure 5

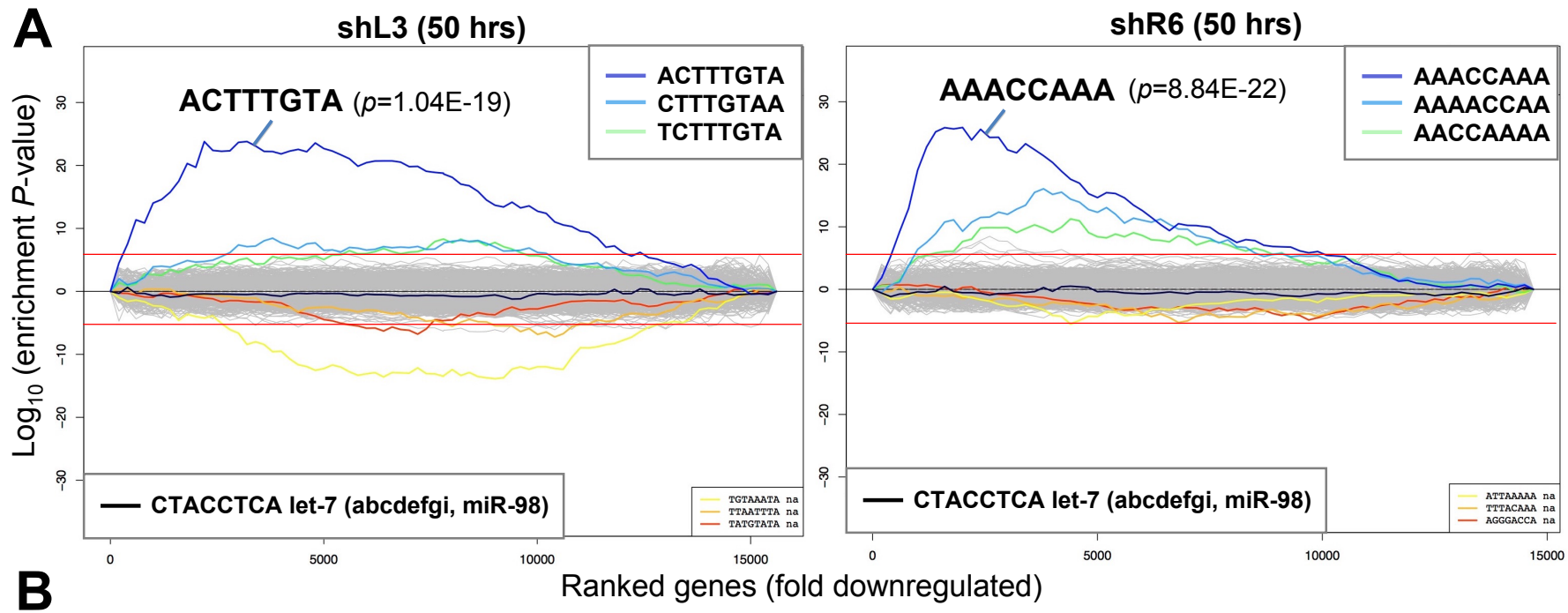

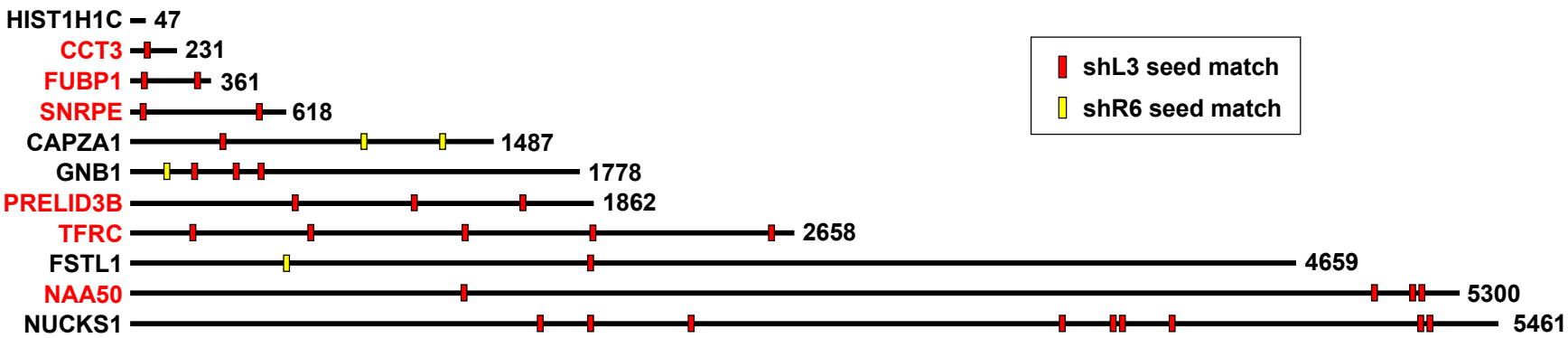

C

Downregulated

		shL3 (50hrs) No	shL3 (50hrs) Yes	shL3 (100hrs) No	shL3 (100hrs) Yes	shR6 (50hrs) No	shR6 (50hrs) Yes	shR6 (100hrs) No	shR6 (100hrs) Yes	shL1 (100hrs) No	shL1 (100hrs) Yes	siL3 (48hrs) No	siL3 (48hrs) Yes
Seed match present	No	825	2	783	48	1113	13	1108	16	600	189	1205	238
	Yes	904	55	850	109	612	40	619	31	746	259	244	93
	P-value	2.83E-13		2.58E-05		6.65E-09		4.31E-05		0.38		5.74E-06	

Figure 5 - figure supplement 1

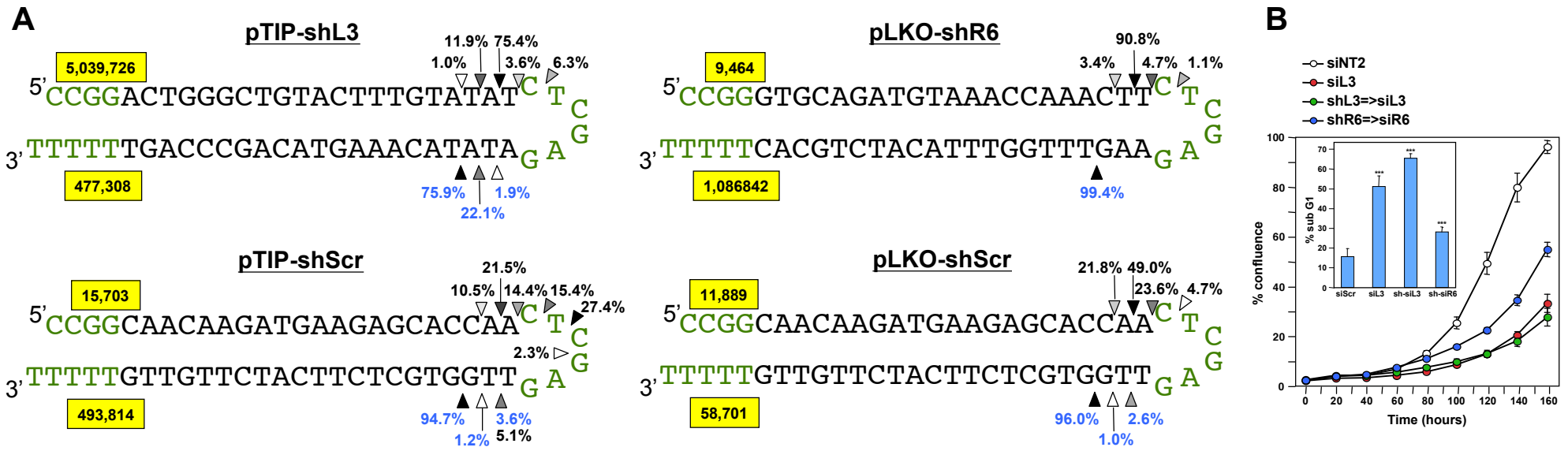

Figure 5 - figure supplement 2

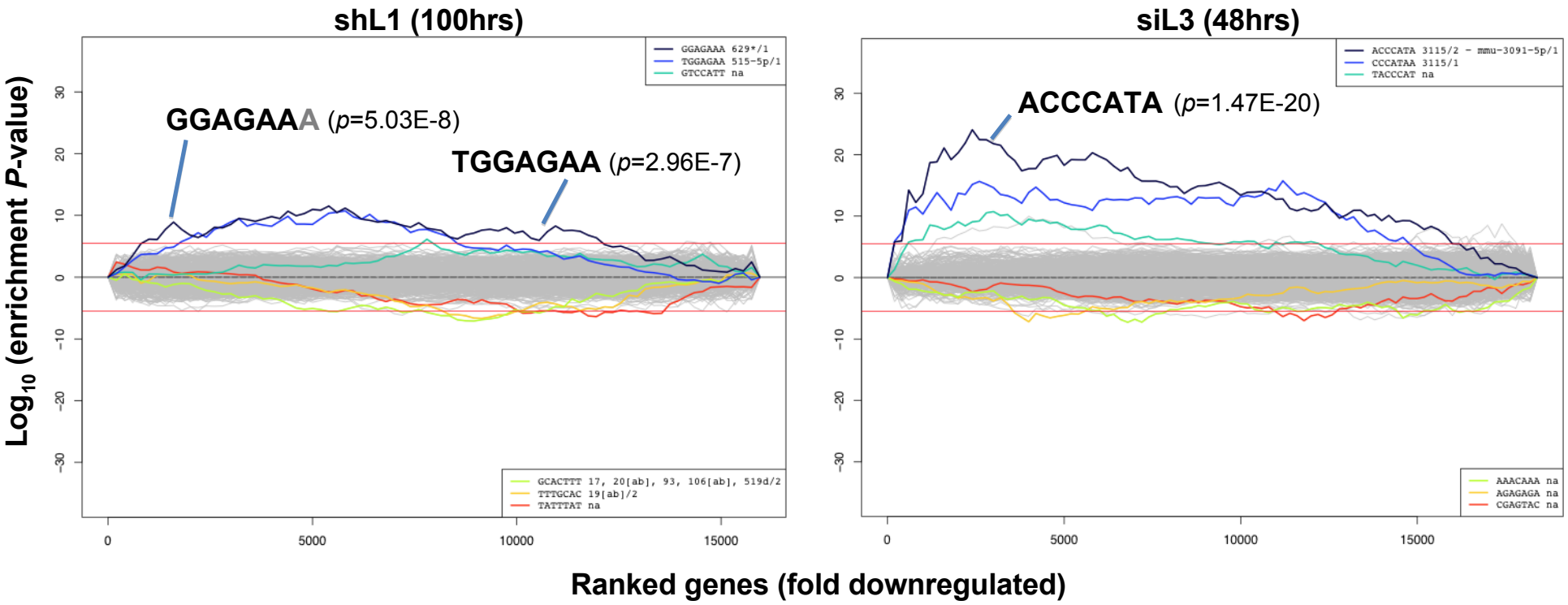

Figure 5 - figure supplement 3

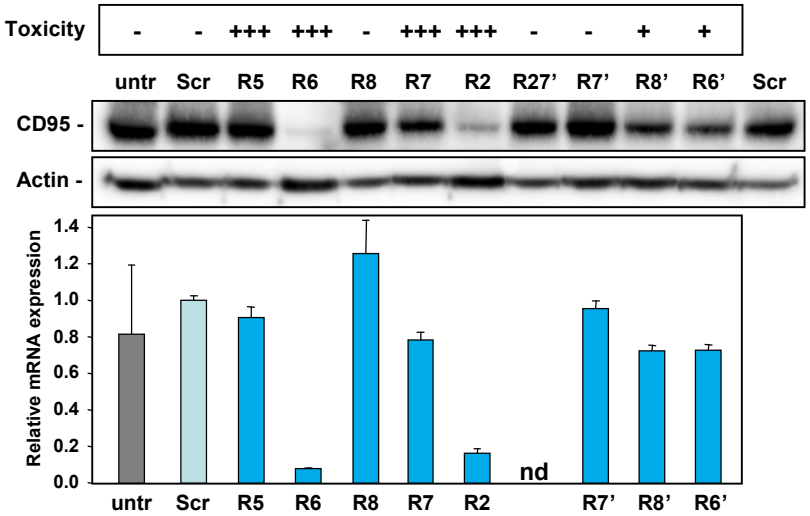

Figure 6

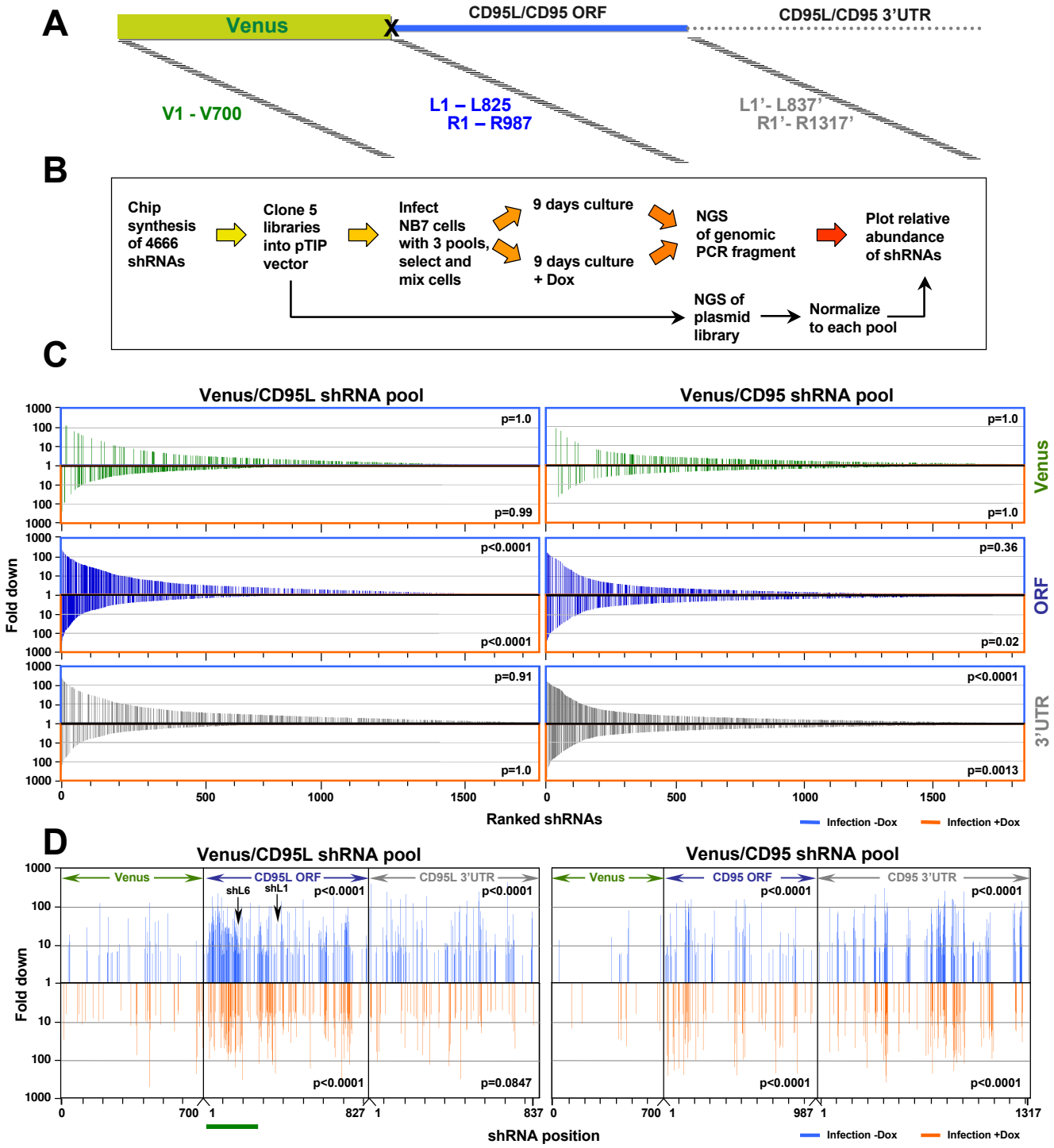
A
Venus
CD95L/CD95 ORF
CD95L/CD95 3'UTR
V1 - V700
L1 – L825
R1 – R987
L1'- L837'
R1'- R1317'
B
Chip synthesis of 4666 shRNAs
Clone 5 libraries into pTIP vector
Infect NB7 cells with 3 pools, select and mix cells
9 days culture
9 days culture + Dox
NGS of genomic PCR fragment
Plot relative abundance of shRNAs
NGS of plasmid library
Normalize to each pool
C
Venus/CD95L shRNA pool
Venus/CD95 shRNA pool
Fold down
Venus
ORF
3'UTR
p=1.0
p=0.99
p<0.0001
p=0.36
p=0.02
p=0.91
p=0.0013
Ranked shRNAs
Infection -Dox
Infection +Dox
D
Venus/CD95L shRNA pool
Venus/CD95 shRNA pool
CD95L ORF
CD95L 3'UTR
CD95 ORF
CD95 3'UTR
shL6
shL1
p<0.0001
p=0.0847
shRNA position

Figure 6 - figure supplement 1

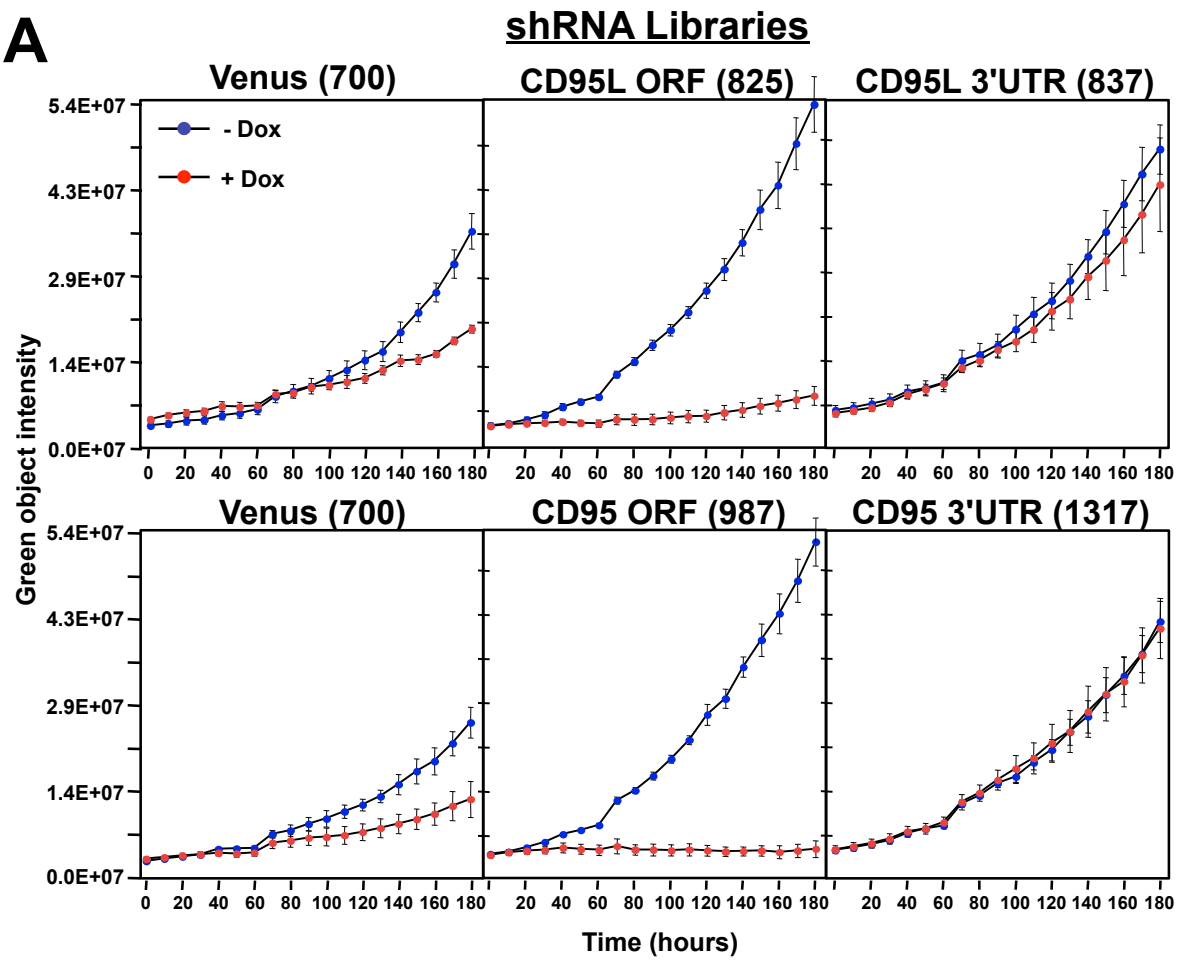

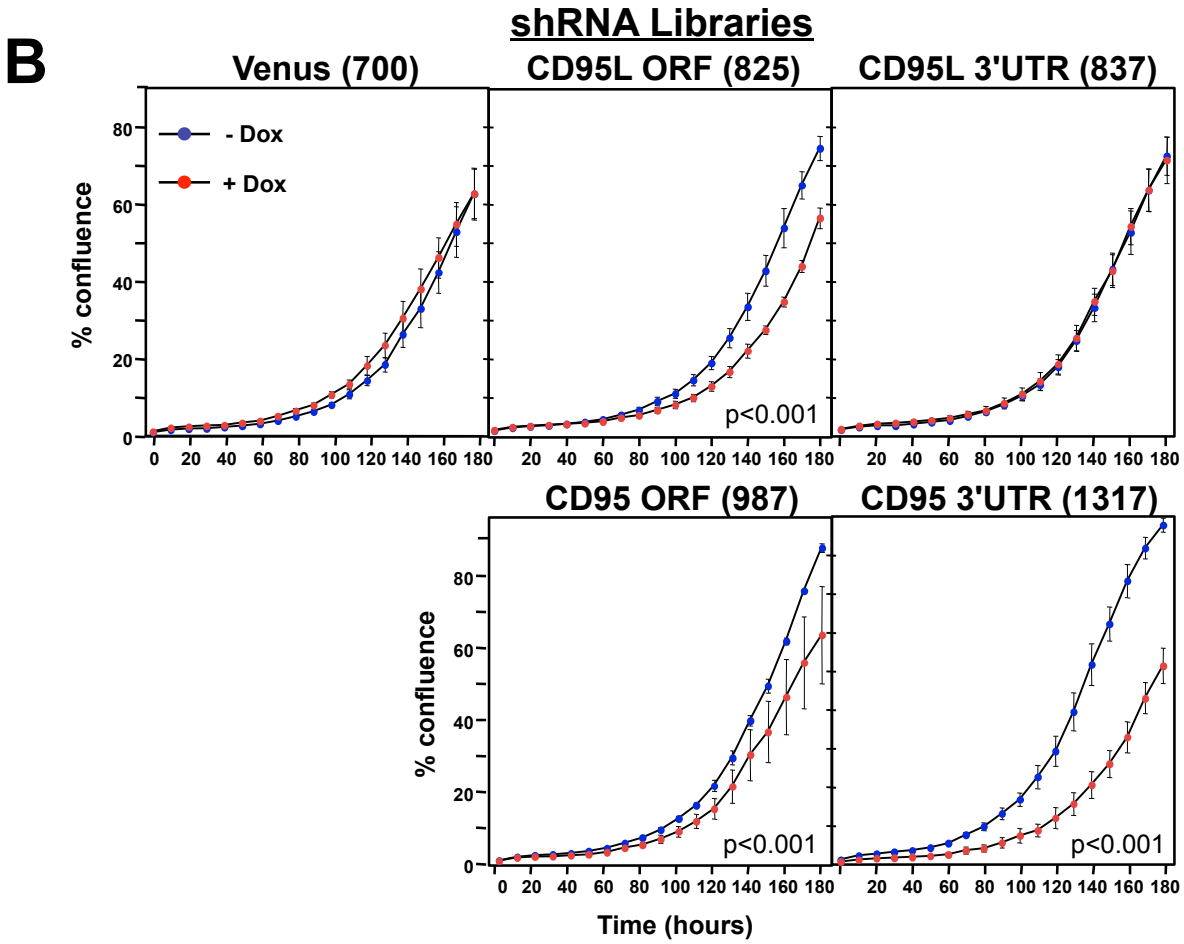

Figure 6 - figure supplement 2

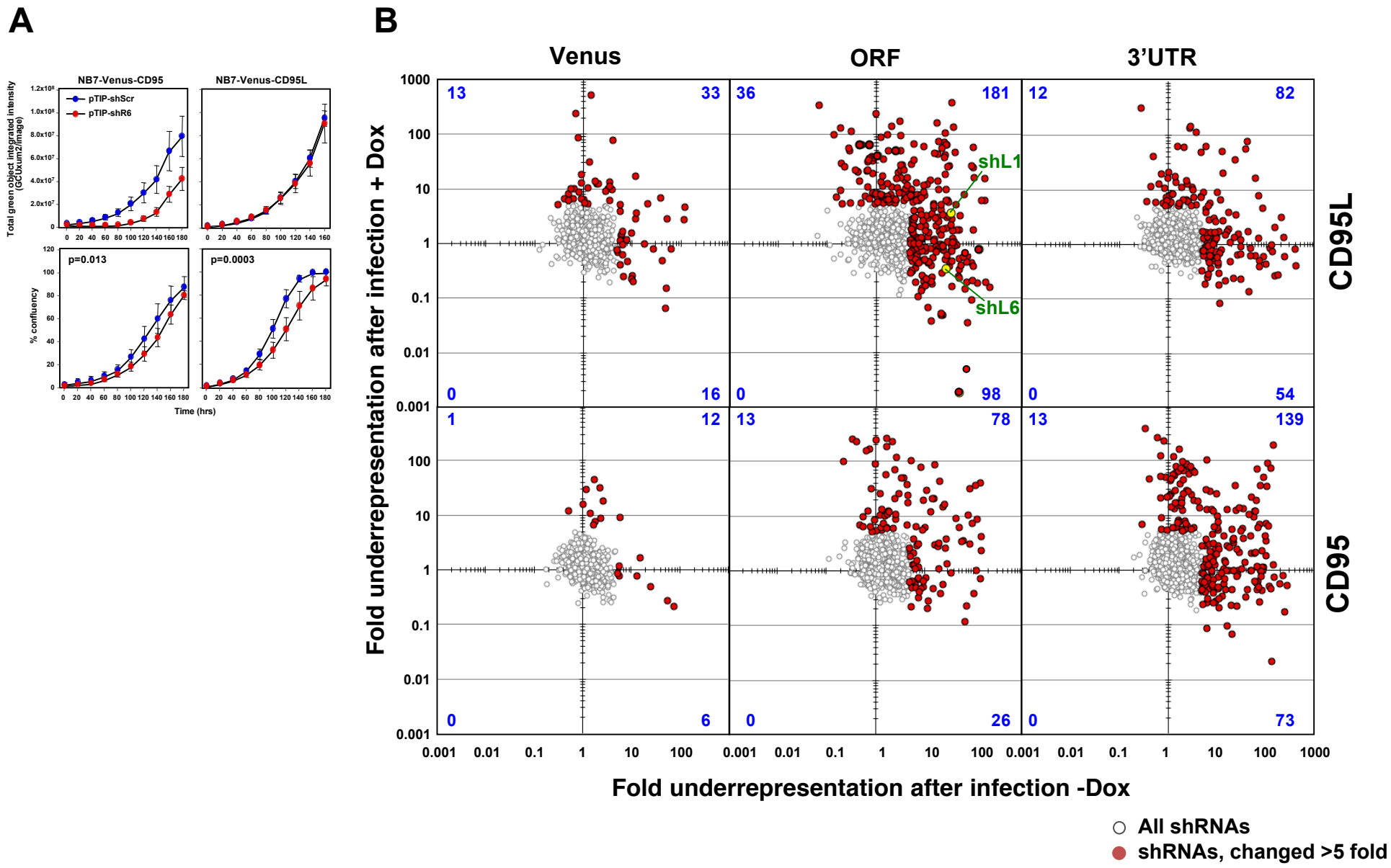

Figure 7

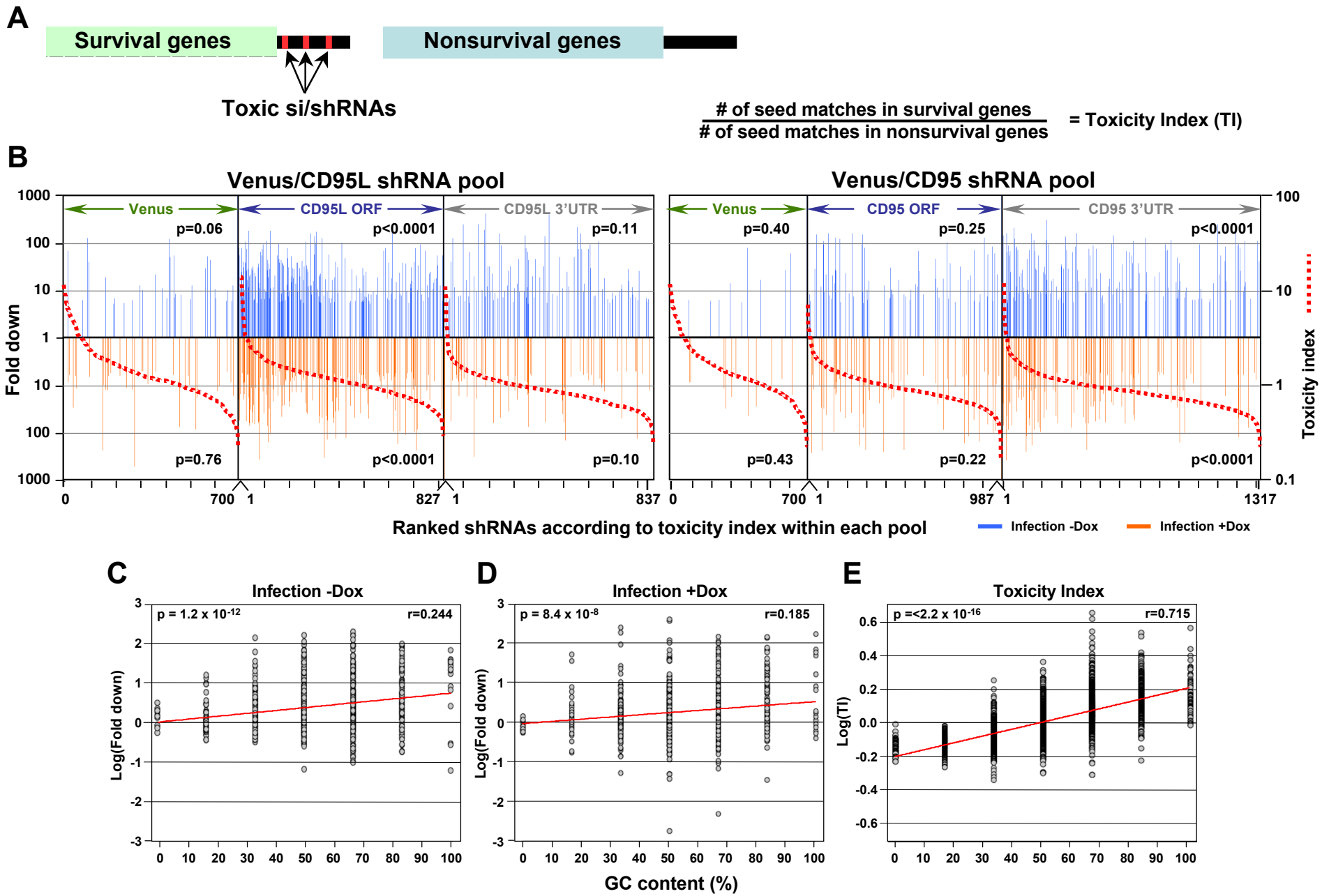
A
Survival genes
Nonsurvival genes
Toxic si/shRNAs
# of seed matches in survival genes
# of seed matches in nonsurvival genes
= Toxicity Index (TI)
B
Venus/CD95L shRNA pool
Venus/CD95 shRNA pool
Venus
CD95L ORF
CD95L 3'UTR
CD95 ORF
CD95 3'UTR
p=0.06
p<0.0001
p=0.11
p=0.40
p=0.25
p<0.0001
p=0.76
p<0.0001
p=0.10
p=0.43
p=0.22
p<0.0001
Fold down
Toxicity index
Ranked shRNAs according to toxicity index within each pool
Infection -Dox
Infection +Dox
C
Infection -Dox
p = 1.2 x 10-12
r=0.244
Log(Fold down)
D
Infection +Dox
p = 8.4 x 10-8
r=0.185
Log(Fold down)
E
Toxicity Index
p =<2.2 x 10-16
r=0.715
Log(TI)
GC content (%)
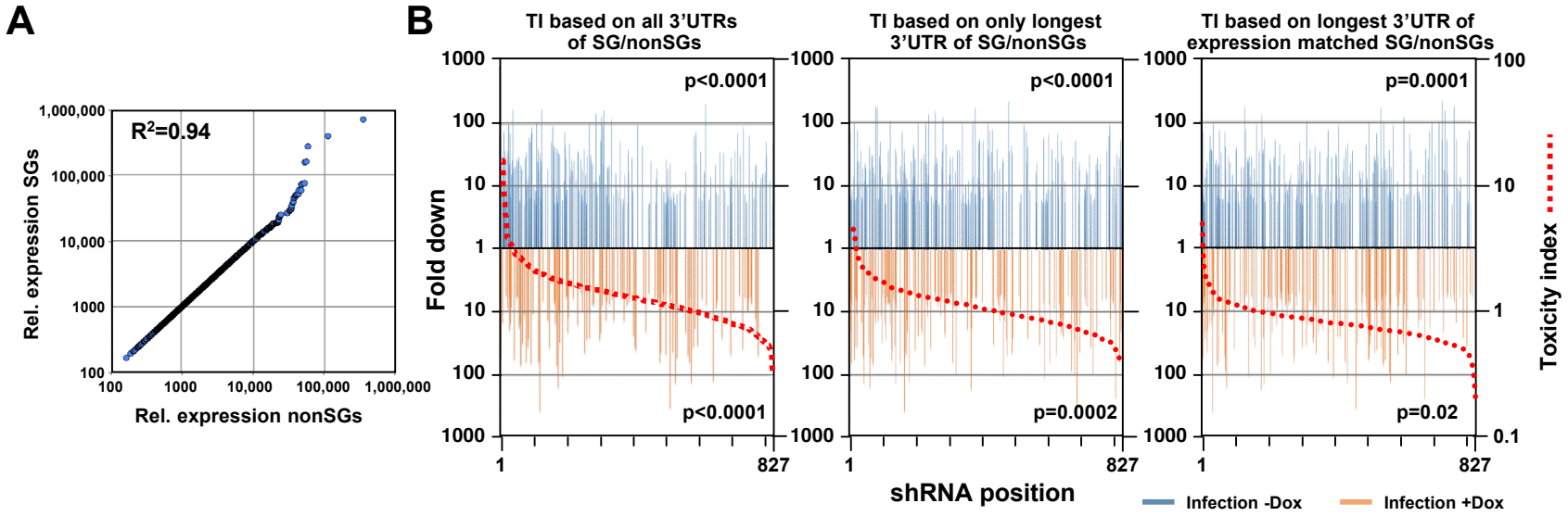
Figure 7 - figure supplement 1